11-7-2019 10:45 AM

Discovery of Novel Mechanisms Regulating Cancer Extravasation in the Chorioallantoic Membrane Model

Yohan Kim, *The University of Western Ontario*

Supervisor: Khan, Zia A., *The University of Western Ontario*
Co-Supervisor: Chakraborty, Chandan, *The University of Western Ontario*
A thesis submitted in partial fulfillment of the requirements for the Doctor of Philosophy degree in Pathology and Laboratory Medicine
© Yohan Kim 2019

Recommended Citation

Abstract

Cancer metastasis is a multistep process that begins with the invasion of tumour cells into the stroma and migration towards the blood vessels. Tumour cells that have entered the bloodstream must then survive and leave by a process known as extravasation. Finally, extravasated cells proliferate and establish the secondary site in the metastatic cascade. Although extravasation encompasses key events during cancer cell invasion to aid in the development of effective treatments, an *in vivo* model that rapidly, reproducibly and economically recapitulates cancer cell extravasation is needed. Therefore, the objectives of my research were to 1) establish and validate an *in vivo* model of cancer cell extravasation, and 2) identify novel cellular and molecular events.

I used the chorioallantoic membrane of chicken embryos as a model system of extravasation as it provides an accessible and highly vascularized structure. The combination of the chorioallantoic membrane of chicken embryos, nanoscale flow cytometry, and confocal microscopy-based intravital imaging allowed me to observe that extravasating prostate cancer cells exhibited significant cell volume reduction. This reduction is suggestive of an invasive cell phenotype. However, cell volume reduction at certain threshold also decreased cancer cell extravasation efficiency. I also found that cancer cell released extracellular vesicles during extravasation, and an increase in extracellular vesicle release caused cell volume reduction. I then tested the hypothesis that extracellular vesicle release and extravasation may be linked to modes of cell death. Real-time imaging of cancer cells that released extracellular vesicles during extravasation did not show activation of caspase-3. Activation of necroptosis, however, increased extracellular vesicle release and decreased cell extravasation and secondary colony formation. These results suggest that necroptosis may be targeted to induce extracellular vesicle release, decrease extravasation, and halt cancer metastasis.

Collectively, my work lays out the protocols for the use of the chorioallantoic membrane of chicken embryos as a model system to investigate cancer cell extravasation and invasion. Use of this model system allowed me to identify extracellular vesicle release during extravasation and discover that necroptosis may be a potential regulator of cancer metastasis.

Summary for Lay Audience

Cancer spreading to different areas in the body is known as metastasis and is the main cause of cancer-related deaths. Many underlying events in cancer metastasis are still poorly understood. To provide new insights, I first established a new model to study metastasis. I injected human prostate cancer cells into the blood vessel of chicken embryo lungs. I then monitored the cancer cells in real-time using microscopy. This technique was optimized, and results were published to allow other researchers to study metastasis in this quick, economical, and reliable model. For the second part of my part, I investigated the changes that take place in cancer cells when the cells move from the injected area to different areas. I observed that cancer cells shrink their sizes when they move out of the blood stream to enter different sites. My results also indicate that this shrinking of cancer cells may have been made possible by a release of small portions of the cell. I reasoned that if this release can be artificially increased, it would possibly kill more cancer cells and provide a new target to stop metastasis. Indeed, my results show that increasing the release of cell portions reduces the ability of cancer cells to move to secondary sites. Therefore, my studies lay the foundation for a new therapeutic target for cancer patients.

Keywords

Co-Authorship Statement

I completed all studies presented in this thesis in the laboratory of Dr. Hon Leong (University of Western University, 2015-2017) for the first 2 years, and the Urology Research Laboratory (being led by Dr. Fabrice Lucien, 2018-2019) at Mayo Clinic for the last 2 years. Dr. Hon Leong contributed to the design, analysis, interpretation, and manuscript preparation for chapter 3 and 4. Dr. Fabrice Lucien also contributed to design, analysis, interpretation, and manuscript preparation for chapter 4. Dr. Chandan Chakraborty and Dr. Zia Khan contributed to interpretation and manuscript preparation for chapter 4.

Chapter 3: Dr. Karla Williams developed the animal models and performed extravasation studies with me. Carson Gavin and Emily Jardin assisted with these extravasation experiments. Dr. Karla Williams and Dr. Anne Chambers participated in manuscript preparation and are co-authors on the published study.

__Kim Y__, Williams KC, Gavin CT, Jardine E, Chambers AF, Leong HS. 2016. Quantification of Cancer Cell Extravasation In Vivo. Nature Protocols. 11(5): 937-948.

Chapter 4: Andrew Poon assisted with all *in vivo* quantification and imaging studies of cancer cell extravasation. Andrew Poon also participated in manuscript preparation. Matthew Aurora and Carson Le assisted with *in vivo* quantification of cancer cell extravasation. Matthew Lowerison assisted with all statistical tests. Janice Gomes contributed to nanoscale flow cytometry-based quantification of cancer cell extracellular vesicle release. Ke Deng helped with intravenous cancer cell injections into the CAM and flow cytometry-based quantification of cancer cell extracellular vesicle release. Yaroslav Fedyshyn helped with the preparation of zsGreen PC-3/PC-3M-LN4 human prostate cancer cells.

Planned publication: __Kim Y__, Poon A, Aurora M, Le Carson, Lowerison M, Gomes J, Deng K, Fedyshyn Y, Leong H, Lucien F. Necroptosis Mediates Cancer Cell Extravasation and Metastasis throughout Cancer Cell Extracellular Vesicle Release.

Acknowledgments

I would like to humbly acknowledge my mentors, Dr. Chandan Chakraborty and Dr. Zia Khan. I am forever grateful that I have two excellent mentors. Not only did Dr. Chandan Chakraborty and Dr. Zia Khan provide me limitless support and guidance throughout my PhD training, they also fostered an environment of creative, critical, and enjoyable science. I have been extremely lucky because I could not have finished my doctorate degree without my mentors. To Dr. Chakraborty, thank you for accepting me as your trainee and all the constructive feedback through my training. I believe that I have developed into a better scientist and human being because of your kindness and supervision. Dr. Khan, I really thank you for giving me motivation and encouragement through every part of my research from the beginning to the end. You especially always encouraged me when I struggled with confronting unexpected events during my training. I have been also greatly benefited from your constructive advice in scientific writing, presentation, and expanding ideas in my research. I could not have imagined having better life mentors than both of you. I will also never forget the discussion in science and life we had during the office hours. Again, I really thank you for everything and treating me like a nephew and a younger brother.

I also want to thank my previous mentor Dr. Hon Leong. Thank you for providing me the opportunity and all the resources over the first 3 year of my doctoral training. I refined myself as a scientist by receiving your guidance. I also want to thank you for helping me foster scientific maturity, leadership, and execution. I really appreciate your support on establishing my career in science and I wish you all the best.

I greatly acknowledge Dr. Fabrice Lucien and Dr. Kelly Paulson at Mayo clinic. Dr. Fabrice Lucien stepped up as my secondary mentor at Mayo Clinic, and always supported and motivated me. Dr. Fabrice Lucien supervised me throughout the last year of my training, helping me finish my publication without any further delays. As both a great colleague and friend of mine, I am very fortunate that we completed not only our training together but also, we will work together to perform excellent translational science that will bring positive impacts on cancer patient care. Dr. Kelly Paulson, a research administrator in the department of Urology, supported me providing all resources to manage and finish my work at Mayo clinic. I want to give a special thank to Dr. Kelly Paulson for treating me like her son.

I want to acknowledge my advisory mentorship at the Mayo clinic: Dr. Mark McNiven, Dr. David Katzmann, Dr. Gina Razidlo. I appreciate their great advice and discussion that led to the development of this thesis. They guided me in the right direction, helped me expand my scientific knowledge and provided constructive feedback.

I would like to acknowledge the Lawson Health Research Institute and Ontario Graduate Scholarship for supporting my studies and allowing me to take the next steps in my career.

Dear heavenly father, thank you for your great plan for me even before I was born. You are my strength and shelter so that I could achieve this milestone to help people in the world. I will always follow you until the end of my life on Earth. Amen.

To the most beautiful woman in the world, my wife Kwiyoung, I could accomplish this milestone because of your presence beside me. I want to say I really thank you for your sacrifice and support you made over last 3 years. When I couldn't escape from the "dark days", you have always held my chin up and made me push forward. I have really enjoyed the time we laughed and cried together. I really look forward to the next chapter of our life with our son Joshua. Thank you again and I love you so much with all my heart.

To my mom and dad, I want to say I truly love you with all my heart and thank you. No one can love me and provide me with wise counsel and sympathetic ears like you do. You are always there for me. I really thank you for the moral and financial support throughout my life. Without you, I wouldn't have made it up to this point. You have always encouraged me to move forward when I was feeling low on myself. I can proudly say that I always learn every single value of life by watching the hard work you do every given day. Again, mom and dad, you deserve all my respect and love.

To my only and beloved brother, I really thank you for being my best friend and supporter. I am very proud to be your brother and best friend as well. I have watched you build up your career as a professional kinesiologist and perform an excellent job in helping patients rehabilitate. I hope you keep up your passion for helping patients and I will keep you in my prayer forever.

To my colleagues, Andrew and Janice, we created a great team and produced a great work all together. I will never forget the time we spent together during our training. You guys are my

life-time friends forever. All the best for you in pursuing veterinary medicine and doctoral training!

Table of Contents

List of Tables

List of Figures

List of Abbreviations

AFM Atomic Force Microscopy

ALIX Programmed Cell Death 6-Interacting Protein

Akt1 Rac-alpha serine/threonine-protein kinase

ANGPTL4 Angiopoietin-Like 4

Apaf-1 Apoptosis Activating Factor-1

Apo-EV Apoptotic Extracellular Vesicle

ARF6 ADP-ribosylation Factor 6

ARP2/3 Actin-related Protein 2/3 Complex

ATM Ataxia-telangiectasia mutated

ATP Adenosine Triphosphate

BCL-XL B-cell Lymphoma-extra large

BMDC Bone Marrow-derived Dendritic Cell

BM-MSC Bone Marrow-derived Mesenchymal Stem Cell

CAD Caspase-activated DNAse

CAM Chorioallantoic Membrane

cAMP Cyclic Adenosine Monophosphate

cANGPTL4 C-terminal Fibrinogen-like domain of Angiopoietin-Like 4

cAR1 cAMP Receptor

Caspase Cystine-dependent Aspartate-driven Proteases

CCL2 C-C Motif Chemokine Ligand 2

CHMP2A Charged Multivesicular Body Protein 2A

CHMP4B Charged Multivesicular Body Protein 4B

cIAP1/2 Cellular Inhibitor of Apoptosis Protein

CSF1R Colony Stimulating Factor 1 Receptor

CTC Circulating Tumor Cell

CTSD Cathepsin D

CXCR2 Chemokine (C-X-C motif) receptor

CXCL Chemokine (C-X-C motif) Ligand

CYLD Cylindromatosis

DAMPs Danger-associated Molecular Patterns

DIAPH3 Diaphanous-related Formin-3

DMF Dimethyl Fumarate

DNA Deoxyribose Nucleic Acid

EC Endothelial Cell

ECM Extracellular Matrix

EndMT Endothelial-to-mesenchymal Transition

ESCRT Endosomal Sorting Complexes Required for Transport

EGFR Epidermal Growth Factor Receptor

EMT Epithelial-to-mesenchymal transition

ERα Estrogen Receptor-α

ERK Extracellular Signal-Regulated Kinase

EV Extracellular Vesicle

FADD Fas-Associated Death Domain

FasL Tumor Necrosis Factor Ligand

FN Fibronectin

FITC Fluorescein Isothiocyanate

FOS-1A Fos Proto-oncogene, Activating Protein-1 Transcription Factor Subunit

FRET Föster Resonance Energy Transfer

FSC Forward-scattered Light

GPCR G Protein-coupled Receptor

HIF Hypoxia-inducible factor

IL Interleukin

ILV Intraluminal Vesicle

LALS Large Angle Light Scatter

LHX2 LIM/Homeobox protein 2

LPS Lipopolysaccharides

Ly6C Lymphocyte Ag 6C

MAMs Metastasis Associated Macrophages

MAPK Mitogen-activated Protein Kinase

MAT Mesenchymal Amoeboid Transition

MAVS Mitochondrial Antiviral Signaling Protein

MET Mesenchymal-Epithelial Transition

MFI Mean Fluorescent Intensity

MHC II Major Histocompatibility Complex II

MLC Myosin Light Chain

MLCK Myosin Light Chain Kinase

MLKL Mixed Lineage Kinase Domain-like Protein

MMP Matrix Metalloproteinase

mRNA Messenger Ribonucleic Acid

MSC Mesenchymal Stem Cell

MVB Multivesicular Body

Nec-1 Necrostatin 1

NETs Neutrophil Extracellular Traps

nFC Nanoscale Flow Cytometry

NF-κB Nuclear Factor κ Light Chain Enhancer of Activated B Cells

NHE-1 Sodium-hydrogen antiporter 1

NOD Non-obese Diabetic

NTA Nanoparticle Tracking Analysis

N-WASP Neural Wiskott-Aldrich Syndrome Protein

PBMC Peripheral Blood Mononuclear Cell

PDX Patient-derived Xenograft

PE Phycoerythrin

PLD Phospholipase D

PI3K Phosphoinositide 3-Kinase

PMT Photomultiplier Tube

PS Phosphatidylserine

PSMA Prostate Specific Membrane Antigen

PTEN Phosphatase and Tensin Homolog

P2X7 Purinoceptor 7

P2Y$_2$ Purinoceptor 2

RBM11 The RNA Recognition Motif Protein 11

RIPK Receptor-interacting Serine/Threonine-protein Kinase

ROCK RHO-associated Protein Kinase

ROI Region of Interest

qRT-PCR Quantitative Reverse Transcriptase Polymerase Chain Reaction

SCID Severe Combined Immunodeficient

SEM Scanning Electron Microscopy

siRNA Small interfering RNA

SMA α-smooth muscle actin

SALS Small Angle Light Scatter

Src Proto-oncogene Tyrosine-protein Kinase (homology to the Rous Sarcoma Virus Oncogene Protein PP60)

SSC Side-scattered Light

STS Staurosporine

TEM Transmission Electron Microscopy

TF Tissue Factor

TGF-α Transforming Growth Factor-α

TGF-β Tumor growth factor β

TKS5 Tyrosine Kinase Substrate with Five Src Homology 3 Domains

TLR Toll-like Receptor

TNFR1 Tumor Necrosis Factor Receptor

TRADD Tumor Necrosis Factor Receptor Type 1 Associated Death Domain Protein

TRAF TNF Receptor-Associated Factor

TRITC Tetramethylrhodamine

TSG101 Tumor Susceptibility Gene 101

tTG Tissue Transglutaminase

u-PA Urokinase-type Plasminogen Activator

VEGF Vascular endothelial growth factor

VE-cadherin Vascular Endothelial cadherin

VPS Vacuolar Protein Sorting-Associated Protein

ZMP-1 Zinc Metalloprotease 1

<div align="center">Chapter 1</div>

1   Introduction

1.1   Underlying cellular process during cancer metastasis

1.1.1   Dogma of cancer metastasis

Cancer is an extremely heterogeneous disease. There are more than 200 different cancer types[1]. However, certain cellular and molecular events are shared between these various cancer types, and are termed the hallmarks of cancer[2]. Advances in basic scientific research have identified therapeutic targets in many different cancers, which alone, or in combination have yielded promising initial results[3]. Unfortunately, despite these advances, many patients still succumb to cancer recurrence and relapse.

Metastasis is a critical event in cancer progression, contributing to over 90% mortality in cancer patients[4]. Metastasis and its level, inform the stage of cancers and provide information on the survival chance of patients. The most invasive cancers (for example, triple negative breast cancer, kidney cancer, prostate cancer, and melanomas) metastasize to several distant organs or tissues such as the bone, liver, brain, and lungs[5]. This movement of cancer cells from the primary site to a secondary site is a multistep process termed the metastatic cascade[6]. Accumulation of genetic mutations and changes to the tissue microenvironment facilitates cell transformation, uncontrollable cell growth and proliferation, and establishment of the primary tumour[2]. As the primary tumour confronts microenvironmental stresses such as changes in oxygen and nutrient levels, pH, growth factors, chemokines and cytokines, cells in the tumour assume an invasive phenotype to find secondary growth sites and maintain their proliferation[2,6,7]. Alteration of metastasis suppressor genes plays a significant role in these processes[8–11]. For example, highly metastatic murine K-1735 melanoma cells exhibit reduced NM23 gene expression and form metastases in rats[12].

Once cancer cells migrate to secondary organs, the stroma at these sites provides a sustainable niche that allows tumour cells to adapt and proliferate. Certain cancers migrate towards specific secondary organs to form colonies, according to the Paget's "seed and

soil" theory (**Table 1**)[13]. For example, breast and prostate cancer cells preferably metastasize to the bone. It is believed that processes at these secondary sites may facilitate homing of the cancer cells. In the case of bones, bone remodeling secretes chemokines, growth factors, and angiogenic factors that may facilitate breast and prostate cancer secondary colony formation[14]. However, certain cancers such as brain, pancreatic, and ovarian cancers do not exhibit bone metastases[15]. Instead, pancreatic and ovarian cancer metastasize to peritoneum, a site not assaulted by breast and prostate cancer.

Heterogeneity in metastatic potential and intensity may also exist within the cancer type. Therefore, cancer metastasis varies in origin, underlying molecular process, intensity of the spread, and secondary site. In addition, since invasive tumours can utilize different molecular pathways to succeed in metastasis, clear understanding of each molecular mechanism is required to develop multiple therapeutic strategies to halt both localized and metastasized tumours.

Cancer Type	Primary Site	Principal Site of Metastasis
Breast Cancer	Breast	Bone, lung, liver, and brain
Small Cell Carcinoma	Lung	Brain, liver and bone
Malignant Melanoma	Skin	Lung, brain and liver
Prostate Cancer	Prostate	Bone
Testicular Cancer	Tastis	Liver
Colorectal Cancer	Colon/rectum	Liver and lung
Neuroblastoma	Mediastinum/abdomen	Liver

Table 1: Tumour type specific metastatic sites based on Paget's "seed and soil" theory[13]

Table is reproduced here for educational purpose only and not for any commercial use. Table is included in the Ph.D. dissertation with attribution[13]

1.1.2   Limits of current therapeutics targeting metastatic cancers

Currently, chemotherapy is commonly used with radiation or hormonal therapy after surgery to target localized and metastasized tumours. However, most chemotherapeutic agents show general cytotoxicity[16,17]. This cytotoxicity is partially due to high doses of chemotherapeutic drugs that are needed to contain cancer growth. Cells within the tumour respond to anti-cancer drugs differently, necessitating a high dose[18]. Most primary tumours comprise highly heterogenous cells. Chromosomal instability in cancer cells causes somatic mutagenesis and epigenetic heterogeneity. Metastatic cancers adopt genetic and epigenetic alterations allowing some subpopulations of cancer cells to resist anti-cancer drugs and grow after drug treatment is stopped[19]. Tumour cells may also acquire intrinsic resistance to cytotoxic chemoradiotherapies[20]. Numerous metastatic cancers (for example, colorectal cancer and breast cancer) show lower levels of reactive oxygen species production and the activation of ataxia telangiectasia mutated (ATM)-dependent DNA-

damage repair process to escape chemotherapy-induced changes. Furthermore, many cancers can develop multidrug resistance by repelling chemotherapeutic agents out and impairing drug delivery[21]. Therefore, understanding the underlying cellular and molecular processes involved in cancer metastasis may provide novel avenues to develop effective and fast-acting therapies.

1.1.3   The metastatic cascade

Cancer becomes life-threatening by spreading to different organs throughout successive steps of the metastatic cascade[6,22,23]. Throughout this sequence, cancer cells confront pressures that they must overcome. Initially, cancer growth is contained at the primary site. Acquisition of invasive phenotypes allows cancer cells to migrate towards blood or lymphatic conduits. Degradation of vessel basement membranes and migration across the endothelial lining allow the cells access to other tissues. Cancer cells now must survive the circulation, stall in small capillaries, cross the endothelial lining, and establish a metastatic colony in secondary organs.

Cancer cells generate hypoxic regions that induce endothelial cell migration and proliferation[24]. Hypoxic environment is kin to the activation of the hypoxia-inducible factor (HIF) pathway[25]. Cancer cells in hypoxic regions increase the expressions of angiogenic and hematopoietic growth factors such as vascular endothelial growth factor (VEGF)[26]. Elevated local VEGF and other angiogenic factors increase endothelial cell permeability, migration, and proliferation. The increase in vascular permeability and density may facilitate cancer cells to intravasate into the bloodstream[27]. The newly formed blood vessels in tumours are highly atypical, tortuous, and may lack directional blood flow. These abnormal vessels also reduce pH and increase interstitial fluid pressure, which hamper immune cell functions and allow cancer cells to escape through leaky vessels[28,29].
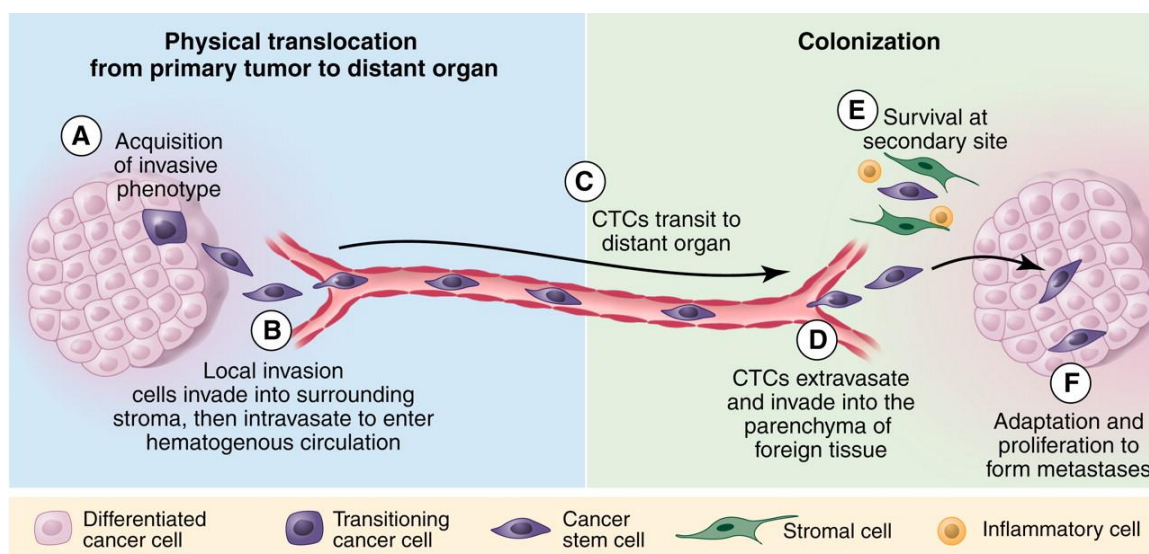
Figure 1: The metastatic cascade comprises local invasion, intravasation, hematogenous migration, extravasation, and metastatic colony formation[30]**.** (A) Cancer cells acquire an invasive phenotype by undergoing epithelial-to-mesenchymal transition (EMT). This transition allows cancer cells to become motile by losing epithelium characteristics such as E-cadherin. (B) Cancer cells with an invasive phenotype intravasate through the leaky blood vessels and begin their journey in the circulation. (C) Cancer cells migrate across the circulatory system during that cells confront shearing forces, immune surveillance, and cell death. (D) Cancer cells arrest in small blood vessels such as capillaries at secondary sites and extravasate into the stromal space. (E) Extravasated cancer cells either survive or undergo cell deaths. Surviving cancer cells can also then continue their proliferation or become dormant. (F) A secondary metastatic colony is formed when a permissive microenvironment allows surviving cancer cells to proliferate.

Figure is reproduced here for educational purpose only and not for any commercial use. Figure is included in the Ph.D. dissertation with attribution[30].

The migration of cancer cells from the primary site (intravasation) requires morphological changes that allow cancer cells to become invasive and migratory (**Figure 1A, B**). This phenotypic change manifests as cytoskeleton rearrangement, loss of apical-basal polarity, and acquisition of a mesenchymal phenotype (termed epithelial-to-mesenchymal transition (EMT)) (**Figure 1A**). Apical-basal polarity is a hallmark of epithelial cells, and is mainly regulated by epithelial cadherin (E-cadherin) and cytokeratin[31]. E-cadherin and cytokeratin facilitate tight junctions, adherens junctions, gap junctions, and assembling desmosomes. Cancer cells receive extracellular cell- and tissue-specific stimulating factors to induce the

activation of several genes involved in motility and intravasation. An increase of transforming growth factor-β (TGF-β) expression leads to the activation of downstream colony stimulating factor 1 receptor (CSF1R), among other proteins. CSF1R is involved in cellular motility and the inhibition of CSF1R has been shown to reduce cancer cell motility and intravasation *in vivo*[32]. CSF1R also suppresses keratins and claudins, which are involved in a reduction of cancer cell invasion and intravasation[33]. TGF-β also activates LIM/homeobox protein (LHX2), which enhances cancer cell intravasation and metastasis[32,34]. The expression of epidermal growth factor receptor (EGFR; Erb2 and Erb3) on cancer cells also affects the level of cancer cell invasiveness and intravasation[35]. Although EGFR is mainly involved in stimulating tumour growth, overexpression of EGFR induces intravasation by phosphoinositide 3-kinase (PI3K) and neural Wiskott-Aldrich syndrome protein (N-WASP) that induce invadopodia formation[36]. Loss of E-cadherin and expression of mesenchymal genes such as N-cadherin, fibronectin, and vimentin[37], facilitate disassembly of cytoskeleton anchored to desmosomes, allowing the cancer cells to form invadopodia and become motile. As a result, cancer cells can proceed to intravasation and enter the circulation.

Intravasated cells, termed circulating tumour cells (CTCs), migrate along the circulatory system before lodging/stalling at the capillaries of secondary sites (**Figure 1C**)[38]. CTCs confront an extremely stressful extracellular milieu consisting of innate immune system, oxidative stress, and shear forces from blood pressure[39,40]. In this environment, only about 0.1% of CTCs survive to attempt colony formation at secondary sites[41]. To avoid innate immune system-mediated attacks, CTCs can attach to platelets and myeloid cells, and avoid circulating immune cells. In addition, CTCs associate with fibrin to anchor to the blood vessel endothelium, which allows the cells to escape into the stroma before immune cells mount an attack[42,43]. Primary tumours may also release clusters of cells that form microemboli. Such microemboli formation can lead to local metastatic foci and increase metastatic efficiency[44].

Perhaps a key determinant of metastatic spread is extravasation. Although most single tumour cells extravasate into the stroma first and proliferate later, some tumour cells may also proliferate in the blood vessel before extravasating[45]. It is plausible that tumour proliferation in circulation is an attempt to increase the frequency of extravasation or likelihood of survival of extravasating cells. Increased expression of endothelial adhesion molecules such as integrins facilitates adherence of CTCs to endothelial cells. Tumour cells may also get support from platelets to adhere to the endothelium via β_3 integrin interaction[46,47]. Studies have shown that $a_v\beta_3$ integrins on MDA-MB-435 cells increase the expression of matrix metallopeptidase 9 (MMP9) resulting in more migration and metastatic foci in the lungs[48,49]. Combination of TGF-β and $a_v\beta_3$ also prevents anoikis of tumour cells[50]. Tumour cell-activated platelets also release dense granule-derived ATP which modulates endothelial junctions and creates spaces that allow cancer cells to transmigrate[51]. As tumour cells arrive at the secondary sites, a mesenchymal-epithelial transition (MET) takes place[52–54]. A recent study documented histological evidence of an epithelial phenotype of metastases, which was similar to the primary tumour[55,56]. Cytoskeletal changes that accompany MET allow cancer cells to recruit granulocytes (for example, neutrophils) by building a chemoattractant gradient comprised of CXCL5 and CXCL7[57,58]. CXCL5 and CXCL7 bind to CXCR2 chemokine receptors on neutrophils at the sites of extravasation. Once neutrophils detect circulating tumour cells, neutrophils form neutrophil extracellular traps (NETs) by degranulating to sequester tumour cells[59]. In this process, β_1 integrins can help tumour cells attach to the endothelium and MMP-9 secreted by neutrophils can degrade the endothelial basement membrane barrier so that tumour cells can pass through. Tumour cells also release CC-chemokine ligand 2 (CCL2) that binds to CC-chemokine receptor 2 (CCR2) of Ly6C-positive circulating monocytes. Recruited monocytes differentiate into metastasis-associated macrophages (MAMs) that release VEGF to increase the permeability of the blood vessels[60,61]. In addition, tumour cells can secret VEGF themselves to induce further endothelial leakiness, promoting tumour cell extravasation[62]. Tumour cells can also enhance extravasation by secreting angiopoietin-like 4 (ANGPTL4)/C-terminal fibrinogen-like domain (cANGPTL4) that loosens the tension of vascular endothelium and tight junctions[63]. Secreted cANGPTL4

can temporarily interact with $\alpha_5\beta_1$, vascular endothelial-cadherin, and clautin-5 that help facilitate metastasis[64].

Most cancer cell extravasation (**Figure 1D**) is paracellular migration wherein tumour cells pass through endothelial cells. However, tumour cells can also pass through individual cell bodies by a process called transcellular migration[65,66,67]. Extravasation appears to be challenging due to more restricted endothelium of mature blood vessels near distant organs. However, single tumor cells from the primary tumor generally undergo intravasation easily due to malformed and irregular tumor blood vessels exhibiting loss of endothelium and disrupted cell junctions[29]. To facilitate extravasation, tumour cells form finger like protrusive structures termed invadopodia that are rich in actin and degrade the extracellular matrix[36,66]. Invadopodia formation is a highly coordinated process due to the involvement of multi-regulatory proteins. Tumour cells form invadopodia by responding to growth factors and extracellular matrix-mediated integrin signalling. Upon receiving stimulating signals, actin regulatory proteins (N-WASP, cortactin, and ARP2/3) facilitate local F-actin nucleation[68]. TKS4 and TKS5, other regulatory and adaptor proteins, are also involved in invadopodia formation and maturation. Cancer cell invadopodia mainly facilitate the degradation of extracellular matrix[23,68].

Tumour cells that enter the stroma of secondary sites need to survive, enter dormancy or undergo cell death[6] (**Figure 1E, F**). Tissues rich in growth promoting factors (TGF-β, insulin-like growth-factor-1) such as bones and breast can provide sustainable nutrient-rich environment to tumour cells[69]. The presence of specific growth factor receptors can also affect tumour cell metastatic efficiency. EGFR on colon and other cancer cells can respond to transforming growth factor-α (TGF-α) from the liver that helps cancer cells adapt to the liver environment and facilitate metastatic growth[70,71]. Lastly, tumour cells can change gene-expression patterns in response to organ-specific microenvironment. Human renal cell carcinoma KG-2 cells implanted in the kidney of athymic nude mouse form both local tumours and metastases in the lungs, whereas KG-2 cells implanted subcutaneously only form local tumours[72]. Associated with this behaviour, KG-2 cells implanted in the kidney showed significantly higher expression of urokinase-type plasminogen activator (u-PA) compared to KG-2 cells implanted subcutaneously[72].

1.1.4   Cancer extravasation is a realistic target to combat cancer metastasis

Emerging studies on cancer extravasation have highlighted its significance in the metastatic cascade. Extravasation is not only limited to transendothelial migration of leukocytes and cancer cells but represents quite a common biological process. In cancer progression, however, extravasation is a crucial step. Only a very small number of disseminated cancer cells end up forming metastatic colonies in experimental metastasis assays[6]. *In vivo* assays show that only 10% of extravasated B16F10 melanoma cells successfully formed secondary colonies *in vivo*[73]. Therefore, it appears that extravasation is a rate-limiting step in the metastatic cascade. Many potential drugs targeting invadopodia formation in invasive cancer cells are under development. As outlined above, morphological changes in cancer cells facilitate extravasation through invadopodia formation[66,74,75]. Invadopodia formation and maturation are regulated by several proteins which include TKS4 and TKS5. A previous study showed that impaired invadopodia formation throughout siRNA-mediated TKS4 and TKS5 knockdown resulted in the abrogation of breast cancer cell extravasation and cancer cell colony formation in mouse lungs[66]. Studies also show that Src kinase regulates invadopodia biogenesis in extravasating cancer cells by interacting with cortactin and F-actin[74,76]. Bowden *et al.* and Mader *et al.* demonstrated enhanced invadopodia formation upon constitutive Src expression, and decreased invadopodia formation and degradation of ECM upon Src knockdown in human breast cancer MDA-MB-231 cells[77,78]. SU6656, a Src inhibitor, significantly reduced invadopodia formation, migration, and metastatic colony formation in MDA-MB-231 cells[74]. It is not surprising that studies on invadopodia inhibition have flourished recently, and various potential therapeutics are being tested for evidence of extravasation inhibition.

1.1.5   Animal model systems for studying cancer metastasis

Identification of cellular and molecular mechanisms underlying cancer cell extravasation is dependent on appropriate *in vivo* models. *In vitro* culture studies on cancer migration or invasion offer an economical and versatile assessment of metastatic potential. Cancer cells with genetic modification/chemical treatment can be cultured and monitored readily and offer valuable information. However, all observations made in these *in vitro* studies need to be validated in *in vivo* models. In addition to offering a more realistic context, cancer cells spreading to preferred sites can also be investigated in *in vivo* systems. Currently, *in vivo* metastasis models include non-mammalian and mammalian systems. Select systems will be discussed here.

1.1.6   Non-mammalian models

Dictyostelium discoideum and *Caenorhabditis elegans* are useful models to study cancer chemotaxis and invasion[79]. *D. discoideum* shows amoeboid migration towards cAMP. Interaction between cAMP and cAMP receptor (cAR1) polarizes and prepares cells to migrate through G_{α} and $G_{\beta\gamma}$[79,80]. *D. discoideum* shows not only a transient increase in cell polarity upon uniform chemoattractant stimulation, but also a persistent and spatially restricted increase in cell polarity in response to a chemoattractant gradient.

C. elegans is a simple model of basement membrane invasion. It has a very unique body component called the single cell that breaches two underlying basement membranes[81]. The single cell can form an anchor, similar to invadopodia, which is formed by FOS-1A[82] activation. Zinc metalloprotease 1 (ZMP-1), downstream of FOS-1A, degrades basement membranes[83,84]. These non-mammalian models are certainly valuable in providing mechanistic insights into specific cellular events such as protrusive structure formation which may be similar to cancer cell invasion and metastasis.

1.1.7   Mouse models of metastasis

The mouse model has become the gold standard in cancer research[85] and offers multiple advantages. Gene homology between human and mouse allows investigators to study cancer metastasis in mouse cell lines derived from carcinogen-induced tumours, spontaneous tumours, or normal cells that are transformed in culture[86]. Cancer cells implanted to create syngeneic and xenograft models of the cancer[87]. Implanting human cancer cells and tissues is also widely used[88]. However, there may be species differences that may limit the biological significance of some findings.

One of the advantages of using the mouse model is that it provides an appropriate context/microenvironment to the tumour cells to study primary tumour growth, assess metastasis, and tropism. Experimental models in which cancer cells are injected into blood vessels allow researchers to monitor cell extravasation and metastatic colony formation[88]. The different means of administering cancer cells have been recently reviewed by Khanna and Hunter[89]. Cancer cells can be injected into the lateral tail vein, portal vein, carotid artery, and left ventricle of the heart. Of these, tail vein injection is the most common route to administer cancer cells and reliably generates lung metastases. Intracardiac injection is used to study bone and brain metastasis. In this case, cancer cells are injected into the left ventricle of the heart. Depending on the cancer type introduced, intracardiac injection can allow cancer cells to spread through most organs in the body. However, breast and prostate cancer metastases are mainly found in the bone from the intracardiac injection. Intra-portal or intrasplenic injection directly introduces cancer cells into the liver.

Metastasis models are designed to examine the metastatic cascade but do not provide information on primary tumour growth and intravasation[88]. To overcome this limit, cancer cells or tissues can be transplanted ectopically or orthotopically to create spontaneous metastasis model. These models allow rapid tumour growth under the skin which is highly vascularized and tumour growth can be easily measured by calipers[88]. Orthotopic transplantation is also suitable to examine initial phases of the metastatic cascade as tumours are generated at the original primary tumour sites[88].

Cancer cells that are introduced in mice may be compromised by the host immune system. Immunodeficient mice such as athymic nude mice and severe combined immunodeficient (SCID) mice can resolve the host immune system issue[90,91]. Although these mice are deficient in the adaptive immune system, endogenous innate immunity still remains. However, these mice models are expensive and labour-intensive, require several high-level techniques including surgical skills, injections, and restraint techniques. Therefore, animal models that are easy, reliable, cost-effective, high-throughput, and allow modulation of genes and testing of potential treatments are needed.

1.1.8 Chorioallantoic membrane (CAM) of avian embryo metastasis model.

The chorioallantoic membrane (CAM) of avian embryos is not a new/recent model. It has been utilized as a cancer xenograft model for almost a hundred years[92]. In 1912, transplantation of mouse and rat tumours on the CAM of chicken embryo showed not only tumour growths but identified tumours that were passed from eggs to eggs[92]. Advantages of utilizing the CAM in cancer research are mostly due to the structure of the CAM. Avian embryos utilize the CAM as the respiratory organ to exchange oxygen and carbon dioxide. The CAM shows a highly vascularized structure and a fully developed lymphatic system that have similar functions and molecular compositions as the mammalian system[93]. Histological examination of the CAM shows the presence of two epithelial layers and a thin layer of stroma in between. Chicken embryos cultured *ex ovo* expose the CAM to the outside so that the structure provides easy access to the vasculature. Because of this open structure, researchers may use the CAM model to study the development of the vasculature. It only takes 6-7 days for the development of vasculature[94]. The accessibility and short period of development make the CAM model easier to handle compared to the mouse model. Although it was reported that the CAM has a slow development of non-specific immune system from day 15 onwards, the system is still naturally immunodeficient compared to the mouse model[95]. Another advantage of the CAM of chicken embryo is that it is cost-effective and overcomes the inadequacy of power in studies. In addition, CAM allows investigators to perform a high-throughput screen.

Xenografts of several cancer cell lines and tumour tissues successfully grow on the CAM[96,97,98,99,100]. Klingenberg *et al*. reported that xenografts of the Burkitt lymphoma cell lines BL2B95 on the CAM of day 10 chicken embryos exhibited growth[101]. Histological examination confirmed the establishment of the tumour. Transmission electron microscopy-based imaging also highlighted tumour structures and infiltrating granulocytes and macrophages. Immunofluorescence labeling in the CAM showed BL2B95 cells forming tumours and lymphatic metastases. Time-lapse imaging of the CAM also showed the spreading of BL2B95 cells to distant sites.

Dr. Ann F. Chambers' group[102] modified the CAM assay in 1980s to study metastasis. Instead of creating an *ex ovo* model, top of eggshell was removed by drilling and cancer cells were injected intravenously into the CAM of day 11 chicken embryos [103]. Since then, the metastatic efficiency of different cancer cells have been evaluated in the CAM assay by monitoring survival and homing of injected cancer cells[104]. Studies also have assessed vascular permeability of the CAM with various sizes of dextrans and intravital imaging. Pink *et al*. showed that the rates of 158-kDa TRITC-dextran leakage were higher in non-tumour tissue, tumour tissue, and necrotic core sites, compared to the rates of 2000-kDa FITC-dextran[105]. In addition, CAMs, which were exposed to VEGF, showed more leakage of doxorubicin[105]. This study shows that the vascular permeability of the CAM can be modulated, which is valuable in studies of cancer extravasation. There are still a number of unanswered questions, such as inherent blood vessel permeability of different ages of chicken embryos. There is a need to further characterize and optimize the experimental CAM metastasis model.

1.2 Cancer cell extracellular vesicle biogenesis and potential roles in cancer metastasis

1.2.1 The biogenesis and roles of extracellular vesicles

In 1967, Dr. Peter Wolf discovered platelet extracellular vesicles (EVs) as platelet dust encapsulated in lipid-rich transmembrane[106]. These structures were still able to perform a biological activity, anticoagulation in plasma and serum[106]. Since then, research on these

cell dust particles has centered around characterizing which cell types generate them and what their biological roles are. EV is a collective term which is used to describe heterogenous membrane vesicles, and includes exosomes, microparticles, and apoptotic bodies. It is now known that the content of EV cargoes is decided by the releasing cells. The physiological and pathological states that induce EV release are also being characterized.

Exosomes are derived from the maturation of multivesicular bodies (MVB) and secreted by exocytosis[107]. Exosomes are smaller (50-100 nm in diameter) compared to plasma membrane-derived vesicles termed microparticles/ectosomes (greater than 100nm and over 1μm)[108,109]. Exosomes participate in intercellular communication in both normal and pathological states. Maturation process of MVB plays a key role in exosome biogenesis, by generating intraluminal vesicles (ILVs). ILVs are generated by the inward budding and fission of limiting late endosomal membrane. Resulted ILVs are carried by the endosomal sorting complexes required for transport (ESCRT) machinery comprising of ESCRT-II and III. The ESCRT complex with the ESCRT-III subunit, vacuolar protein sorting-associated protein 32 (VPS32), makes contact between ILV and programmed cell death 6-interacting protein (ALIX). Later ILVs undergo fusion with the cell surface and secretion by exocytosis[108,109].

Stein and Luzio in 1991 found that neutrophils shed vesicles embraced by isotope labelled-cellular plasma membrane lipids through ectocytosis[110]. Larger EVs (microparticles, ectosomes) are released when cells are activated by intra- and/or extra-cellular stimuli and initiate cytoskeletal remodeling. Endocytosis and cargo recycling may also initiate large EV biogenesis with the help of ADP-ribosylation factor 6 (ARF6). Several cytoskeletal remodeling-associated small GTPases, such as ARF6, activate phospholipase D (PLD) and extracellular signal-regulated kinase (ERK), allowing for the formation and shedding of membrane blebs[75,111,112]. RhoA and RHO-associated protein kinase (ROCK) are other important regulators of actin organization and microparticle biogenesis. ROCK, downstream from RhoA, activates Lim kinase-cofilin which is involved in the formation

of plasma membrane derived microparticles[113]. In addition to the cytoskeletal remodeling by ARF6, cytosolic Ca^{2+} levels are involved in microparticle biogenesis. Changes in cytosolic Ca^{2+} levels activate aminophospholipid translocases (flippases and floppases), scramblases and calpain, which then regulate plasma membrane phospholipid asymmetry. The asymmetry of phospholipids allows the plasma membrane to undergo restructuring of actin cytoskeleton, leading to the plasma membrane blebbing and microparticle release[114]. Inhibiting scramblases suppresses phosphatidylserine exposure (PS) on blood platelets and reduces microparticle production[115]. Microparticle release also consists of several regulator proteins including ARF6 and ATPase VPS4. ARF6 phosphorylates myosin light chain (MLC) that induces actomyosin contraction followed by shedding microparticles from the plasma membrane. VPS4 induces scission of microparticles derived from the interaction between arrestin domain-containing protein-1 and tumour susceptibility gene 101 (TSG101) on the plasma membrane[116]. Lastly, microparticle release can be initiated in a ATP-dependant manner by P2X7 receptors maneuvering rearrangement of the plasma membrane[117,118].

One of the most significant findings in EV research is the discovery of EV-specific protein markers[119]. Similar to cell body, EVs are encapsulated by fatty acids constituting the plasma membrane: EV membrane is enriched in sphingomyelin, PS, cholesterol, and saturated fatty acids. However, outer EV membrane is more PS-rich compared to cell plasma membrane. This somewhat unique feature has implicated PS as a potential EV surface marker. EVs also inherit many of the surface and cytosolic proteins of the cells from where they originate. Advanced techniques such as ultracentrifugation of the EVs and subsequent proteomic analysis have allowed a map of EV embedding proteins to be devised (Exocarta and Vesiclepedia)[120–123]. Most representative EV surface proteins include tetraspanins (CD9, CD63, and CD81) and major histocompatibility complex II (MHC II), which are present on both exosomes and larger EVs[119].

1.2.2   Cancer cell EVs and their potential roles

In addition to the documented role of EVs in anticoagulation[106] and removal of unwanted cellular materials, new roles of EVs from different cell types are being recognizied[124]. EVs are released from different types of cancers as well and it is believed that these messengers are involved in inter- and intra-cellular communication in tumours. EVs may transfer oncogenes, regulate angiogenesis, modulate the immune system, and establish pre-metastatic niche. Similar to normal cell EVs, cancer-derived EVs are heterogenous in biogenesis, size-spectrum and potential roles (**Figure 2**). In addition, the molecular pathways involved in the release of cancer-derived large EVs are similar to those discovered in normal cells. Cancer cells actively release large EVs upon the activation of small GTP-binding proteins, ARF1 and 6. ARF1 and 6 phosphorylate MLC, inducing actomyosin contraction and membrane blebbing[112,125]. Intracellular calcium can also activate scramblase and calpain in cancer cells to induce cytoskeleton rearrangement, a loss of plasma membrane asymmetry, and membrane blebbing. Cancer cell EV release is also regulated by the ESCRT machinery.
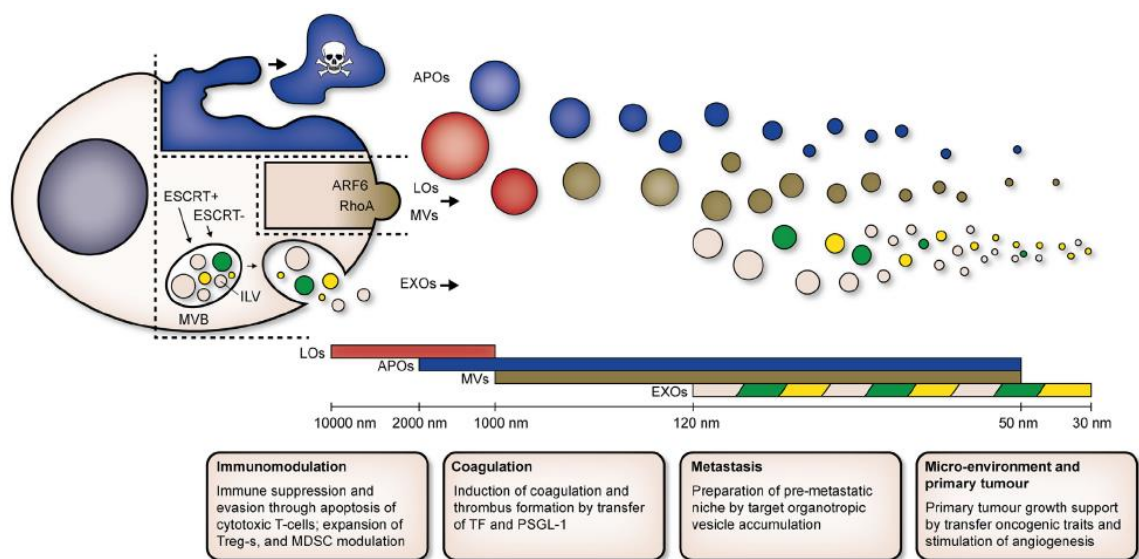
Figure 2: The heterogeneity of cancer cell EVs and their potential roles[126]. Cancer cells release exosomes, microparticles (microvesicles), and large oncosomes. Apoptotic cancer cells also release apoptotic EVs (APOs or Apo-EVs) as an EV subset. Different molecular pathways in cancer cell EV biogenesis cause the heterogeneity of cancer cell EVs.

Figure is reproduced here for educational purpose only and not for any commercial use. Figure is included in the Ph.D. dissertation with attribution[126].

Cancer cell-derived EVs can travel to distant sites and interact with different cell types. A recent study has shown that cancer-derived EVs transfer EGFR to induce tumourigenesis in nearby recipient cells[127]. Al-Nedawi *et al*. also reported that EGFRvIII overexpressing U373 human astrocytoma cells transfer EGFRvIII to recipient U373 cells through microvesicles. These recipient U373 cells started to express EGFRvIII, increased the expression of VEGF, and increased colony formation in soft agar[127]. Antonyak *et al*. showed that microvesicles from MDA-MB 231 breast cancer cells and U87 glioblastoma cells transform normal NIH-3T3 cells. MDA-MB-231 and U87 cell-derived microvesicles contained tissue transglutaminase (tTG) linking to fibronectin allowed 3T3 cells to acquire anchorage-independent growth *in vitro* and *in vivo*[128]. Studies also illustrate how cancer cell-derived EVs can compromise the host immune system. Taylor *et al*. showed that ovarian cancer patient serum-derived EVs are enriched in FasL. The exposure of Jurkat T cells to ovarian cancer-EVs induced apoptosis, which was mediated by FasL[129]. Cancer-

derived EVs have also been shown to cause CD8$^+$ T cell apoptosis and proliferation of CD4$^+$CD25$^+$FOXP3$^+$ T$_{reg}$ cells[130,131].

In addition to microvesicles and exosomes, cancer cells generate large 'oncosomes'. Large oncosomes appear to be unique to cancer cells and are typically 1-10 μm in diameter. Studies have shown that oncosomes are detected from amoeboid cell-enriched tumour tissues and plasma samples of metastatic prostate cancer patients, but not from benign tissues or plasma samples. Oncosomes are generated from non-apoptotic plasma membrane blebbing and fission, processes similar to microparticles. Acquisition of an amoeboid phenotype is facilitated by the overexpression of certain oncoproteins such as myristoylated Akt1, heparin-binding epidermal growth factor, and caveolin-1. Cancer cells may also lose cytoskeletal regulator Diaphanous-related formin-3 (DIAPH3) or activate Akt1 and EGFR pathways to induce oncosome formation[126,132]. In comparison to normal cell-derived large EVs, oncosomes show the presence of caveolin-1 and are enriched in cytokeratin-18. Levels of tetraspanins (CD9, CD63, CD81), however, is low [133]. Despite these differences, oncosomes share select exosome- and large EV-specific proteins such as ALIX and ARF6[126,134].

As the name suggests, oncosomes carry materials that may be categorized as oncogenic. Minciacchi *et al.* showed that oncosomes derived from prostate cancer cell lines or plasma of metastatic prostate cancer patients contain active AKT1 (phosphorylated form) that activates MYC in fibroblasts. The activation of MYC in fibroblasts increased the size of DU145 xenografts and induced angiogenesis[135]. Another mechanism by which oncosomes facilitate cancer progression is remodeling of extracellular matrices in metastatic niche[136].

1.2.3 Intravascular cancer cell death and its involvement in cancer cell EV biogenesis

As mentioned earlier, intravasated cancer cells experience stressors while in the circulation. Cancer cells are highly susceptible to different types of cell death including apoptosis, anoikis, and necroptosis in the circulation[137]. These cell death pathways are also involved in cancer cell EV release and will be discussed here.

1.2.3.1 Apoptosis

Apoptosis is a programmed cell death that removes old, damaged or unneeded cells. Apoptosis triggered by multiple factors that include endogenous stimuli (ageing and cellular damage) and exogenous stimuli (infection, inflammation, engagement of pro-apoptotic receptors)[138]. The hallmarks of apoptosis are plasma membrane blebbing, caspase activation, nucleus condensation, and generation of apoptotic bodies which are engulfed by macrophages, neutrophils, and dendritic cells[139]. Cystine-dependent aspartate-driven proteases (Caspases) are the main effector proteins in apoptosis[138]. Pro-apoptotic signals cause cytochrome C release from mitochondria, forming complexes with apoptosis activating factor-1 (Apaf-1)[140]. Caspase-9 joins the complexes to form apoptosome that activates caspase-3, an executioner caspase. Activated caspase-3 cleaves the C-terminus of Rho-associated coiled-coil containing protein kinase 1 (ROCK1) and induces constitutively active myosin light chain kinase (MLCK) that phosphorylates the light chain of myosin II. MLCK activates myosin II and following cortical actin contraction by sliding myosin II, which increases intracellular hydrostatic pressure producing membrane blebs. Maturing blebs clear the original actin lining and are released. Growing blebs contain nuclear DNA fragments generated by caspase-activated DNAse (CAD) which is also activated by caspase-3. Membrane blebs also pack other cellular organelles such as the Golgi apparatus, endoplasmic reticulum, and mitochondria. During this packaging process, apoptotic bodies or apoptotic EVs (Apo-EV) are released into the bloodstream[141]. Lastly, lipid scramblases and phospholipases expose PS ("find-me" and "eat-me" signal), attracting phagocytes. If apoptotic cells are not phagocytosed, uncleared apoptotic cells or

apoptotic bodies/Apo-EVs can become unstable and undergo membrane rupture, causing the release of intracellular materials through a process called secondary necrosis[141]. Secondary necrosis can cause chronic inflammation and autoimmune disease.

Emerging studies show that Apo-EVs of cancer cells exhibit oncogenic effects rather than simply dead cell debris which is engulfed by phagocytes. Apo-EVs can carry nuclear proteins (histones) and organelles (mitochondria, endoplasmic reticulum, and ribosomes), whereas other EV subsets typically carry proteins and genetic material. Hayakawa *et al*. showed the presence of bioactive mitochondria in astrocyte-derived Apo-EVs[142]. They also showed that transferring these EVs improved survival and differentiation of neurons in infarcted regions[142]. Similarly, Pavlyukov *et al*. showed that apoptotic mouse glioblastoma cells upregulated spliceosome protein RBM11 and EVs released from these apoptotic cells transferred RBM11 to recipient glioblastoma cells[143]. The recipient cells exhibited increased cyclin D1 and mouse double minute 4 (MDM4), proteins regulating cell cycling. In addition, spliced isoforms of cyclin D1 (D1a) and MDM4 (4s), which are pro-oncogenic, were found[143]. These studies show that cancer cell Apo-EVs may be involved in cancer progression, and perhaps recurrence following initial treatment.

1.2.3.2   Anoikis

Detachment of cells from extracellular matrix or lack of required substratum may induce a form of programmed cell death called anoikis (loss of "home" or "homelessness")[144]. Anoikis is also a defence mechanism which prevents reattachment of detached cells at abnormal sites and dysplastic growth. Failure in anoikis can cause ectopic cell proliferation and even lead to tumour formation. However, cancer cells can develop resistance to anoikis by switching their integrins, undergoing EMT, constitutively activating pro-survival signaling, and manipulating their metabolic processes.

Interaction of cells with extracellular matrix is primarily mediated through integrin receptors [26,27,147,148,149]. Cancer cells exhibit differential integrin expression patterns compared to normal counterparts, which allow the cells to grow and avoid cell death

mechanisms. Human melanoma cells, for example, express $\alpha_v\beta_3$ integrins which are not expressed in benign nevi or normal melanocytes[48,150]. Invasive and androgen-resistant prostate cancer cell lines also show $\alpha_v\beta_3$ expression, whereas androgen-sensitive and non-invasive LNCaP cell lines do not[151]. Integrin $\alpha_v\beta_5$ has also been shown to counter anokis, although its level is quite low compared to other integrins[152]. Expression of pro-survival integrins such as $\alpha_v\beta_6$ integrin can induce resistance to anoikis and maintenance of an invasive phenotype as well[153]. Overexpression of the β_6 subunit induced cancer cell migration and secretion of metalloproteinase-3 (MMP-3), and prolonged EMT in cancer cells[153].

Cancer cells undergoing EMT acquire an invasive phenotype and an anti-apoptotic and pro-survival gene patterns[154]. Snail, ZEB1/2, Twist, nuclear factor-κB, and HIF1/2 are common transcription factors associated with EMT[155]. Twist also increases Bcl-2[144]. Snail-1 has been shown to inhibit Bid, caspase-6, and PTEN to evade anoikis[144]. Inhibition of PTEN leads to the activation of PI3K/Akt pathway and the discharge of Bad[156]. HIF-1 can activate Twist and Snail to maintain EMT and anoikis resistance in cells[156]. HIF-1 can also increase EGF expression and activate the MAPK pathway, inducing degradation of pro-apoptotic proteins such as Bim and Bmf[156].

1.2.3.3   Necroptosis

Over last two decades, "extrinsic" apoptotic cell death has been shown to switch to programmed necrotic cell death. In contrast to homeostatic and anti-inflammatory apoptosis, necroptosis causes inflammation. The best-characterized extrinsic necroptosis pathway is mediated via the tumour necrosis factor receptor-1 (TNFR1) complex[157]. Tumour necrosis factor-α (TNF-α) extrinsically induces apoptosis by activating TNFR1 and the formation of TNFR1 signaling complex (TNF-RSC, complex 1). The complex 1 recruits receptor-interacting serine/threonine-protein kinase 1 (RIPK1), TNFR1-associated Death Domain protein (TRADD), Fas-Associated Death Domain (FADD), TNFR-associated Factor 2/5 (TRAF2/TRAF5), and cellular Inhibitor of Apoptosis Protein (cIAP1/2). If caspase-3 is inactivated or RIPK1 undergoes deubiquitination (for example,

by cylindromatosis (CYLD)), TNFR1-driven signaling switches to necroptosis. In addition, deficiency in cIAP1/2 in the presence of activated RIPK1, leads to recruitment of RIPK3 to form an alternative protein complex called the complex IIb or necrosome. Activated RIPK3 then recruits mixed lineage kinase domain-like protein (MLKL) to the complex IIb and phosphorylates it. Activated MLKL proteins form an oligomer and translocate from the cytosol to the plasma membrane. Plasma membrane-localized MLKL oligomers create pores and cause a rapid influx of Ca^{2+} into the cell, which subsequently leads to membrane lipid scrambling and PS exposure[158]. Such plasma membrane disruption compromises membrane integrity and induces the release of cellular contents.

Although RIPK1-dependant necroptosis is considered the canonical pathway, toll-like receptor (TLR) 3 and 4 also participate in necroptosis in response of innate immune system to pathogens such as bacteria, virus, as well as several endogenous threats[159]. Signaling through TLR3 and 4 enhances TNF-α production and may also induce the formation of lysosomal cathepsin D (CTSD) and mitochondrial antiviral signaling protein (MAVS) complex that recruits RIPK1 and activates necroptosis[159].

Although necroptosis is primarily viewed as a player in inflammatory diseases, emerging studies show the involvement of necroptosis in neoplasia. Yatim *et al*. have shown that RIPK3-RIPK1-dependant necroptosis in NIH-3T3 induces NF-κB expression and enhances dendritic cell maturation and antigen presentation to cytotoxic $CD8^+$ T cells[160]. This study suggests that necroptosis may be utilized against cancer cells to increase T cell priming. Yang *et al*. have demonstrated that RIPK3 induces type 1 interferon (IFN) response in necroptotic mouse colorectal and lung cancer cells[161]. These necroptotic cells released ATP and high mobility group box-1 (HMGB1) that recruited $CD11c^+CD86^+$ dendritic cells and $CD3^+CD8^+$ cytotoxic T cells[161].

Similar to apoptosis, necroptosis has been linked to EV release (**Figure 3**). Gong *et al*. have shown that ESCRT-III complex participates in MLKL-induced plasma membrane disruption[162]. In their study, ESCRT-III complex translocated to the sites of MLKL-induced plasma membrane holes and repaired membranes by shedding EVs. Yoon *et al.* also showed that MLKL-induced necroptosis in human liver and colorectal cancer cells

releases EVs[163]. Specifically, the researchers showed that MLKL-depleted HepG2 hepatoma cells had a reduction in ILVs within MVBs, whereas the size of MVBs increased. Decreased number of ILVs resulted in a decrease in MLKL-induced EV release. MLKL-depleted HT-29 colon cancer cells also exhibited a decrease in EVs[163]. Immunoprecipitation of EVs from necroptotic HT-29 cells showed that MLKL proteins interacted with ESCRT and flotillin 1 and 2 proteins. These results imply that MLKL proteins interact with ESCRT to induce EV release during necroptosis. Lastly, a study identified phosphorylated MLKL in EVs from necroptotic mouse bone marrow-derived dendritic cells, possibly suggesting that extrusion of EVs with phosphorylated MLKL is an adaptive mechanism to suppress cell death[163]. Together, these studies illustrate the involvement of necroptosis in EV release that may participate in cancer progression.
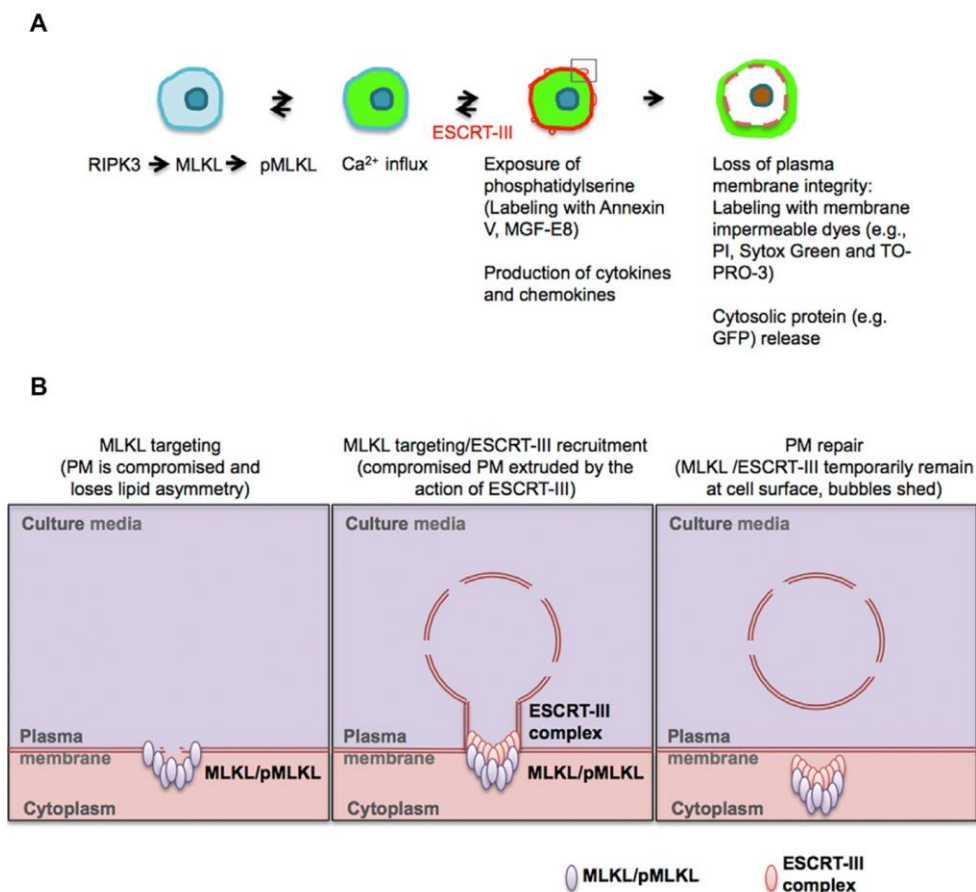
Figure 3: Participation of ESCRT-III complex in MLKL-induced necroptosis causes cellular EV release[162]. (A) RIPK3-MLKL signal transduction during cell necroptosis can induce the exposure of PS to the outer plasma membrane. ESCRT-III complex can intervene in the plasma membrane repair process. During this process, necroptotic cell can shed parts of damaged plasma membrane as EVs to resuscitate or cells undergo membrane rupture if they have overwhelming plasma membrane damages. (B) ESCRT-III complex is recruited to the site of MLKL-induced plasma membrane damage and induces EV biogenesis and release to repair the damage.

Figure is reproduced here for educational purpose only and not for any commercial use. Figure is included in the Ph.D. dissertation with attribution[162].

1.2.4 Current methods of cancer cell EV isolation and detection

EV studies require precise methods of identification, quantification and purification. The nature of biofluids from which EVs are harvested also poses challenges. Investigating protein compositions of EVs is also confronted with contaminants such as soluble proteins and platelets. Fortunately, there are a few established techniques of EV detection, purification and quantification to adopt for different biofluids.

1.2.4.1 Microscopy-based EV imaging

Imaging of cancer cell-derived EVs can be performed both *in vitro* and *in vivo*. *In vitro* EV imaging can identify the presence of surface antigens as biomarkers. *In vivo* imaging can contribute to the understanding of molecular and biological mechanisms of EV biogenesis and release. Transmission electron microscopy (TEM) and scanning electron microscopy (SEM) can reconstruct a clean image and topography of EVs in a broad size spectrum by using electron beams[164]. Atomic force microscopy (AFM) also creates a topographic image of EV by using a probe made by silicon or silicon nitride. AFM can image most EVs with a resolution limit close to 1 nm[164].

Fluorescent fusion proteins allow real-time visualization of EV release from cancer cells. Wallace *et al*. tagged a palmitoylation signal with enhanced GFP (EGFP) and tdTomato red fluorescent proteins to label the inner plasma membrane of glioblastoma cells and 293T cells[165]. Confocal microscopy-based live cell imaging revealed that GBM and 293T cells exchanged EVs. Mittelbrunn *et al*. introduced GFP-tagged CD63 in Raji B and J77 T cells and collected EVs. These EVs were then introduced to unmodified Raji B and J77 T cells. They observed uptakes of GFP-tagged CD63 in the recipient cells[166]. In addition to labeling proteins, fluorescent dyes such as DiD (DiIC18(5); 1,1`-dioctadecyl-3,3,3`,3`-tetramethylindodicarbocyanine, 4-chlorobenzenesulfonate) and PKH dyes (PKH67 and PKH26) may also be utilized to track EVs. Grange *et al*. labeled mesenchymal stem cells (MSCs) and MSC-derived EVs with DiD[167]. PKH67 and PKH26 dyes are also lipophilic and bind to the lipid bilayer of the plasma membrane of cells[168,169]. Carboxyfluorescein

diacetate succinimidyl ester (CFDA), commonly used to measure proliferation, can also label both cancer cells and EVs derived from the labeled cells[170].

1.2.4.2   Nanoscale flow cytometry

Nanoscale flow cytometry (nFC) in studying cancer cell EV quantification has emerged as a preferred technique. It allows the analysis of individual EVs and the detection of multiple surface antigens by using fluorophore-tagged antibodies. nFC utilizes enhanced optics comprising of large angle light scatter (LALS) and small angle light scatter (SALS), and highly sensitive photomultiplier tube (PMT) (**Figure 4**)[171] to determine EV size (between 100 nm and 1000 nm)[171–174]. The combination of multi-channeled laser and two-way light scattering strategy can allow researchers to analyze the presence of several surface antigens in different EV subsets. Gomes *et al*. have standardized nFC detection and quantification of EVs in the laboratory and clinic[172]. They showed that nFC provides an accurate detection of platelet-derived microparticles in various human plasma samples. They also showed that nFC provided a consistent CD41-positive microparticle quantification between light scattering-only detection and fluorescence-only detection (**Figure 4**)[172].

The biggest advantage of nFC is that it can quantify specific EVs in a high-throughput manner. Biggs *et al*. showed that nFC detected different amounts of prostate-specific microparticles among healthy volunteer plasma samples and samples from prostate cancer patients with different metastatic stages. They detected microparticles with light scattering detection and prostate-specific membrane antigen (PSMA)-tagged antibody. They confirmed their results by detecting and quantifying microparticles in the culture media of PSMA-positive human prostate cancer cell lines PC-3 and LnCAP[171]. Despite restricted size detection (100-1000 nm), nFC technique is highly recommended to detect and quantify cancer-specific EVs from both cell culture and patient plasma samples.
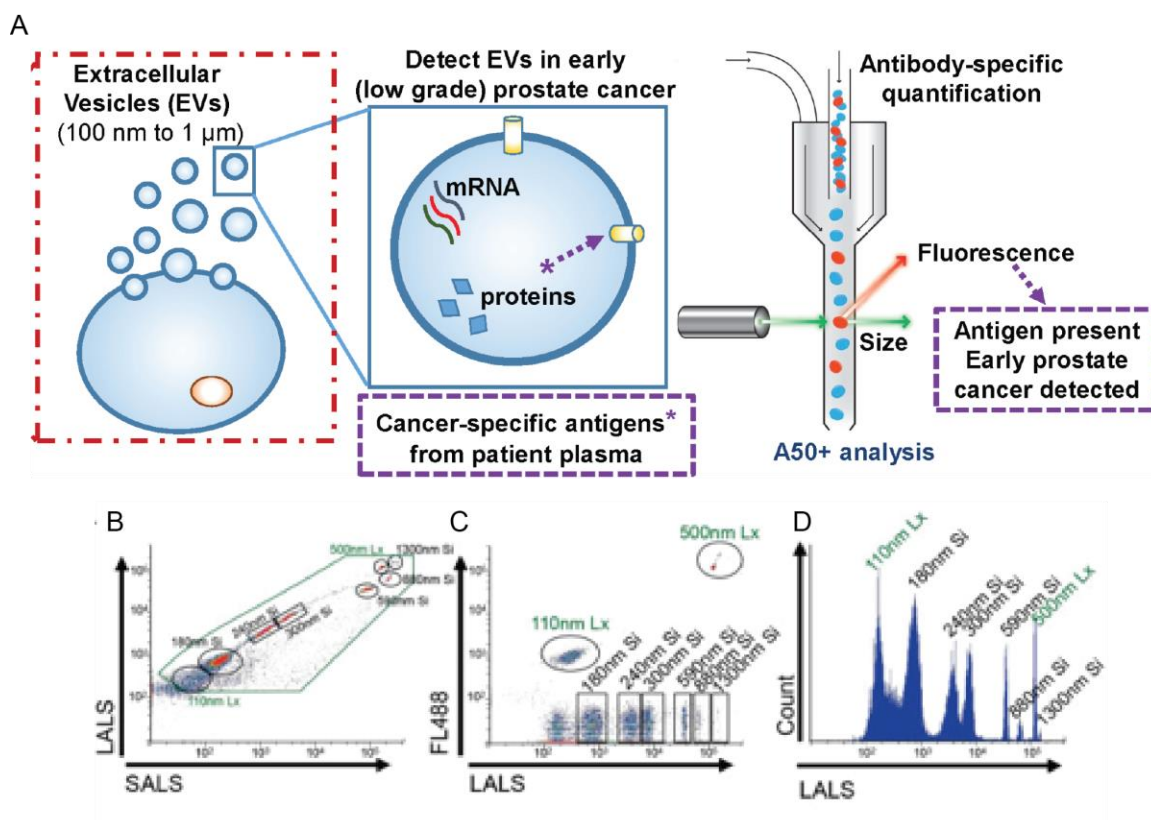
Figure 4: Nanoscale flow cytometry detects cancer EVs by using calibration sized beads[172,173]. (A) nFC uses light scattering and fluorescence to detect EVs with cancer specific antigens between 100 nm and 1000 nm. (B) Light scatter (large angle light scatter and small angle light scatter) based nFC calibration with non-fluorescent silica beads of different sizes. (C) Fluorescent latex and non-fluorescent silica beads based nFC calibration. (D) Histogram displays individual counts of each size-calibration bead.

Figures (top and lower panel) are reproduced here for educational purpose only and not for any commercial use.

Figures are included in the Ph.D. dissertation with attribution[172,173].

1.2.4.3 Ultracentrifugation

Centrifugation-based EV isolation techniques for a small EV collection from conditioned medium have been well-established. Kowal *et al*. showed that high centrifugal forces (≥ 100,000 xg) could afford a preparation of small EV pellets[119]. Studies utilizing this technique remove cell debris and EVs larger than 220 nm to isolate small EVs. Cell culture conditioned media and various biofluids (for example, blood, urine, cerebrospinal fluid)

can be spun with low centrifugal force (300 xg) to remove cell debris and apoptotic bodies, followed by higher centrifugal force (2,000 xg) to remove additional cell debris and dead cells. Once dead cells and debris are removed, high speed spins from 10,000 xg up to 50,000 xg can precipitate large EVs (microparticles and oncosomes)[125,175]. A final spin with high speed over 100,000 xg can precipitate both large and small EVs. Collected EVs can be stored in phosphate buffered saline (PBS) at -80°C and used for EV protein characterization and biomarker discovery with the aid of mass spectrometry, western blot, and immunoprecipitation[176].

1.2.4.4   Ultrafiltration

Ultracentrifugation is highly versatile in separating different EV subsets and the quality of EV subset separation is also reliable. However, ultracentrifugation requires specialized equipment capable of spinning samples at 200,000 xg. In addition, ultracentrifugation-specific tubes are needed, which are expensive. Instead of expensive equipment, polyethersulfone nanomembrane filter with 100 kDa molecular mass cut-off can be used to collect EVs by concentrating samples[177]. In addition, any bench-top centrifuge can spin ultrafiltration tubes to collect EVs. Ultrafiltration is also faster and simpler to isolate EVs, and easily paired with nFC to quantify EVs. Miranda *et al*. showed that ultrafiltration can provide similar urinary EV concentration with the one collected from ultracentrifugation[178]. Therefore, ultrafiltration is an economical and time-saving EV isolation technique for high-throughput EV quantification.

1.3   Motivation and hypothesis

1.3.1   Motivation

Although there is an urgent need to combat cancer metastasis, targeting the multiple steps in the metastatic cascade has been limited. My work centers around the notion that cancer cell extravasation must be inhibited to effectively prevent metastasis. Cell extravasation involves changes of cancer cell phenotype to an invasive one, which is critical to

metastasis. Extravasation is also the last key step before cancer cells home to a secondary site. If we are able to alter the efficiency of cancer cell extravasation to secondary sites, we may be able to contain cancer spread. However, to understand the cellular and molecular changes that play a role in extravasation, an *in vivo* system that allows these mechanisms of extravasation to be examined in real-time is needed. Towards this goal, I focused on the economical CAM of chicken embryo to view and quantify cancer cell extravasation (Chapter 3). Observations made in this CAM assay using prostate cancer cells led to the discovery of cell volume changes as perhaps necessary events in extravasation. These cell volume changes were associated with the release of extracellular vesicles (EV). Extravasation and EV release were also associated with induction of cell death pathways (Chapter 4). Together, my studies developed an *in vivo* model of extravasation and highlighted an important role of cell death pathways in extravasation.

1.3.2   Hypothesis

Modelling cancer cell extravasation using the chorioallantoic membrane platform will allow real-time monitoring of the cellular events required in the process and discovery of novel underling mechanisms.

1.3.3   Research Objectives of the Study

There are three main objectives:

1. To optimize *in vivo* quantification of cancer cell extravasation using the CAM of chicken embryos and the reproducibility of the model (Chapter 2).

2. To elucidate the relationships between cancer cell volume changes and metastatic efficiency, and extracellular vesicle release and cell volume change (Chapter 3).

3. To determine whether cell death pathways are involved in cell volume change and extracellular vesicle release (Chapter 3)

1.4   Bibliography

1.   Lambert, A. W., Pattabiraman, D. R. & Weinberg, R. A. Emerging Biological Principles of Metastasis. *Cell* **168,** 670–691 (2017).

2.   Hanahan, D. & Weinberg, R. A. Hallmarks of Cancer: The Next Generation. *Cell* **144,** 646–674 (2011).

3.   Bayat Mokhtari, R. *et al.* Combination therapy in combating cancer. *Oncotarget* **8,** 38022–38043 (2017).

4.   Seyfried, T. N. & Huysentruyt, L. C. On the origin of cancer metastasis. *Crit. Rev. Oncog.* **18,** 43–73 (2013).

5.   Arvelo, F., Sojo, F. & Cotte, C. Cancer and the metastatic substrate. *Ecancermedicalscience* **10,** 701 (2016).

6.   Chambers, A. F., Groom, A. C. & MacDonald, I. C. Dissemination and growth of cancer cells in metastatic sites. *Nat. Rev. Cancer* **2,** 563–72 (2002).

7.   Shurin, M. R. *et al.* Intratumoral cytokines/chemokines/growth factors and tumor infiltrating dendritic cells: friends or enemies? *Cancer Metastasis Rev.* **25,** 333–356 (2006).

8.   Yan, J., Yang, Q. & Huang, Q. Metastasis suppressor genes. *Histol. Histopathol.* **28,** 285–92 (2013).

9.   Steeg, P. S. Metastasis suppressors alter the signal transduction of cancer cells. *Nature Reviews Cancer* **3,** 55–63 (2003).

10.   Müller, A. *et al.* Involvement of chemokine receptors in breast cancer metastasis. *Nature* **410,** 50–56 (2001).

11.   Seraj, M. J., Samant, R. S., Verderame, M. F. & Welch, D. R. Functional evidence for a novel human breast carcinoma metastasis suppressor, BRMS1, encoded at

chromosome 11q13. *Cancer Res.* **60,** 2764–9 (2000).

12. Steeg, P. S. *et al.* Evidence for a novel gene associated with low tumor metastatic potential. *J. Natl. Cancer Inst.* **80,** 200–4 (1988).

13. Akhtar, M., Haider, A., Rashid, S. & Al-Nabet, A. D. M. H. Paget's "Seed and Soil" Theory of Cancer Metastasis. *Adv. Anat. Pathol.* 1 (2018). doi:10.1097/PAP.0000000000000219

14. van der Pluijm, G. *et al.* Interference with the Microenvironmental Support Impairs the *De novo* Formation of Bone Metastases *In vivo*. *Cancer Res.* **65,** 7682–7690 (2005).

15. Budczies, J. *et al. The landscape of metastatic progression patterns across major human cancers*. **6,**

16. Gidwani, B. & Vyas, A. A Comprehensive Review on Cyclodextrin-Based Carriers for Delivery of Chemotherapeutic Cytotoxic Anticancer Drugs. *Biomed Res. Int.* **2015,** 1–15 (2015).

17. Moorthi, C., Manavalan, R. & Kathiresan, K. *Nanotherapeutics to Overcome Conventional Cancer Chemotherapy Limitations*. *J Pharm Pharmaceut Sci (www.cspsCanada.org)* **14,** (2011).

18. Gambara, G., Gaebler, M., Keilholz, U., Regenbrecht, C. R. A. & Silvestri, A. From Chemotherapy to Combined Targeted Therapeutics: In Vitro and in Vivo Models to Decipher Intra-tumor Heterogeneity. *Front. Pharmacol.* **9,** 77 (2018).

19. Wilting, R. H. & Dannenberg, J.-H. Epigenetic mechanisms in tumorigenesis, tumor cell heterogeneity and drug resistance. *Drug Resist. Updat.* **15,** 21–38 (2012).

20. Ganci, F. *et al.* in *Contemporary Issues in Head and Neck Cancer Management* (InTech, 2015). doi:10.5772/60081

21. Muralidharan-Chari, V. *et al.* Microvesicle removal of anticancer drugs contributes to drug resistance in human pancreatic cancer cells. *Oncotarget* **7,** 50365–50379 (2016).

22. Mehlen, P. & Puisieux, A. Metastasis: a question of life or death. *Nat. Rev. Cancer* **6,** 449–58 (2006).

23. Leong, H. S. *et al.* Invadopodia Are Required for Cancer Cell Extravasation and Are a Therapeutic Target for Metastasis. *Cell Rep.* **8,** 1558–1570 (2014).

24. Watnick, R. S. The Role of the Tumor Microenvironment in Regulating Angiogenesis. *Cold Spring Harb. Perspect. Med.* **2,** a006676 (2012).

25. Ziello, J. E., Jovin, I. S. & Huang, Y. Hypoxia-Inducible Factor (HIF)-1 regulatory pathway and its potential for therapeutic intervention in malignancy and ischemia. *Yale J. Biol. Med.* **80,** 51–60 (2007).

26. Zimna, A. & Kurpisz, M. Hypoxia-Inducible Factor-1 in Physiological and Pathophysiological Angiogenesis: Applications and Therapies. *Biomed Res. Int.* **2015,** 549412 (2015).

27. Carmeliet, P. & Jain, R. K. *Principles and mechanisms of vessel normalization for cancer and other angiogenic diseases*. *Nat Rev Drug Discov.* **10,** 417-427 (2011).

28. Carmeliet, P. & Jain, R. K. Principles and mechanisms of vessel normalization for cancer and other angiogenic diseases. *Nat. Rev. Drug Discov.* **10,** 417–427 (2011).

29. Rankin, E. B., Erler, J. & Giaccia, A. J. in *Abeloff's Clinical Oncology: Fifth Edition* 40–51.e5 (Elsevier Inc., 2013). doi:10.1016/B978-1-4557-2865-7.00003-5

30. Chaffer, C. L. & Weinberg, R. A. *A Perspective on Cancer Cell Metastasis Author(s)*. *New Series* **331,** (2011).

31. Lamouille, S., Xu, J. & Derynck, R. Molecular mechanisms of epithelial-mesenchymal transition. *Nat. Rev. Mol. Cell Biol.* **15,** 178–96 (2014).

32. Chiang, S. P. H., Cabrera, R. M. & Segall, J. E. Tumor cell intravasation. *Am. J. Physiol. Cell Physiol.* **311,** C1–C14 (2016).

33. Patsialou, A. *et al.* Autocrine CSF1R signaling mediates switching between invasion and proliferation downstream of TGFβ in claudin-low breast tumor cells. *Oncogene* **34,** 2721–31 (2015).

34. Bill, R. & Christofori, G. The relevance of EMT in breast cancer metastasis: Correlation or causality? *FEBS Lett.* **589,** 1577–1587 (2015).

35. Xue, C. *et al.* ErbB3-Dependent Motility and Intravasation in Breast Cancer Metastasis. *Cancer Res.* **66,** 1418–1426 (2006).

36. Peláez, R., Pariente, A., Pérez-Sala, Á. & Larrayoz, I. M. Integrins: Moonlighting Proteins in Invadosome Formation. *Cancers (Basel).* **11,** (2019).

37. Wu, Y., Sarkissyan, M. & Vadgama, J. V. Epithelial-Mesenchymal Transition and Breast Cancer. *J. Clin. Med.* **5,** (2016).

38. Hou, J.-M. *et al.* Circulating tumor cells as a window on metastasis biology in lung cancer. *Am. J. Pathol.* **178,** 989–96 (2011).

39. Chen, L., Bode, A. M. & Dong, Z. Circulating Tumor Cells: Moving Biological Insights into Detection. *Theranostics* **7,** 2606 (2017).

40. Micalizzi, D. S., Maheswaran, S. & Haber, D. A. A conduit to metastasis: circulating tumor cell biology. *Genes Dev.* **31,** 1827–1840 (2017).

41. Krebs, M. G., Hou, J.-M., Ward, T. H., Blackhall, F. H. & Dive, C. Circulating tumour cells: their utility in cancer management and predicting outcomes. *Ther. Adv. Med. Oncol.* **2,** 351–65 (2010).

42. Francart, M.-E. *et al.* Epithelial-mesenchymal plasticity and circulating tumor cells: Travel companions to metastases. *Dev. Dyn.* **247,** 432–450 (2018).

43. Xu, X. R., Yousef, G. M. & Ni, H. *Cancer and platelet crosstalk: opportunities*

and challenges for aspirin and other antiplatelet agents. (2018).

44. Azevedo, A. S., Follain, G., Patthabhiraman, S., Harlepp, S. & Goetz, J. G. Metastasis of circulating tumor cells: favorable soil or suitable biomechanics, or both? *Cell Adh. Migr.* **9,** 345–56 (2015).

45. Au, S. H. *et al.* Clusters of circulating tumor cells traverse capillary-sized vessels. *Proc. Natl. Acad. Sci. U. S. A.* **113,** 4947–52 (2016).

46. Uppal, A., Wightman, S. C., Ganai, S., Weichselbaum, R. R. & An, G. Investigation of the essential role of platelet-tumor cell interactions in metastasis progression using an agent-based model. *Theor. Biol. Med. Model.* **11,** 17 (2014).

47. Gawaz, M. *et al.* Vitronectin Receptor (α $_v$ β $_3$) Mediates Platelet Adhesion to the Luminal Aspect of Endothelial Cells. *Circulation* **96,** 1809–1818 (1997).

48. Felding-Habermann, B. *et al. Integrin activation controls metastasis in human breast cancer*.

49. Rolli, M. *et al. Activated integrin v3 cooperates with metalloproteinase MMP-9 in regulating migration of metastatic breast cancer cells*. *PNAS August* **5,** (2003).

50. Blandin, A.-F. *et al.* β1 Integrins as Therapeutic Targets to Disrupt Hallmarks of Cancer. *Front. Pharmacol.* **6,** (2015).

51. Schumacher, D., Strilic, B., Sivaraj, K. K., Wettschureck, N. & Offermanns, S. Platelet-Derived Nucleotides Promote Tumor-Cell Transendothelial Migration and Metastasis via P2Y2 Receptor. *Cancer Cell* **24,** 130–137 (2013).

52. Yao, D., Dai, C. & Peng, S. Mechanism of the Mesenchymal-Epithelial Transition and Its Relationship with Metastatic Tumor Formation. (2011). doi:10.1158/1541-7786.MCR-10-0568

53. Hugo, H. *et al.* Epithelial--mesenchymal and mesenchymal--epithelial transitions in carcinoma progression. *J. Cell. Physiol.* **213,** 374–83 (2007).

54. Chaffer, C. L., Thompson, E. W. & Williams, E. D. Mesenchymal to epithelial transition in development and disease. in *Cells Tissues Organs* **185,** 7–19 (2007).

55. Banyard, J. & Bielenberg, D. R. The role of EMT and MET in cancer dissemination. *Connect. Tissue Res.* **56,** 403–13 (2015).

56. Yeung, K. T. & Yang, J. Epithelial-mesenchymal transition in tumor metastasis. *Mol. Oncol.* **11,** 28–39 (2017).

57. Lam, F. W., Vijayan, K. V. & Rumbaut, R. E. Platelets and Their Interactions with Other Immune Cells. *Compr. Physiol.* **5,** 1265–80 (2015).

58. Strilic, B. & Offermanns, S. Cancer Cell Review Intravascular Survival and Extravasation of Tumor Cells. (2017). doi:10.1016/j.ccell.2017.07.001

59. Najmeh, S. *et al.* Neutrophil extracellular traps sequester circulating tumor cells via β1-integrin mediated interactions. *Int. J. Cancer* **140,** 2321–2330 (2017).

60. Qian, B. *et al.* A Distinct Macrophage Population Mediates Metastatic Breast Cancer Cell Extravasation, Establishment and Growth. doi:10.1371/journal.pone.0006562

61. Qian, B.-Z. *et al.* CCL2 recruits inflammatory monocytes to facilitate breast-tumour metastasis. *Nature* **475,** (2011).

62. Prager, G. W. *et al.* Targeting of VEGF-dependent transendothelial migration of cancer cells by bevacizumab. (2010). doi:10.1016/j.molonc.2010.01.002

63. Tan, M. J., Teo, Z., Sng, M. K., Zhu, P. & Tan, N. S. Emerging Roles of Angiopoietin-like 4 in Human Cancer. *Mol. Cancer Res.* **10,** 677–688 (2012).

64. Huang, R.-L. *et al.* ANGPTL4 modulates vascular junction integrity by integrin signaling and disruption of intercellular VE-cadherin and claudin-5 clusters. *Blood* **118,** 3990–4002 (2011).

65. Khuon, S. *et al.* Myosin light chain kinase mediates transcellular intravasation of

breast cancer cells through the underlying endothelial cells: a three-dimensional FRET study. *J. Cell Sci.* **123,** 431 LP-440 (2010).

66. Leong, H. S. *et al.* Invadopodia Are Required for Cancer Cell Extravasation and Are a Therapeutic Target for Metastasis. *Cell Rep.* **8,** 1558–1570 (2014).

67. Tremblay, P.-L., Huot, J. & Auger, F. A. Mechanisms by which E-Selectin Regulates Diapedesis of Colon Cancer Cells under Flow Conditions. *Cancer Res.* **68,** 5167 LP-5176 (2008).

68. Beaty, B. T. *et al.* β1 integrin regulates Arg to promote invadopodial maturation and matrix degradation. *Mol. Biol. Cell* **24,** 1661–75, S1-11 (2013).

69. Feitelson, M. A. *et al.* Sustained proliferation in cancer: Mechanisms and novel therapeutic targets. *Semin. Cancer Biol.* **35,** S25–S54 (2015).

70. Sasaki, T. *et al.* Modification of the Primary Tumor Microenvironment by Transforming Growth Factor α-Epidermal Growth Factor Receptor Signaling Promotes Metastasis in an Orthotopic Colon Cancer Model. *Am. J. Pathol.* **173,** 205–216 (2008).

71. Wee, P. & Wang, Z. Epidermal Growth Factor Receptor Cell Proliferation Signaling Pathways. *Cancers (Basel).* **9,** (2017).

72. Gohji, K. *et al. Organ-Site Dependence for the Production of Urokinase-Type Plasminogen Activator and Metastasis by Human Renal Cell Carcinoma Cells. American Journal ofPathology* **151,** (1997).

73. Cameron, M. D. *et al.* Temporal Progression of Metastasis in Lung : Cell Survival , Dormancy , and Location Dependence of Metastatic Inefficiency Temporal Progression of Metastasis in Lung : Cell Survival , Dormancy , and. *Cancer Res.* 2541–2546 (2000).

74. Balzer, E. M. *et al.* c-Src differentially regulates the functions of microtentacles and invadopodia. *Oncogene* **29,** 6402–6408 (2010).

75. Muralidharan-Chari, V. *et al.* ADP-Ribosylation factor 6 regulates tumorigenic and invasive properties in vivo. *Cancer Res.* **69,** 2201–2209 (2009).

76. Tornin, J. *et al.* FUS-CHOP Promotes Invasion in Myxoid Liposarcoma through a SRC/FAK/RHO/ROCK-Dependent Pathway. *Neoplasia* **20,** 44–56 (2018).

77. Bowden, E. T. *et al.* Co-localization of cortactin and phosphotyrosine identifies active invadopodia in human breast cancer cells. *Exp. Cell Res.* **312,** 1240–53 (2006).

78. Mader, C. C. *et al.* An EGFR-Src-Arg-cortactin pathway mediates functional maturation of invadopodia and breast cancer cell invasion. *Cancer Res.* **71,** 1730–41 (2011).

79. Stuelten, C. H., Parent, C. A. & Montell, D. J. Cell motility in cancer invasion and metastasis: insights from simple model organisms. *Nat. Rev. Cancer* **18,** 296–312 (2018).

80. Nichols, J. M., Veltman, D. & Kay, R. R. Chemotaxis of a model organism: progress with Dictyostelium. *Curr. Opin. Cell Biol.* **36,** 7–12 (2015).

81. Sherwood, D. R. & Sternberg, P. W. Anchor cell invasion into the vulval epithelium in C. elegans. *Dev. Cell* **5,** 21–31 (2003).

82. Sherwood, D. R., Butler, J. A., Kramer, J. M. & Sternberg, P. W. FOS-1 Promotes Basement-Membrane Removal during Anchor-Cell Invasion in C. elegans. *Cell* **121,** 951–962 (2005).

83. Ozanne, B. W., Spence, H. J., McGarry, L. C. & Hennigan, R. F. Transcription factors control invasion: AP-1 the first among equals. *Oncogene* **26,** 1–10 (2007).

84. Hastie, E. L. & Sherwood, D. R. A new front in cell invasion: The invadopodial membrane. *Eur. J. Cell Biol.* **95,** 441–448 (2016).

85. Lampreht Tratar, U., Horvat, S. & Cemazar, M. Transgenic Mouse Models in

Cancer Research. *Front. Oncol.* **8,** 268 (2018).

86. de Jong, M. & Maina, T. Of mice and humans: are they the same?--Implications in cancer translational research. *J. Nucl. Med.* **51,** 501–4 (2010).

87. Talmadge, J. E., Singh, R. K., Fidler, I. J. & Raz, A. Murine Models to Evaluate Novel and Conventional Therapeutic Strategies for Cancer. *Am. J. Pathol.* **170,** 793 (2007).

88. Gómez-Cuadrado, L., Tracey, N., Ma, R., Qian, B. & Brunton, V. G. Mouse models of metastasis: progress and prospects. *Dis. Model. Mech.* **10,** 1061–1074 (2017).

89. Khanna, C. & Hunter, K. Modeling metastasis in vivo. *Carcinog.* **26,** 513–523 (2005).

90. Belizário, J. E. *Immunodeficient Mouse Models: An Overview*. *The Open Immunology Journal* **2,** 79-85 (2009).

91. Zhang, B., Duan, Z. & Zhao, Y. Mouse models with human immunity and their application in biomedical research. *J. Cell. Mol. Med.* **13,** 1043–1058 (2009).

92. Karnofsky, D. A., Ridgway, L. P. & Patterson, P. A. TUMOR TRANSPLANTATION TO THE CHICK EMBRYO. *Ann. N. Y. Acad. Sci.* **55,** 313–329 (1952).

93. Papoutsi, M. *et al.* Endogenous origin of the lymphatics in the avian chorioallantoic membrane. *Dev. Dyn.* **222,** 238–251 (2001).

94. Kain, K. H. *et al.* The chick embryo as an expanding experimental model for cancer and cardiovascular research. *Dev. Dyn.* **243,** 216–228 (2014).

95. Ribatti, D. *The chick embryo chorioallantoic membrane in the study of angiogenesis and metastasis*. (Springer, 2010).

96. Klagsbrun, M., Knighton, D. & Folkman, J. Tumor angiogenesis activity in cells

grown in tissue culture. *Cancer Res.* **36,** 110–4 (1976).

97.   Fergelot, P. *et al.* The experimental renal cell carcinoma model in the chick embryo. *Angiogenesis* **16,** 181–194 (2013).

98.   Sys, G. M. L. *et al.* The In ovo CAM-assay as a Xenograft Model for Sarcoma. *J. Vis. Exp.* e50522 (2013). doi:10.3791/50522

99.   Adar, Y. *et al.* Imidazoacridinone-dependent lysosomal photodestruction: a pharmacological Trojan horse approach to eradicate multidrug-resistant cancers. *Cell Death Dis.* **3,** e293–e293 (2012).

100.   Weiss, A. *et al.* Low-dose angiostatic tyrosine kinase inhibitors improve photodynamic therapy for cancer: lack of vascular normalization. *J. Cell. Mol. Med.* **18,** 480–491 (2014).

101.   Klingenberg, M., Becker, J., Eberth, S., Kube, D. & Wilting, J. The chick chorioallantoic membrane as an in vivo xenograft model for Burkitt lymphoma. *BMC Cancer* **14,** 339 (2014).

102.   Wilson, S. M. & Chambers, A. F. Experimental Metastasis Assays in the Chick Embryo. *Curr. Protoc. Cell Biol.* **21,** 19.6.1--19.6.24 (2003).

103.   Chambers, A. F., Shafir, R. & Ling, V. *A Model System for Studying Metastasis Using the Embryonic Chick1*. (1982).

104.   Chambers, A. F. & Ling, V. Selection for experimental metastatic ability of heterologous tumor cells in the chick embryo after DNA-mediated transfer. *Cancer Res.* **44,** 3970–5 (1984).

105.   Pink, D. B. S., Schulte, W., Parseghian, M. H., Zijlstra, A. & Lewis, J. D. Real-Time Visualization and Quantitation of Vascular Permeability In Vivo: Implications for Drug Delivery. *PLoS One* **7,** e33760 (2012).

106.   Wolf, P. The nature and significance of platelet products in human plasma. *Br. J.*

Haematol. **13,** 269–88 (1967).

107. Zhang, Y., Liu, Y., Liu, H. & Tang, W. H. Exosomes: biogenesis, biologic function and clinical potential. *Cell Biosci.* **9,** 19 (2019).

108. Brett, S. I., Kim, Y., Biggs, C. N., Chin, J. L. & Leong, H. S. Extracellular vesicles such as prostate cancer cell fragments as a fluid biopsy for prostate cancer. *Prostate Cancer Prostatic Dis* **18,** 213–220 (2015).

109. Pasquier, J. *et al.* Microparticles mediated cross-talk between tumoral and endothelial cells promote the constitution of a pro-metastatic vascular niche through Arf6 up regulation. *Cancer Microenviron.* **7,** 41–59 (2014).

110. Stein, J. M. & Luzio, J. P. *Ectocytosis caused by sublytic autologous complement attack on human neutrophils The sorting of endogenous plasma-membrane proteins and lipids into shed vesicles. Biochem. J* **274,** (1991).

111. Fackler, O. T. & Grosse, R. Cell motility through plasma membrane blebbing. *Journal of Cell Biology* **181,** 879–884 (2008).

112. Clancy, J. W. *et al.* Regulated delivery of molecular cargo to invasive tumour-derived microvesicles. *Nat. Commun.* **6,** 6919 (2015).

113. Li, B., Antonyak, M. A., Zhang, J. & Cerione, R. A. RhoA triggers a specific signaling pathway that generates transforming microvesicles in cancer cells. (2012). doi:10.1038/onc.2011.636

114. Morel, O., Jesel, L., Freyssinet, J.-M. & Toti, F. Cellular Mechanisms Underlying the Formation of Circulating Microparticles. *Arterioscler. Thromb. Vasc. Biol.* **31,** 15–26 (2011).

115. Fujii, T., Sakata, A., Nishimura, S., Eto, K. & Nagata, S. TMEM16F is required for phosphatidylserine exposure and microparticle release in activated mouse platelets. *Proc. Natl. Acad. Sci. U. S. A.* **112,** 12800–5 (2015).

116.   Nabhan, J. F., Hu, R., Oh, R. S., Cohen, S. N. & Lu, Q. Formation and release of arrestin domain-containing protein 1-mediated microvesicles (ARMMs) at plasma membrane by recruitment of TSG101 protein. doi:10.1073/pnas.1200448109

117.   Bianco, F. *et al.* Astrocyte-Derived ATP Induces Vesicle Shedding and IL-1β Release from Microglia. *J. Immunol.* **174,** 7268–7277 (2005).

118.   Thomas, L. M. & Salter, R. D. on TLR4 by Phospholipids and Is Partially Dependent Mediated Microvesicles from Myeloid Cells Is-Induced 7 Activation of Macrophages by P2X. *J Immunol* **185,** 3740–3749 (2010).

119.   Kowal, J. *et al.* Proteomic comparison defines novel markers to characterize heterogeneous populations of extracellular vesicle subtypes. doi:10.1073/pnas.1521230113

120.   Kalra, H. *et al.* Vesiclepedia: A Compendium for Extracellular Vesicles with Continuous Community Annotation. *PLoS Biol.* **10,** e1001450 (2012).

121.   Joy, A. P. *et al.* Proteome profiling of extracellular vesicles captured with the affinity peptide Vn96: comparison of Laemmli and TRIzol© protein-extraction methods. *J. Extracell. vesicles* **7,** 1438727 (2018).

122.   Pircher, A., Treps, L., Sedger, L. M. & Jaiswal, R. Intercellular Vesicular Transfer by Exosomes, Microparticles and Oncosomes - Implications for Cancer Biology and Treatments. *Front. Oncol. | www.frontiersin.org* **1,** 125 (2019).

123.   Keerthikumar, S. *et al.* ExoCarta: A Web-Based Compendium of Exosomal Cargo. *J. Mol. Biol.* **428,** 688–692 (2016).

124.   Colombo, M., Raposo, G. & Théry, C. Biogenesis, Secretion, and Intercellular Interactions of Exosomes and Other Extracellular Vesicles. *Annu. Rev. Cell Dev. Biol* **30,** 255–289 (2014).

125.   Muralidharan-Chari, V. *et al.* ARF6-Regulated Shedding of Tumor Cell-Derived Plasma Membrane Microvesicles. *Curr. Biol.* **19,** 1875–1885 (2009).

126. Willms, E., Cabañas, C., Mäger, I., Wood, M. J. A. & Vader, P. Extracellular Vesicle Heterogeneity: Subpopulations, Isolation Techniques, and Diverse Functions in Cancer Progression. *Front. Immunol.* **9,** 738 (2018).

127. Al-Nedawi, K. *et al.* Intercellular transfer of the oncogenic receptor EGFRvIII by microvesicles derived from tumour cells. *Nat. Cell Biol.* **10,** 619–624 (2008).

128. Antonyak, M. A. *et al.* Cancer cell-derived microvesicles induce transformation by transferring tissue transglutaminase and fibronectin to recipient cells. *Proc. Natl. Acad. Sci. U. S. A.* **108,** 4852–7 (2011).

129. Taylor, D. D., Içek Gerçel-Taylor, C. ̧, Lyons, K. S., Stanson, J. & Whiteside, T. L. *T-Cell Apoptosis and Suppression of T-Cell Receptor/CD3-by Fas Ligand-Containing Membrane Vesicles Shed from Ovarian Tumors*. (2003).

130. Wieckowski, E. U. *et al.* Tumor-derived microvesicles promote regulatory T cell expansion and induce apoptosis in tumor-reactive activated CD8+ T lymphocytes. *J. Immunol.* **183,** 3720–30 (2009).

131. WHITESIDE, T. Immune suppression in cancer: Effects on immune cells, mechanisms and future therapeutic intervention. *Semin. Cancer Biol.* **16,** 3–15 (2006).

132. Vlaeminck-Guillem, V. Extracellular Vesicles in Prostate Cancer Carcinogenesis, Diagnosis, and Management. *Front. Oncol.* **8,** 222 (2018).

133. Di Vizio, D. *et al.* Oncosome formation in prostate cancer: association with a region of frequent chromosomal deletion in metastatic disease. *Cancer Res.* **69,** 5601–9 (2009).

134. Morello, M. *et al.* Large oncosomes mediate intercellular transfer of functional microRNA. *Cell Cycle* **12,** 3526–3536 (2013).

135. Minciacchi, V. R. *et al.* MYC Mediates Large Oncosome-Induced Fibroblast Reprogramming in Prostate Cancer. *Cancer Res.* **77,** 2306–2317 (2017).

136. Vizio, D. Di *et al.* Large Oncosomes in Human Prostate Cancer Tissues and in the Circulation of Mice with Metastatic Disease. **181,** 1573–1584 (2012).

137. Su, Z., Yang, Z., Xu, Y., Chen, Y. & Yu, Q. Apoptosis, autophagy, necroptosis, and cancer metastasis. *Mol. Cancer* **14,** 48 (2015).

138. Elmore, S. Apoptosis: a review of programmed cell death. *Toxicol. Pathol.* **35,** 495–516 (2007).

139. Zhang, Y., Chen, X., Gueydan, C. & Han, J. Plasma membrane changes during programmed cell deaths. *Cell Res.* **28,** 9–21 (2018).

140. Hausmann, G. *et al.* Pro-apoptotic apoptosis protease-activating factor 1 (Apaf-1) has a cytoplasmic localization distinct from Bcl-2 or Bcl-x(L). *J. Cell Biol.* **149,** 623–34 (2000).

141. Caruso, S. & Poon, I. K. H. Apoptotic Cell-Derived Extracellular Vesicles: More Than Just Debris. *Front. Immunol.* **9,** 1486 (2018).

142. Hayakawa, K. *et al.* Transfer of mitochondria from astrocytes to neurons after stroke. *Nature* **535,** 551–555 (2016).

143. Pavlyukov, M. S. *et al.* Apoptotic Cell-Derived Extracellular Vesicles Promote Malignancy of Glioblastoma Via Intercellular Transfer of Splicing Factors. *Cancer Cell* **34,** 119–135.e10 (2018).

144. Paoli, P., Giannoni, E. & Chiarugi, P. Anoikis molecular pathways and its role in cancer progression ☆. (2013). doi:10.1016/j.bbamcr.2013.06.026

145. Frisch, S. M. & Francis, H. Disruption of epithelial cell-matrix interactions induces apoptosis. *J. Cell Biol.* **124,** 619–626 (1994).

146. Frisch, S. M. & Ruoslahti, E. Integrins and anoikis. *Curr. Opin. Cell Biol.* **9,** 701–6 (1997).

147. Reddig, P. J. & Juliano, R. L. Clinging to life: cell to matrix adhesion and cell

survival. *Cancer Metastasis Rev.* **24,** 425–439 (2005).

148. Giancotti, F. G. Complexity and specificity of integrin signalling. *Nat. Cell Biol.* **2,** E13–E14 (2000).

149. Boudreau, N. J. & Jones, P. L. Extracellular matrix and integrin signalling: the shape of things to come. *Biochem. J.* **339 (Pt 3),** 481–8 (1999).

150. Gehlsen, K. R., Davis, G. E. & Sriramarao, P. Integrin expression in human melanoma cells with differing invasive and metastatic properties. *Clin. Exp. Metastasis* **10,** 111–20 (1992).

151. Zeng, Q. *et al.* Endothelial cell retraction is induced by PAK2 monophosphorylation of myosin II. *J. Cell Sci.* **113 (Pt 3),** 471–82 (2000).

152. Janes, S. M. & Watt, F. M. Switch from alphavbeta5 to alphavbeta6 integrin expression protects squamous cell carcinomas from anoikis. *J. Cell Biol.* **166,** 419–31 (2004).

153. Ramos, D. M. *et al.* Expression of integrin β6 enhances invasive behavior in oral squamous cell carcinoma. *Matrix Biol.* **21,** 297–307 (2002).

154. Shirkoohi, R. Epithelial mesenchymal transition from a natural gestational orchestration to a bizarre cancer disturbance. (2012). doi:10.1111/cas.12074

155. Yan, L., Xu, F. & Dai, C.-L. Relationship between epithelial-to-mesenchymal transition and the inflammatory microenvironment of hepatocellular carcinoma. *J. Exp. Clin. Cancer Res.* **37,** 203 (2018).

156. Whelan, K. A. *et al.* Hypoxia Suppression of Bim and Bmf Blocks Anoikis and Luminal Clearing during Mammary Morphogenesis. *Mol. Biol. Cell* **21,** 3829–3837 (2010).

157. Najafov, A., Chen, H. & Yuan, J. Necroptosis and Cancer. *Trends in Cancer* **3,** 294–301 (2017).

158. Najafov, A., Chen, H. & Yuan, J. Necroptosis and Cancer. doi:10.1016/j.trecan.2017.03.002

159. Galluzzi, L., Kepp, O., Ka-Ming Chan, F. & Kroemer, G. Necroptosis: Mechanisms and Relevance to Disease. *Annu. Rev. Pathol. Mech. Dis. 2017* **12,** 103–133 (2016).

160. Yatim, N. *et al.* RIPK1 and NF-κB signaling in dying cells determines cross-priming of CD8^{+} T cells. *Science* **350,** 328–34 (2015).

161. Yang, H. *et al.* Contribution of RIP3 and MLKL to immunogenic cell death signaling in cancer chemotherapy. *Oncoimmunology* **5,** e1149673 (2016).

162. Gong, Y.-N. *et al.* ESCRT-III Acts Downstream of MLKL to Regulate Necroptotic Cell Death and Its Consequences. *Cell* **169,** 286–300.e16 (2017).

163. Yoon, S., Kovalenko, A., Bogdanov, K. & Wallach, D. MLKL, the Protein that Mediates Necroptosis, Also Regulates Endosomal Trafficking and Extracellular Vesicle Generation. *Immunity* **47,** 51–65.e7 (2017).

164. Chuo, S. T.-Y., Chien, J. C.-Y. & Lai, C. P.-K. Imaging extracellular vesicles: current and emerging methods. *J. Biomed. Sci.* **25,** 91 (2018).

165. Wallace, P. K. *et al.* Tracking antigen-driven responses by flow cytometry: Monitoring proliferation by dye dilution. *Cytom. Part A* **73A,** 1019–1034 (2008).

166. Mittelbrunn, M. *et al.* Unidirectional transfer of microRNA-loaded exosomes from T cells to antigen-presenting cells. *Nat. Commun.* **2,** 282 (2011).

167. Grange, C. *et al.* Biodistribution of mesenchymal stem cell-derived extracellular vesicles in a model of acute kidney injury monitored by optical imaging. *Int. J. Mol. Med.* **33,** 1055–63 (2014).

168. Fick, J. *et al.* The extent of heterocellular communication mediated by gap junctions is predictive of bystander tumor cytotoxicity in vitro. *Proc. Natl. Acad.*

Sci. U. S. A. **92,** 11071–5 (1995).

169. Askenasy, N. & Farkas, D. L. Optical Imaging of PKH&hyphen;Labeled Hematopoietic Cells in Recipient Bone Marrow In Vivo. *Stem Cells* **20,** 501–513 (2002).

170. Parish, C. R. Fluorescent dyes for lymphocyte migration and proliferation studies. *Immunol. Cell Biol.* **77,** 499–508 (1999).

171. Biggs, C. N. *et al.* Prostate extracellular vesicles in patient plasma as a liquid biopsy platform for prostate cancer using nanoscale flow cytometry. *Oncotarget* **7,** 8839–49 (2016).

172. Gomes, J. *et al.* Analytical Considerations in Nanoscale Flow Cytometry of Extracellular Vesicles to Achieve Data Linearity. *Thromb. Haemost.* **118,** 1612–1624 (2018).

173. Poon, A. C. *et al.* Nanoscale flow cytometry of patient plasma for the detection of prostate cancer-associated extracellular vesicles. *STEM Fellowsh. J.* **3,** 1–2 (2017).

174. van der Pol, E. *et al.* Absolute sizing and label-free identification of extracellular vesicles by flow cytometry. *Nanomedicine Nanotechnology, Biol. Med.* **14,** 801–810 (2018).

175. Baj-Krzyworzeka, M. *et al.* Tumour-derived microvesicles carry several surface determinants and mRNA of tumour cells and transfer some of these determinants to monocytes. *Cancer Immunol. Immunother.* **55,** 808–818 (2006).

176. Momen-Heravi, F. *et al.* Current methods for the isolation of extracellular vesicles. doi:10.1515/hsz-2013-0141

177. Cheruvanky, A. *et al.* Rapid isolation of urinary exosomal biomarkers using a nanomembrane ultrafiltration concentrator. *Am. J. Physiol. Physiol.* **292,** F1657–F1661 (2007).

178. Miranda, K. C. *et al.* Nucleic acids within urinary exosomes/microvesicles are potential biomarkers for renal disease. *Kidney Int.* **78,** 191–199 (2010).

Chapter 2

2 Quantification of Cancer Cell Extravasation *In Vivo*

Contents of this chapter are published in Nature Protocols. Kim Y, Williams KC, Gavin CT, Jardine E, Chambers AF, Leong HS. Nat Protoc. 2016; 11(5):937-48. Only formatting changes were made to include the published work in this thesis.

2.1 Introduction

Metastasis is the process by which a primary tumour releases tumour cells into the hematogenous or lymphatic system, resulting in the downstream colonization of distant sites such as the brain, liver, lung and bone marrow[1]. There are four main steps in the metastatic cascade: intravasation[2–4]; transit in the blood or lymphatic system[5–7]; extravasation[8,9]; and adaptation to the secondary site[10–13]. Intravasation is the entry of tumour cells into the circulation at the primary tumour site, and it is thought to require migration past the endothelial cells of vessels distributed throughout the tumour. When tumour cells enter the circulation, they are carried away from the site of intravasation and arrest in the capillary beds of distant sites such as the liver, brain, bone marrow and lung. After intravascular arrest at these distant sites, tumour cells may undergo extravasation, which is the movement of cancer cells from the vessel lumen into the underlying tissue. Studies using the CAM of chicken embryos and mouse lungs have shown that the vast majority of metastases are found in the extravascular space and are rarely present in the intravascular space (vessel lumen), suggesting that cancer cell extravasation is a key step in the metastatic cascade[9,14]. Extravasation occurs at all distant sites, with varying efficiencies[15], and only a small percentage of extravasated tumour cells will successfully adapt to the local microenvironment and proliferate to form a metastatic colony[15–17].

In this protocol, we describe a technique to evaluate cancer cell invasiveness by quantifying *in vivo* rates of cancer cell extravasation in the CAM of chicken embryos. Our laboratory and others have used this protocol in recent research investigating the efficacy of target genes[9,18–20] or drugs[9,20–22] in inhibiting or promoting cancer cell extravasation.

This assay can also be used to study metastatic inefficiency (whereby only a small number of tumour cells form metastases[16]), which can occur at various steps of the metastatic cascade, including intravasation[23], extravasation[15] and adaptation to the new local microenvironment[24]. Highly aggressive cancer cells, such as B16F10, tend to form large numbers of metastases (particularly in the lung and liver), whereas less aggressive variants, such as B16F1, form considerably fewer metastases[25]. Clones of tumour cells with invasive phenotypes are able to persist because of their ability to overcome local restrictions (for example, nutrient deprivation and hypoxia)[26,27]. Many metastatic cancer cells form membrane protrusions known as invadopodia that mediate cancer cell extravasation and, when blocked by depletion of invadopodia-specific factor Tks4/5 (tyrosine kinase substrate with four/five Src homology 3 domains), have considerably reduced metastatic colony formation[9,28]. However, various other cancer cell lines are also able to extravasate with varying efficiencies with little to no invadopodia formation capacity, as determined by gelatin-degradation assays[29], suggesting that proteases might not always be integral for transendothelial migration.

2.1.1   Comparison with other methods

Cancer cell extravasation has been studied using the *in vitro* Transwell assay, in which cancer cells are seeded onto a Transwell filter pore system and allowed to translocate across a well containing chemotaxis factors such as fetal bovine serum (FBS)[30,31]. This assay has been used extensively to evaluate the effects of various genetic factors and pharmacologic compounds on cancer cell invasion in a system analogous to the process of cancer cell extravasation (**Figure 5a**). As a result of the Transwell assay, many molecular mechanisms and cellular components have been implicated in cancer cell extravasation, such as various Rho GTPase effectors[18,32,33], chemokines[34,35], integrins[8,36,37], proteases[38,39] and cytoskeletal proteins[40–42]. However, there are three major caveats with *in vitro*–based assays. First, translocation of cell volume in Transwell assays occurs through 2D circular pores ranging from 3 to 12 µm in diameter, whereas extravasation probably occurs along endothelial junctions belonging to an architecturally complex 3D microvasculature network[43,44]. Second, *in vitro* assays are hemodynamically static, whereas both plasma proteins and

circulating blood cells are key to promoting and counteracting biophysical forces acting upon tumour cells as they attempt to extravasate. Most of the *in vitro* assays use cell culture media supplemented with 10–15% FBS and not 100% uncoagulated plasma, so *in vitro* experiments are missing the full range of plasma proteins and their rheological impact on microcirculation. Recent publications have highlighted the use of endothelial cells to form cell monolayers to simulate transendothelial migration[45–47], but these systems lack the full range of platelets, red blood cells and leukocytes needed to recreate *in vivo* hemodynamics. Moreover, these microfluidic chips are not readily commercially available and require trypsinization to remove cells (which may also remove the gelatin coatings needed for new cell layers to form)[48]. Furthermore, they require continuous perfusion throughout the chip and continuous monitoring (no monitoring is required after cancer cell injections in the CAM). Third, most cells will eventually translocate across the Transwell over a 24- to 48-h period of incubation *in vitro*, highlighting the permissive-ness of the Transwell filter. In fact, given that very few cells die *in vitro* if they fail to translocate (whereas large numbers would die *in vivo*), the Transwell assay uses an arbitrary time frame to compare treatments or cell genotypes. Given the technical limitations of *in vitro*–based invasion assays, *in vivo* cancer cell extravasation studies are rapidly gaining popularity.
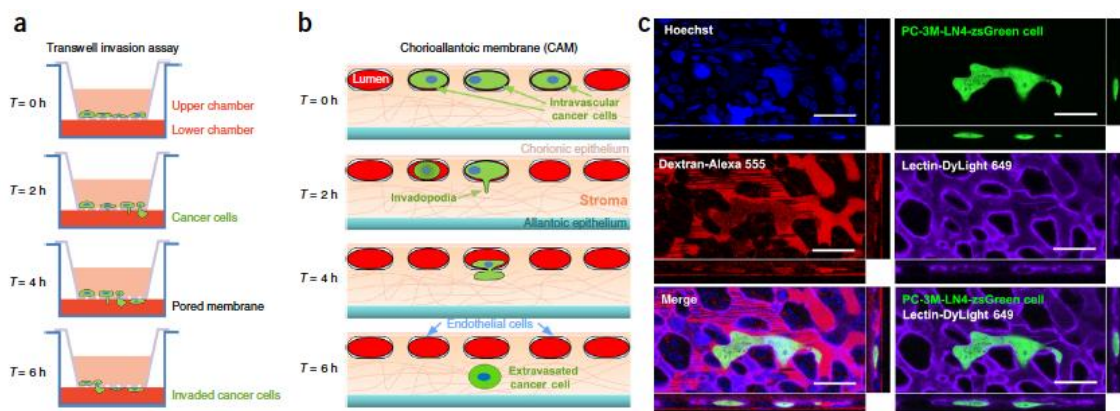
Figure 5: Comparison of transwell invasion assay with the chorioallantoic membrane (CAM) to quantify cancer cell extravasation and imaging intravascular and extravascular cancer cells in the CAM. (a) Schematic of in vitro transwell invasion assay in which cancer cells of interest are plated into the upper chamber of the Transwell system and migrate across a pore membrane system to gain access to the lower chamber filled with a chemotactic agent. (b) Schematic of *in vivo* cancer cell extravasation assay in which cancer cells are injected intravenously (i.v.) and arrest within the capillary bed of the CAM. Over time, a fraction of cells will successfully undergo transendothelial migration into the stroma of the CAM. (c) Intravital image using confocal resonance scanning microscopy of a cultured human prostate PC-3M-LN4 cancer cell in the intravascular space of the CAM. When various other labeling agents are injected, such as Hoechst 33456 to stain nuclei (blue), lectin-DyLight 649 to label the endothelial walls (purple) and Dextran-Alexa 555 to reveal the vessel lumen space (red), cancer cells such as PC-3M-LN4 (green) can be properly visualized in the CAM capillary bed to determine whether the cells are intravascular or extravascular. Scale bars, 10 μm.

Although murine preclinical models remain the gold standard for simulating the metastatic process *in vivo*, it can be difficult to study cancer cell extravasation rates in commonly colonized mouse organs such as the lung and liver, as capillary beds are not accessible for imaging. In contrast, the CAM of chicken embryos is well-suited for evaluating cancer cell extravasation rates because it offers a flat, extensive capillary bed for imaging key steps of the metastatic cascade, in some ways resembling a '2D lung'[4,9,43,49–52]. When labeling agents such as fluorescently-conjugated lectins (*Lens culinaris* agglutinin), which label the luminal surface of endothelial cells, or dextrans, which label the vessel lumen, are injected intravenously (i.v.) into the CAM, the capillary bed becomes evident and appears as a thin sheet in the middle of the CAM, with the stroma space immediately below it (**Figure 5b**).

When cancer cells are injected into CAM veins, the cells will be present immediately within this capillary bed and, over time, extravasate into the underlying stroma, which is not labeled by the lectin, providing a clear distinction between intravascular and extravasated cancer cells.

2.1.2   Advantages and limitations

This *in vivo* assay enables the investigator to evaluate the effects of a target gene or drug at a specific step of the metastatic cascade, cancer cell extravasation. This preclinical model can be used to determine the number of cancer cells that initially arrest in the embryonic lung and the proportion of cancer cells that extravasate in the region of interest (ROI) within 24 h. The key strength of this model is that cancer cells immediately arrest within the capillary bed of the CAM, which is a 2D microvasculature network that spans above and across the entire embryo when *ex ovo*. When cancer cells extravasate, the majority will translocate into the stroma layer immediately below the CAM's capillary bed (**Figure 5b**). In some instances, the cancer cells will displace stromal cells, which appear as circular voids throughout the CAM's capillary bed (**Figure 5c**). When fluorescently labeled lectins are injected into CAM veins, the identification of cells as intravascular or extravasated becomes straightforward and rapid (**Figure 5c**). *L. culinaris* agglutinin lectins are powerful reagents because of their high affinity for the glycocalyx of chicken embryo endothelial cells, and they are relatively inexpensive, as only ~5 µg of lectins is needed for each embryo. This enables the user to determine extravasation efficiency in a binary manner and to generate quantitative data proficiently and in a high-powered manner. This technique is also an excellent means of performing drug screens for compounds that inhibit invasion or cancer cell extravasation in an *in vivo* environment. To begin these drug screens, pretreatment of the cells before injection or co-injection of drugs can be performed to determine the drugs' effect on cancer cell extravasation. Subsequent drug administration after the initial injection of cells is not necessary because cancer cell extravasation occurs primarily within the first 12 h after the injection of cells, and drug bioavailability *in vivo* is not normally an issue during that time frame. Moreover, given the small blood volume of avian embryos (1.3–3.4 mL total), the use of biologics such as inhibitory antibodies or

peptides is economically feasible with this model, as opposed to performing the same experiments in mice, where more complex pharmacodynamic consideration is required. This technique is also economically and scientifically scalable, as several different treatments can be performed in the same day, using at least $N > 6$ for each treatment group or genotype. The ability to generate experiments within 24 h that can evaluate various groups or genotypes offers a high-throughput means of attaining *in vivo* results that are meaningful to cancer cell metastasis without reliance on a rodent model. Although performing end-point assays in immunocompromised mice will continue to be the gold standard for oncology preclinical models, the opportunity to evaluate several groups or treatments in this intermediate model is valuable, especially because mouse models are more expensive and time-consuming to use.

Because of the low cost of each chick embryo ($0.50–1.00 per embryo), CAM assays for each cell group or treatment group can be sufficiently powered ($N > 15$ embryos per group) to readily achieve statistical significance between groups. Moreover, because of the highly accessible nature of the CAM, cancer cells within the capillary bed or stroma can be readily visualized using either wide-field or confocal fluorescence microscopy, without any hair, adipocytes or skin obscuring the visualization of fluorescently labeled cells. The CAM assay is also rapid; the injection of fluorescently labeled lectins that label the luminal surface of endothelial cells allows the researcher to quickly and easily distinguish intravascular cancer cells from extravasated cancer cells within just 24 h[53].

A limitation of this assay is that only fluorescently labeled cells can be used, either by expression of fluorescent proteins or by pretreatment with lipophilic fluorescent dyes such as CellTracker (Thermo Fisher) dyes. In addition, although this model has been used to understand many steps of angiogenesis and cancer metastasis in mammals, another limitation may arise from the fact that mammalian tumour cells are operating in an avian xenograft microenvironment. If the cancer cells require specific endocrinological factors for viability, then this should be considered when performing extravasation assays in embryos. Furthermore, it is essential that the investigator become skilled at the i.v.

injection of cancer cells, and it is our aim with this work to provide a complete step-by-step guide to help researchers successfully reproduce this protocol.

2.1.3   Overview of the technique

There are four key stages to this method: preparation of *ex ovo* embryos, preparation of cancer cells for i.v. injection into the CAM of chick embryos, intravital imaging of cancer cells before and after extravasation, and wide-field imaging–based quantification of cancer cell extravasation.

2.1.4   Experimental design

Eggs. There are many breeds and sizes of chicken embryos, but White Leghorn chicken eggs are commonly used for scientific endeavors. A typical extravasation experiment requires $n > 10$ embryos per group. A group can be defined as those embryos that receive an injection of cancer cells that receive an overnight pretreatment of drug/therapy.

Cell lines. Adherent cell lines or those grown in suspension can be used for these experiments. In this protocol, we present images and data obtained with the PC-3M-LN4 prostate cancer cell line. Many different cancer cell lines have been used and injected into the CAM of chick embryos, and the proportion that successfully extravasates *in vivo* is correlated to metastatic efficiency. Ideal positive and negative control cell lines will be off-target control knock-down cells and cells treated with vehicle control (negative control).

Injection techniques. It is essential that the bore width of the microinjector needle have the same diameter as the vein for the injection of cancer cells, as this will minimize blood loss and maximize embryo viability after the injection.

Incubation conditions. Before the fertilized eggs are cracked, incubation of the eggs is necessary at 22 °C in any incubator for up to 3 h before cracking. Chicken embryo incubation units at 39 °C are used for incubation of chicken embryos after cracking and microinjection, and no CO_2 is used. Cancer cell culture conditions are at 37 °C.

Counting techniques. The means of determining extravasation efficiency is the enumeration of cancer cells at $T = 0$ and at $T = 24$ h that are within a 1-inch x 1-inch aluminum foil window as pre- pared by the investigator. Confocal microscopy is used to confirm cancer cell extravasation at $T = 0$ and $T = 24$ h after injection.

Extravasation efficiency. To determine whether cell lines are suitable for extravasation efficiency analysis, the investigator must check that all the cells are extravasated 24 h after injection. Confocal microscopy must be performed on a subset of chick embryos ($N > 4$) to determine the percentage of cells present within the foil window that are intravascular or extravascular. This assay can be readily adapted to study metastatic colony formation by the addition of a 7-d incubation of the embryos after extravasation efficiency analysis ($T = 24$ h). Cancer cell extravasation rates and metastatic colony formation rates can be studied sequentially in a rapid and straightforward manner. When you are performing an extravasation efficiency experiment, always rely on $N > 4$ for each treatment/cohort/cell type. Thus, in the event that 1–2 animals die after the $T = 0$ injection of cancer cells, there will at least be $N = 3$ per group for analysis.

Time course. It is important to be aware that although a typical extravasation experiment takes 24 h to elapse, considerable preparation is required to have the proper number of embryos ready for the number of groups being tested. For this reason, not all groups are evaluated at the same time, and experiments are often split up and performed on different days or weeks.

2.1.5   Reagents

Fertilized white Leghorn eggs. Our experiments were conducted in accordance with guidelines of the Institutional Animal Care and Use Committee at Western University. Consult with your institute's Animal Care and Use Committee to determine whether chicken embryos are considered animals or embryos. At most research institutions, chicken embryos that are maintained from embryonic day 8 to day 22 are not considered animals if the embryos are terminated at day 22. As these experiments require *ex ovo* embryos, the absence of the egg shell will result in the gradual termination of the embryo because of the

lack of calcium needed for embryonic bone development. Cancer cell line of interest used in your research should be regularly checked to ensure that they are authentic and that they are not infected with mycoplasma. Lectin-FITC/lectin-rhodamine/lectin-DyLight 649, *L. culinaris* agglutinin *LCA* (Vector Laboratories, cat. no. FL-1041/FL-1042, always freshly prepare this compound from the stock vial on the day of use).

- dH2O
- Dulbecco's PBS (D-PBS, pH 7.2−7.4; Wisent, cat. no. 311-010-CL)
- FBS (heat inactivated; Wisent, cat. no. 080-910)
- Cell culture medium (unsupplemented) specific to the cell line for experimentation
- Trypsin, 0.05% (wt/vol) and EDTA 0.53 mM (Wisent, cat. no. 325-042-CL)
- 70% ethanol (in dH2O)
- CellTracker green CMFDA (5-chloromethylfluorescein diacetate) dye (Life Technologies, cat. no. C2925)

2.1.6   Equipment

- Digital sportsman egg incubator (GCQ, cat. no. 1502)
- Digital hatcher egg incubator (GCQ, cat. no. 1550)
- Rubbermaid plastic container (Guillevin, cat. no. RH3-228-00-BLU) with 1-cm-diameter holes drilled into sides, spaced 5 cm apart around the side perimeter of each container
- Polystyrene weigh boats for holding *ex ovo* chicken embryos (VWR, cat. no. 12577-01)
- Square Petri dishes as lids for weigh boats containing *ex ovo* chicken embryos (Simport, VWR, cat. no. 25378-115)
- Dremel drill tool
- Dremel cutoff wheel bit no. 36 (Dremel, cat. no. 409)
- Tygon R-3603 laboratory tubing, 50 ft (1/32-inch inner diameter, 3/32-inch outer diameter, 1/32-inch wall thickness; VWR, cat. no. 63009-983)

- Syringes for injections (1-mL maximum volume capacity, box of 100; BD Biosciences, cat. no. 309602)
- Hypodermic needles of injections (18-gauge needles, box of 100; BD Biosciences, cat. no. 305195)
- Intellitemp heat mat (19.7-inch x 11.8-inch, 30 W, Big Apple Herpetologicals)
- Vertical pipette puller (David Kopf Instruments, Model 720)
- Sodium borosillicate capillary tubes (o.d., 1.0 mm; i.d., 0.58 mm; 10 cm length; Sutter Instrument, cat. no. BF100-58-10)
- Circular glass coverslips, no. 1 (18 mm; VWR, cat. no. 16004-300)
- Fine forceps (VWR, cat. no. 25607-856)
- Scissors
- Vacuum grease (VWR, cat. no. 59344-055)
- Avian embryo imaging unit (custom made)
- Aluminum foil
- Pyrex Petri dish (100 x 20 mm; VWR, cat. no. 89000-306)
- Dissecting scope
- Wide-field fluorescence upright microscope fitted with 4x and 10x long-distance objectives
- Refrigerated Benchtop Centrifuge (Eppendorf)
- Kimwipes, 13 x 21 cm, Box/280 (VWR, cat. no. 470173-504)
- Cell culture supplies (cell culture flasks, Falcon tubes, P1000 micropipette, pipette gun and so on)

2.1.7   Reagent set up

Cells

Perform cell culture with various adherent or suspension cancer cell lines as required. To assess the effect of a drug on cancer cell extravasation, ensure that each treatment is performed in a T75 cell culture flask. Each flask should contain cancer cells that are grown to a confluency of ~80–90%. Depending on the injection effectiveness by the investigator,

a single T75 flask may provide enough diluted cells for injection into 6–18 embryos. Although suspension cancer cell lines can be used in this experiment, the following procedure provides instructions for adherent cell lines only.

CellTracker dye

To prepare the dye for cell labeling, add 1 mL of DMSO to a 1.5-mL Eppendorf tube, mix it vigorously and leave it in the dark at −20 °C until needed for Step 17 (up to a maximum of 1 month).

2.1.8   Equipment set up

Microinjection needles Prepare needles drawn from borosilicate glass capillary tubes using a pipette puller (Kopf Instrumentation). Prepare needles that are as long and slowly tapered as possible by adjusting the heat and solenoid settings on the puller. Settings on the 720 Kopf model are generally 16.3 (heater) and 2.3 (solenoid). Needles should be prepared before cell injection, sprayed with 70% ethanol and then stored in a sterile dish with a lid for at most a week. If needles are to be reused, simply spray the needles with 70% ethanol again.

Aluminum foil regions of interest Fold the aluminum foil in half and cut out a window that has an internal width of 1 inch with scissors. The frame of this aluminum foil window should be less than 1/4 inches in width, and the window should be square-shaped. Unfold all foil windows and place them in the Pyrex Petri dish and autoclave before use. The window should have an internal open square dimension of at least 1 inch x 1 inch. For wide-field fluorescence microscopy, we use an Olympus upright microscope that has a Mercury Arc lamp light source and a full set of dichroic filters for visualizing GFP- and RFP-based fluorescence signal. No digital camera is needed for this microscope. For confocal fluorescence microscopy, we use a Nikon Fast A1R confocal upright microscope fitted with several oil-immersion objectives (20x and 60x objectives) and laser lines (405, 488, 561 and 643 nm).

2.2   Protocols

2.2.1   Preparation of *ex ovo* chicken embryos

Timing 9 days

1. When fertilized eggs arrive at the laboratory, place the eggs in the hatcher and incubate them for 4 d at 39 °C at a relative humidity of >70% with rotation as per the instructions for the hatcher.

2. Ideally, eggs are incubated at 39 °C in the hatcher on the day of receipt; however, if this is not possible, place the eggs at 4 °C for up to 3 d for scheduling purposes. Move the eggs from 4 °C to the 22 °C incubator for 3 h before finally placing them in the hatcher incubator at 39 °C for 4 d at a relative humidity of >70% with rotation as per the instructions for the hatcher.

Critical step: Do not wait more than 4 days after fertilization of the eggs to begin step 2.

3. On the day of egg cracking, prepare a Dremel tool (**Figure 6a**) by fitting with a cutting disc (no. 36 cutoff, 15/16-inch diameter, included in the tool set) that is attached to a rod platform and fixed at a user-defined level using a three-finger clamp.

4. Spray down the entire Dremel tool and cutting disc with 70% ethanol.

Critical step: As the cracking step is a major source of contamination of embryos, the cutting disc must be properly sprayed down with 70% ethanol.

5. Place the egg on its side for 10 sec so that the embryo and yolk move to the center of the egg. To crack open the egg shell, hold both ends of the egg with both hands and lightly roll or coat the middle 'waist' of the egg shell with 70% ethanol in a weigh boat.

6. With the Dremel tool operating at medium speed, make four shallow cuts around the middle 'waist' of the egg (**Figure 6b**).

Critical step: Cuts should be equally spaced from one another so that the cracking step (Step 7) is clean and quick.
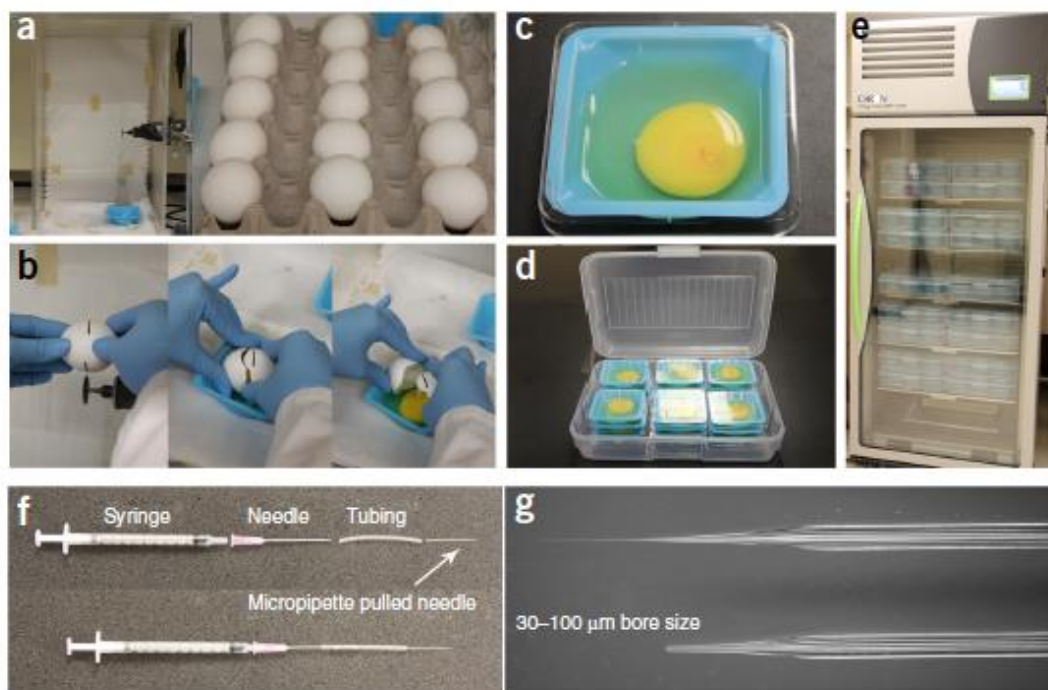
Figure 6: Preparation of ex ovo chicken embryos and microinjector assembly for i.v. injection of cancer cells or labeling agents. (a) Egg-cracking station consists of a plastic shield and a Dremel cutting tool (left image). Eggs are laid on their side before cracking. (b) With the Dremel cutting tool, 2–3 cuts are made along the middle of the egg, and then the egg is gently split open, and the embryo and its yolk are placed into a weigh boat. (c) *Ex ovo* chicken embryos are individually stored in disposable weigh boats and lids. (d) Embryos are stacked and transported in batches using clamshell boxes. (e) Hundreds of embryos are stored in large incubators for experimentation. (f) Unassembled and assembled microinjectors, which are used to i.v. deliver cells and/or labeling agents via small vessels present in the CAM for the extravasation efficiency assay. (g) The pulled microneedles are modified such that the tip is broken so that a bore size (bottom needle) of sufficient size can be used to inject cancer cells and to prevent clogs.

7. Spray a new weigh boat with 70% ethanol. Once the ethanol has dried, lay the egg on the weigh boat on its side and gently roll it back and forth while placing downward pressure on the middle of the egg. The egg shell will gently crack open, and when it is fully split quickly pull the two egg shell halves apart and lay the yolk and its attached embryo in the base of the weigh boat. The fertilization rate will vary depending on the hatchery. Discard unfertilized eggs and reuse weigh boats for other fertilized eggs.

Critical step: To determine whether the embryo is viable, look for a coin shaped red structure on top of the yellow yolk. A beating heart should be observed, which indicates the embryo is alive. Ensure that the yolk is not pierced and that it remains intact immediately after eff shell cutting and splitting. If the yolk is broken open and leaks into the albumin, the chances of mortality considerably increase.

8. Place a transparent square plastic Petri dish cover over the weigh boat that contains the *ex ovo* embryo (**Figure 6c**). Repeat Steps 5–8 for additional eggs as required by the experiment.

Critical step: Although it is possible to reuse weight boats and the transparent lids, they must be washed and sterilized by being sprayed down with 70% ethanol. Omitting this sterilization step increases the risk of contamination.

Pause point: It is best to crack 8-10 eggs at a time before pausing between cuts. Pauses can last anywhere between 10s and 5min.

9. Place fully enclosed embryos into larger plastic containers for transport and storage.

*Critical step: The Rubbbermaid plastic containers must be laid out with six of the transparent square lids and then filled with 200 mL of dH$_2$O. Each container can hold 18 embryos in stacks of three (**Figure 6d**)*

10. Place the containers with embryos into an egg incubator (**Figure 6e**) set at 39 °C with >70% relative humidity with no rocking. If eggs are cracked 4 d after fertilization, incubate the embryos for another 5 d until they are at embryonic day 9.

*Critical step: The base of each container (with a maximum of 18 embryos) must be refilled every day with enough water to cover the bottom of the container. Do not overfill with water, because during shifting of embryos water can enter the inner chamber of the weigh boats and kill the embryos (**Table 2**).*

2.2.2 Preparation of cancer cells for injection

Timing 1–3 h

Critical 1: For optimal counting, perform Steps 11-22 in the morning so that counting can be performed in the early afternoon.

Critical 2: Do not perform experiments with cells grown to full confluency, as they may not extravasate at the same rate as cancer cell lines grown to ~80-90% confluency.

11. Take the T75 flask containing cells grown to ~80–90% confluency and discard the medium into a flask containing 20% bleach, and quickly fill the flask with enough Dulbecco's PBS (D-PBS) to cover the flask surface. Discard D-PBS into the flask containing 20% bleach and repeat this washing step twice.

Critical step: Do not use pipettes or aspiration to remove the medium, because the cells will be exposed to air in the short amount of time needed to aspirate D-PBS. Instead, quickly discard the used medium and quickly fill the flask with D-PBS to wash off any leftover medium. If cells are exposed to air during the wash steps, it will noticeably affect cell viability upon i.v. injection.

12. At the last wash step, discard D-PBS and immediately add 2 mL of 0.05% Trypsin with 0.053 mM EDTA. Ensure even distribution of Trypsin + EDTA (or EDTA for controls) across the entire flask surface that has the cancer cell monolayer. Incubate this flask at 37 °C for 5–8 min. Using an inverted light microscope, ensure that all the cells have 'lifted' off before proceeding.

Critical step: Cell culture techniques for the preparation of cells for injection are cell-line-specific. If the goal is to avoid using Trypsin to harvest cells for use in the extravasation assay, then use EDTA to prepare cells and use 2 mL of 5 mM EDTA in PBS and let it sit for 2 min. Remove EDTA and tap the plate/flask to dislodge cells.

Critical step: Do not leave the cells in Trypsin for more than 15 min; otherwise, receptors and proteins on the cell membrane will be cleaved, making comparisons between groups uncontrolled.

13. Add 7 mL of D-PBS to the flask, collect all cells and transfer them to a sterile 15-mL Falcon tube. Add another 5 mL of D-PBS to the flask to collect all residual cells and add to the 15-mL Falcon tube.

14. Centrifuge the cells at 200 xg for 10 min at room temperature (25 °C). After centrifugation, carefully remove the supernatant and discard it. Add 10 mL of D-PBS and resuspend using a 10-mL-capacity pipette. Centrifuge the cells at 200 xg for 10 min at room temperature. (**Table 2**).

15. After centrifugation, carefully remove the supernatant and discard it. Using a P1000 micropipette, add 1 mL of D-PBS to the cell pellet and resuspend the cells very slowly and gently. The cell pellet will break up into smaller portions, and when drawn into the pipette tip these pieces may become lodged against the side of the pipette tip. To prevent this, gently disturb the cell pellet by shooting the D-PBS into the cell pellet so that smaller fragments are released into the D-PBS.

16.Transfer this cell suspension into a 1.5-mL Eppendorf microcentrifuge tube. With an unused tip, add 0.5 mL of D-PBS to the 15-mL Falcon tube, and then retrieve all residual cells and transfer them to the 1.5-mL tube containing the rest of the cells. Centrifuge this tube at 200 xg for 10 min at room temperature. Remove the supernatant by aspiration and gently resuspend the cell pellet in 1.0 mL of D-PBS.

17. If the cells are already fluorescently labeled, then proceed to Step 19. If not, you will need to label the cells with CellTracker dye at this step. Add 2 μL of diluted CellTracker dye to the cell suspension and mix the entire cell suspension for 10 sec. Leave it on ice for 10 min in the dark. The CellTracker dye will remain bound to the cells for the next 24 h.

18. Centrifuge the cell suspension at 200 xg for 10 min at room temperature. Gently remove the supernatant and resuspend the cell pellet in 1.0 mL of D-PBS. Repeat this wash step.

19. Use a hemocytometer or automated cell-counting machine to determine the concentration of cells in 10 μL of the washed cell suspension. Dilute the cells to 5.0×10^5 cells per mL with D-PBS.

Critical step: If the cell concentration is >5.0 x 10^5 cells per mL, clogs may appear in the needle. If the cell concentration is <5.0 x 10^5 cells per mL, the low density of cells may prevent analyses from reaching sufficient statistical power.

20. If an inhibitory antibody, peptide or ligand is to be evaluated, incubate the diluted cells with the antibody/peptide/ ligand for 15 min in the dark at room temperature. After incubation, repeat Step 19 twice to wash the cells. Dilute the cells to their original volume.

21. Once diluted, keep the diluted cells on ice until i.v. injection into the CAM veins of the chicken embryos (**Table 2**).

Pause Point: The cells can be left on ice for up to 2 h.

2.2.3   i.v. Injection of cancer cells into CAM veins

Timing 1 h, 2–10 min for injection per embryo

22. Assemble the microinjector (**Figure 6f**) by fitting an 18-gauge needle onto a 1-mL syringe. Cut a 5–6-inch piece of Tygon tubing and carefully insert the bevel of the needle into the bore of the tubing. Slowly slide the tubing all the way onto the rest of the needle.

23. Draw 400–500 μL of cell suspension into the microinjector via the tip of the tubing. With the needle facing upward, push the plunger to expel air from the barrel of the syringe. Take care to prevent loss of cancer cells.

Critical step: Be careful not to inject air, as it will kill the embryo.

24. After drawing the cells and eliminating air from the microinjector, add a glass needle (**Figure 6f, g**) that has been altered to have a larger bore.

*Critical step: Ensure that the bore size of the needle is not too narrow. If it is too narrow, cells will clump within the needle and form a clog. To dislodge the clog, pull back the plunger and mix the cell suspension several times with the plunger, and then fill the tubing and glass needle with cell suspension (**Table 2**).*

25. By using a dissecting scope with white-light illumination, place a day 13 embryo onto the stage and locate any small vessels that appear to be bright red (**Figure 7a**). These small vessels are veins, and they carry oxygenated blood back to the embryo because the CAM acts as the 'lung' of the embryo. Vessels with darker red blood are arteries.

*Critical step: Do not inject into arteries and do not inject into large-diameter veins (**Figure 7a**), because blood coagulation will take longer in these injection sites and the embryo will die as a result of excessive blood loss.*
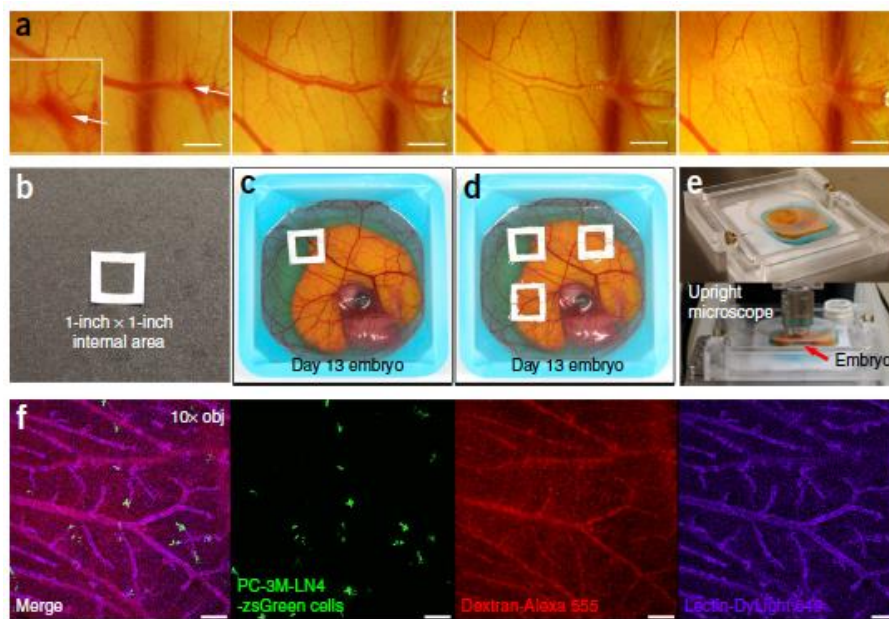
Figure 7: i.v. injections of cells or lectin and setting up the extravasation efficiency assay. (a) The microinjector is used to deliver 10–100 μL of cells or diluted labeling agents i.v. into the CAM. Initial penetration of the needle should result in the release of blood onto the surface of the CAM, analogous to a 'bloom' of blood (far left panel, arrows). Slow injection rate will result in a clear stream of fluid in the vessel (second panel from left), and faster injection rate will result in almost full (second panel from right) to full perfusion of the vessel (far right). Scale bars, 3 mm. (b–e) After injection of cancer cells or labeling agents (a), 1-inch square foils are prepared (b) and placed on day 13 embryos. The experimenter can lay a single square foil ROI per embryo (c) or three of them in a single embryo (d). The embryo is then placed into the chicken incubator unit in which a lid that contains a coverslip is positioned over the square foil ROI (e, top panel). A confocal upright microscope is used to perform intravital imaging to enumerate intravascular cells or extravasated cells (e, bottom panel). (f) When various other labeling agents are injected,

such as lectin-DyLight 649 (purple), which labels the endothelial cell walls or vessels, and Dextran-Alexa 555 (red), which will reveal the vessel lumen space where blood flow occurs, they can help the investigator determine whether their cancer cells (PC-3M-LN4; green) are intravascular, and when using a lower magnification objective (10x) the cancer cell density throughout the CAM can be determined before extravasation efficiency analysis. Obtaining consistent cancer cell density is important for obtaining consistent results across different embryos. Scale bars, 25 μm.

26. Glide the bore of the needle along the vein and traverse back and forth along it, until the bore of the needle catches the CAM. Once this occurs, immediately halt the movement of the needle and slowly raise the CAM by gently raising the needle (the CAM should pull up with the glass needle into the shape of a pitched tent). Gently keep the CAM lifted upward until a small 'bloom' of blood is seen to pop out underneath the needle (**Figure 7a** inset in far-left panel).

*Critical step: Remain patient when you are performing this step. The glass needle will eventually pierce the CAM, releasing a very small amount of blood (**Table 2**).*

27. When this 'bloom' of blood is observed, slowly drop the CAM and then lightly press the plunger of the syringe. Clear fluid should enter the vessel of the CAM and flow toward the body of the embryo.

28. Take notice of the volume markings and press down on the plunger in a light pulsatile manner until 100 μL of cell suspension is injected.

*Critical step: If the needle is not cannulated within the vein, some cell suspension fluid will leak out. If this occurs, lightly push the needle upward and toward the embryo and then apply pressure to the plunger (**Table 2**).*

29. After the cell suspension has been injected, remove the needle and then use rolled-up Kimwipe to absorb all blood and cell suspension from the site of injection. This rolled-up Kimwipe is gently laid over the injection site until the blood is soaked up.

Critical step: Do not press the Kimwipe into the CAM.

30. Apply 2–3 foil windows to the surface of the CAM at sites away from the injection site (**Figure 7b–d**).

Critical step: Ensure that the foil windows completely adhere to the CAM surface.

31. Repeat Steps 23–31 for each embryo according to the needs of the experiment. For each drug treatment or cell line, use N > 4–10 embryos for each group.

2.2.4 Extravasation efficiency data collection using wide-field fluorescence microscopy

Timing: 24 h, 5 min per embryo at T = 0 and T = 24 h

Critical step: When you are performing an extravasation efficiency experiment, always rely on N > 4–10 for each treatment/cohort/cell type. In the event that 1–2 animals die after the T = 0 injection of cancer cells, there will at least be N = 3–7 per group for analysis.

32. By using a wide-field fluorescence microscope and the 10x objective, count all the cells within each foil window immediately after injection. The distribution of cancer cells across the CAM should resemble the density seen in **Figure 3f**. All cells at this time point (T = 0) are intravascular and have not extravasated into the stroma/tissue.

*Critical step: Ensure that counting of all cells occurs within 1 h of Step 30 (**Table 2**).*

33. Ensure that each foil window is counted and record the number of cells enumerated at T = 0 on the plastic square Petri dish, directly over each individual foil window.

Critical step: Ensure that the T = 0 number is written directly over the foil window with an alcohol-resistant felt marker when the lid is placed back on the weigh boat containing the embryo.

34. Place all embryos back in the incubator and incubate for 24 h. (**Table 2**)

35. After 24 h of incubation, either follow option A to use the wide-field fluorescence microscope to analyze extravasation efficiency or follow option B to use the confocal microscope to measure intravascular and extravasated cells. In addition, it is possible to perform option B after option A.
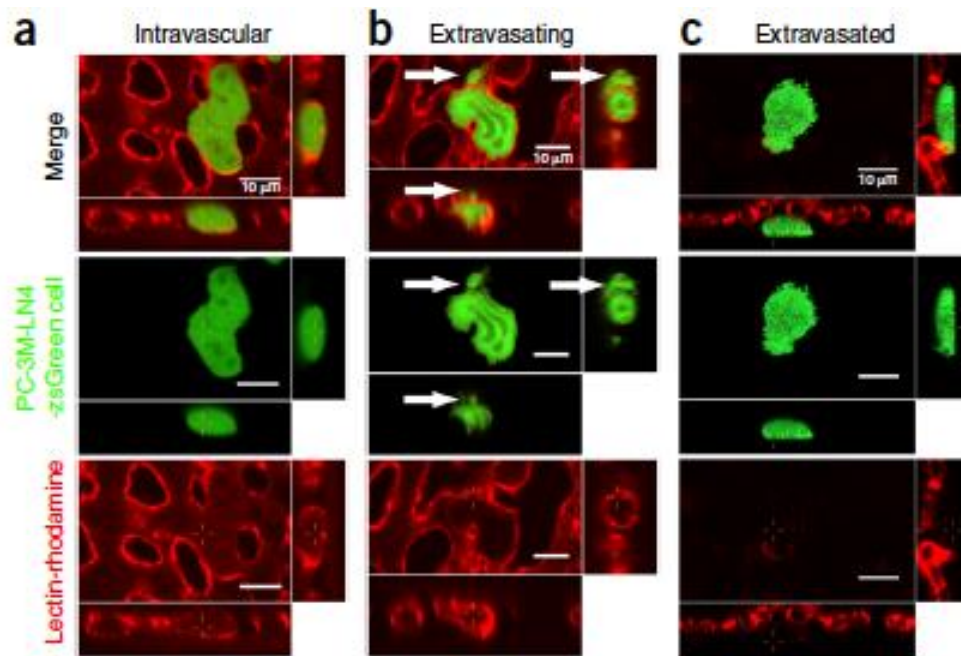
Figure 8: Distinguishing intravascular and extravascular cancer cells in the CAM. (a–c) By using lectin-rhodamine (red), one can easily determine whether cells (green CellTracker dye) are present within the intravascular space (a), in the process of extravasation (b) or extravasated (c). Lectin- rhodamine binds to the glycocalyx present on the luminal surface of endothelial cells. White arrows point to parts of the cell that have breached the endothelial layer. Scale bars, 10 μm.

2.2.5 Analysis of extravasation efficiency

Data-timing 1h

(i) Use the side-field fluorescence microscope to count the number of the cells within each foil window in each embryo as in step 32.

(ii) Record each value on the lid of each embryo and ensure that each value corresponds to each foil window as written at T=24.

(iii) After counting the number of intravascular and extravascular cancer cells present in each window at T=0 and T=24 after i.v. injection of cancer cells, divide the number of extravasated cells at T=24 h by the number of intravascular cells at T = 0 h (**Figure 8a**). If cells in the process of extravasation are observed (**Figure 8b**), do not count them as extravasated and consider them as intravascular cancer cells.

(iv) Calculate mean extravasation efficiencies for all foil windows in the embryos, as shown in **Figure 9**.
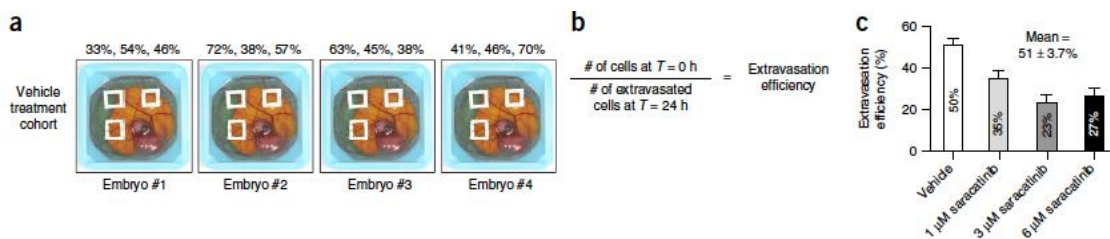
Figure 9: Representative schematic of how an extravasation efficiency assay is performed. (a) Shown is a representative set of embryos (N = 4) injected with cancer cells treated overnight with control vehicle. Three foil ROIs are placed per embryo, and the percentage of cells that successfully extravasate as quantified by wide-field fluorescence microscopy in each of the foil windows is shown above the embryo. (b) Basic calculation of extravasation efficiency as determined for each foil placed on all embryos. (c) Representative data set for PC-3M-LN4 cells pretreated overnight with saracatinib (1, 3 and 6 μM) with no recovery time prior to injection, with underlying data presented in supplementary Data 1. Error bars represent s.e.m.

2.2.6 Confocal microscopy of intravascular versus extravasated cells

Timing: 30 min per embryo

(i) Inject 75 µL of diluted lectin-rhodamine with a microinjector as described in Steps 22–29. The purpose of this step is to determine how many cells are left in the intravascular space, as determined by lectin staining.

Critical step: Only inject the lectin-rhodamine (do not inject any cancer cells), which will label all the endothelial cells of the CAM.

(ii) Wait for 5 min after injection of lectin-rhodamine to perform confocal microscopy.

(iii) Place the injected embryo in the imaging chamber (**Figure 7e**) and place the lid of the imaging chamber such that the coverslip is situated directly over one of the foil windows. The CAM within the foil window will adhere tightly to the coverslip of the imaging chamber lid.

Critical step: Do not press the lid too deeply into the CAM. The coverslip of the imaging chamber lid should be at the same height as the rest of the CAM.

(iv) Place the imaging chamber underneath the 60x objective on a confocal microscope. Using detection protocols for green and red fluorescence signal, use confocal microscopy to determine whether the cells are within the red vasculature (lectin-rhodamine) or whether they have extravasated (in which case the plane of vessels will lie above individual extravasated cells). Determine the proportion of cells that remain in the intravascular space (**Figure 8a–c**). If <5% of all cells are intravascular, collect extravasation efficiency data for the rest of the embryos using wide-field fluorescence microscopy (the high-throughput method most commonly used for determining extravasation efficiency in cancer cells). If >5% of cells remain in the intravascular space at T = 24 h after injection, re-evaluate at 36 h after extravasation. If <5% of cells are then intravascular, perform wide-field fluorescence microscopy, with the assumption that any cells observed in the foil window are extravasated cells.

Critical step: Do not exceed T > 36 h after injection. After 36 h, cell counts may be false (a fraction of these cells may have divided after extravasation).

(v) Dispose of all used and unused embryos by storing at −20 °C overnight before biohazard disposal (**Table 2**).

Troubleshooting advice can be found in **Table 2**.

2.3 Timing

Steps 1 and 2, receiving fertilized eggs and first incubation period: 4–8 d

Steps 3–10, preparation of *ex ovo* embryos: Steps 3 and 4 are 30 min, 5 min for cracking 18 eggs Steps 11–21, preparation of cancer cells for injection: 1–3 h

Steps 22–31, i.v. injection of cancer cells into CAM veins: 1 h, 2–10 min for injection per embryo

Steps 32–34, extravasation efficiency data collection using wide-field fluorescence microscopy: 24 h, 5 min per embryo at T = 0 and T = 24 h

Step 35A, analysis of extravasation efficiency data: 1 h

Step 35B, confocal microscopy of intravascular versus extravasated cells: 30 min per embryo

2.4 Anticipated results

A representative experiment in which a Src kinase inhibitor, saracatinib, is used to pretreat PC-3M-LN4-zsGreen cells overnight at various concentrations (0, 1 μM, 3 μM and 6 μM) is shown in **Figure 9**. To determine the mean extravasation rate, we average all extravasation efficiencies in all windows placed on all embryos. The mean value represents the extravasation efficiency for the treatment group/cohort/cell type for the experiment.

We do not perform mean calculations of extravasation efficiencies that are specific for each embryo before determining the mean extravasation rates between embryos. Instead, we consider the results attained for all foil windows as individual experiments and not specific to the embryo. We have found that pooled analyses are more representative of the variability between animals regardless of any variability among cells injected between embryos, because the density of intravascular cells does not affect extravasation rates. In our experience, most of the cells present in the CAM at T = 24 h after injection have extravasated, with only <5% of cells visualized in the foil ROI window still present in the intravascular space of the CAM and not yet extravasated. However, it is not well understood whether these cells are still viable or whether they are in the process of apoptotic cell death. When the experimenter is sufficiently trained and skilled (in terms of injection efficiency and post-injection embryo viability rates), the number of cells present in the ROI at T = 24 h accurately reflects the extravasation rate. It can be assumed that these cells have successfully extravasated into the stromal space, an act of invasion that is requisite for survival and subsequent proliferation before successful formation of a metastatic colony *in vivo*.

Step	Problem	Possible reason	Solution
10	Embryos die 1–3 d after cracking	Contaminated cutting disc	Spray the disc with 70% ethanol in between egg cracks to minimize contamination
		Water entering the weigh boats	Lower the amount of water added to each rubbermaid container
		Embryos not kept at 22 °C before incubation at 39 °C	Do not allow eggs to be stored at any other temperature
		Incubator not at 39 °C and not at >70% relative humidity	Fix the incubator and all associated parts
		Incubator is the source of contamination	Wash and spray down all components of the incubator with 70% ethanol

(continued)

Step	Problem	Possible reason	Solution
14	Cells remain clumped after centrifugation, resembling a 'cloud' of cells	Cells were left in Trypsin for too long	Minimize the amount of time cells are incubated with Trypsin
		Cells were exposed to air during washing and Trypsin process	Wash cells using the technique described in Step 12. Quickly add Trypsin to cells in Step 13 and minimize the amount of time cells are exposed to air
17	Cells are not green	CellTracker dye is not functional (e.g., expired, exposed to air, not stored properly, did not use the correct diluent)	Purchase new CellTracker dye
21	Cells are clumped	Cells were left too long in the syringe	Eject all cells out of the microinjector into a sterile tube. Using a P1000/P200 micropipette, resuspend the cells gently. Assemble a new microinjector and attempt injections again
24	Needle is clogged	Glass needle bore is too narrow	Eject all cells out of the microinjector into a sterile tube. Using a P1000/P200 micropipette, resuspend the cells gently. Assemble a new microinjector and ensure that a glass needle with a wider bore is used
26 & 28	Cannot inject cells into the vessel	Needle bore is too large	Remove the glass needle and discard it. Make a new glass needle and ensure that it is sharper than the previous one, but do not make the needle too sharp, or the cells will be unable to exit the needle bore and will form a clog
		Cells are clumped	Eject all cells out of the microinjector into a sterile tube. Using a P1000/P200 micropipette, resuspend the cells gently. Assemble a new microinjector and attempt injections again
		Piercing through the CAM	When approaching the CAM, ensure that the needle is no more than 30° above the CAM surface. Approaching the CAM perpendicularly will increase the likelihood of puncturing the CAM
		Vessel chosen is too difficult to approach with the needle	Select another vessel, preferably one that is parallel to the weigh boat wall
		Portion of CAM is too wet	The CAM may be wet because of repeated attempts at that vessel with the release of PBS left on the CAM. This fluid will prevent the needle from 'snagging' or 'catching' the CAM
		CAM is too tough and thick	Choose another portion of the CAM away from the embryo and closest to the wall of the weigh boat. Typically, vessels closest to the weigh boat wall are easiest to inject into. Vessels directly over the embryo are the hardest to inject into
		Injected too many cells or reagent	If more than 150 µl of cell solution is injected, blood flow will stop and it will be difficult to inject more cells at that point. Reattempt in a new embryo if >150 µl of cell solution has been injected but no green cells appear in the CAM

32	Unsure of what a cell is	Only enumerate large fluorescent objects	Refer to **Figure 4a** for examples of intravascular cells. Avoid enumeration of microparticles or dead cells
		Inject fewer cells	Dilute the cells from 5×10^5 cells per ml to 1×10^5 cells per ml. This will aid the experimenter in determining what a cell is if the cells are aggregating in the vessels of the CAM
		Loss of focus on cells	Use a confocal microscope to help determine whether the cells are in focus or not by relying on the lectin-rhodamine signal to locate the Z-plane of the CAM's capillary bed
		Cells on the CAM	If cells are found on two different planes, it means that during the injection some cells were ejected onto the CAM. Remove foil window and enumerate other windows. Ensure that the foil windows are placed away from sites of attempted injections

(continued)

Step	Problem	Possible reason	Solution
34	Embryos have died after injection	Too many cells injected	Dilute the cells from 5×10^5 cells per ml to 1×10^5 cells per ml. This will aid the experimenter in determining what a cell is if the cells are aggregating in the vessels of the CAM
		Drug is too toxic	Decrease the concentration of drug used to pretreat cells or co-injected with cells at $T = 0$
		Embryos were left out at room temperature for too long	Use a heating pad to keep the embryos warm during injections at $T = 0$. Also use a heating pad to keep the embryos warm during enumeration at $T = 0$ and $T = 24$ h
35A(ii)	Cells are fluorescent but not clear	Cells have extravasated	If the fluorescence of the cells appears fuzzy, it is because of light scattering through the hemodynamically active CAM. This is a good sign that the cell has extravasated. Include this cell as extravasated
		Signal is punctate and small	Do not include this event as an extravasated cell. It is probably the remnant of a dead cell or microparticle

Table 2: Troubleshooting, tips and solutions

2.5   References

1. Chambers, A.F., Groom, A.C. & MacDonald, I.C. Dissemination and growth of cancer cells in metastatic sites. Nat. Rev. Cancer 2, 563–572 (2002).

2. Giampieri, S. et al. Localized and reversible TGFbeta signalling switches breast cancer cells from cohesive to single cell motility. Nat. Cell Biol. 11, 1287–1296 (2009).

3. Wyckoff, J.B., Jones, J.G., Condeelis, J.S. & Segall, J.E. A critical step in metastasis: *in vivo* analysis of intravasation at the primary tumour. Cancer Res. 60, 2504–2511 (2000).

4. Zijlstra, A., Lewis, J., Degryse, B., Stuhlmann, H. & Quigley, J.P. The inhibition of tumour cell intravasation and subsequent metastasis via regulation of *in vivo* tumour cell motility by the tetraspanin CD151. Cancer Cell 13, 221–234 (2008).

5. He, W., Wang, H., Hartmann, L.C., Cheng, J.-X. & Low, P.S. *In vivo* quantitation of rare circulating tumour cells by multiphoton intravital flow cytometry. Proc. Natl. Acad. Sci. USA 104, 11760–11765 (2007).

6. Menen, R.S. et al. A rapid imageable *in vivo* metastasis assay for circulating tumour cells. Anticancer Res. 31, 3125–3128 (2011).

7. Patsialou, A. et al. Intravital multiphoton imaging reveals multicellular streaming as a crucial component of *in vivo* cell migration in human breast tumours. Intravital 2, e25294 (2013).

8. Stoletov, K. et al. Visualizing extravasation dynamics of metastatic tumour cells. J. Cell Sci. 123, 2332–2341 (2010).

9. Leong, H.S. et al. Invadopodia are required for cancer cell extravasation and are a therapeutic target for metastasis. Cell Rep. 8, 1558–1570 (2014).

10. Barkan, D., Green, J.E. & Chambers, A.F. Extracellular matrix: a gatekeeper in the transition from dormancy to metastatic growth. Eur. J. Cancer 46, 1181–1188 (2010).

11. Barkan, D. et al. Inhibition of metastatic outgrowth from single dormant tumour cells by targeting the cytoskeleton. Cancer Res. 68, 6241–6250 (2008).

12. Rondeau, G. et al. Effects of different tissue microenvironments on gene expression in breast cancer cells. PLoS One 9, e101160 (2014).

13. Bartkowiak, K., Riethdorf, S. & Pantel, K. The interrelating dynamics of hypoxic tumour microenvironments and cancer cell phenotypes in cancer metastasis. Cancer Microenviron. 5, 59–72 (2012).

14. Cameron, M.D. et al. Temporal progression of metastasis in lung: cell survival, dormancy, and location dependence of metastatic inefficiency. Cancer Res. 60, 2541–2546 (2000).

15. Paku, S., Döme, B., Tóth, R. & Timár, J. Organ-specificity of the extravasation process: an ultrastructural study. Clin. Exp. Metastasis 18, 481–492 (2000).

16. Luzzi, K.J. et al. Multistep nature of metastatic inefficiency: dormancy of solitary cells after successful extravasation and limited survival of early micrometastases. Am. J. Pathol. 153, 865–873 (1998).

17. Schlüter, K. et al. Organ-specific metastatic tumour cell adhesion and extravasation of colon carcinoma cells with different metastatic potential. Am. J. Pathol. 169, 1064–1073 (2006).

18. Arpaia, E. et al. The interaction between caveolin-1 and Rho-GTPases promotes metastasis by controlling the expression of alpha5-integrin and the activation of Src, Ras and Erk. Oncogene 31, 884–896 (2012).

19. MacMillan, C.D. et al. Stage of breast cancer progression influences cellular response to activation of the WNT/planar cell polarity pathway. Sci. Rep. 4, 6315 (2014).

20. Cvetkovic, D. et al. KISS1R induces invasiveness of estrogen receptor-negative human mammary epithelial and breast cancer cells. Endocrinology 154, 1999–2014 (2013).

21. Veiseh, M. et al. Cellular heterogeneity profiling by hyaluronan probes reveals an invasive but slow-growing breast tumour subset. Proc. Natl. Acad. Sci. USA 111, E1731–E1739 (2014).

22. Rytelewski, M. et al. BRCA2 inhibition enhances cisplatin-mediated alterations in tumour cell proliferation, metabolism, and metastasis. Mol. Oncol. 8, 1429–1440 (2014).

23. Weiss, L., Mayhew, E., Rapp, D.G. & Holmes, J.C. Metastatic inefficiency in mice bearing B16 melanomas. Br. J. Cancer 45, 44–53 (1982).

24. Morris, V.L. et al. Mammary carcinoma cell lines of high and low metastatic potential differ not in extravasation but in subsequent migration and growth. Clin. Exp. Metastasis 12, 357–367 (1994).

25. Hill, R.P., Chambers, A.F., Ling, V. & Harris, J.F. Dynamic heterogeneity: rapid generation of metastatic variants in mouse B16 melanoma cells. Science 224, 998–1001 (1984).

26. Ebos, J.M.L. et al. Accelerated metastasis after short-term treatment with a potent inhibitor of tumour angiogenesis. Cancer Cell 15, 232–239 (2009).

27. Pàez-Ribes, M. et al. Antiangiogenic therapy elicits malignant progression of tumours to increased local invasion and distant metastasis. Cancer Cell 15, 220–231 (2009).

28. Eckert, M.A. et al. Twist1-induced invadopodia formation promotes tumour metastasis. Cancer Cell 19, 372–386 (2011).

29. Artym, V.V., Zhang, Y., Seillier-Moiseiwitsch, F., Yamada, K.M. & Mueller, S.C. Dynamic interactions of cortactin and membrane type 1 matrix metalloproteinase at invadopodia: defining the stages of invadopodia formation and function. *Cancer Res.* **66**, 3034–3043 (2006).

30. Albini, A. & Benelli, R. The chemoinvasion assay: a method to assess tumour and endothelial cell invasion and its modulation. *Nat. Protoc.* **2**, 504–511 (2007).

31. Albini, A. & Noonan, D.M. The 'chemoinvasion' assay, 25 years and still going strong: the use of reconstituted basement membranes to study cell invasion and angiogenesis. *Curr. Opin. Cell Biol.* **22**, 677–689 (2010).

32. Reymond, N., Riou, P. & Ridley, A.J. Rho GTPases and cancer cell transendothelial migration. *Methods Mol. Biol.* **827**, 123–142 (2012).

33. Sequeira, L., Dubyk, C.W., Riesenberger, T.A., Cooper, C.R. & van Golen, K.L. Rho GTPases in PC-3 prostate cancer cell morphology, invasion and tumour cell diapedesis. *Clin. Exp. Metastasis* **25**, 569–579 (2008).

34. Wendel, C. *et al.* CXCR4/CXCL12 participate in extravasation of metastasizing breast cancer cells within the liver in a rat model. *PLoS One* **7**, e30046 (2012).

35. Gassmann, P. *et al.* CXCR4 regulates the early extravasation of metastatic tumour cells *in vivo*. *Neoplasia* **11**, 651–661 (2009).

36. Cao, Y. *et al.* Neuropilin-2 promotes extravasation and metastasis by interacting with endothelial β5 integrin. *Cancer Res.* **73**, 4579–4590 (2013).

37. Barthel, S.R. *et al.* Definition of molecular determinants of prostate cancer cell bone extravasation. *Cancer Res.* **73**, 942–952 (2013).

38. Kargozaran, H. *et al.* A role for endothelial-derived matrix metalloproteinase-2 in breast cancer cell transmigration across the endothelial-basement membrane barrier. *Clin. Exp. Metastasis* **24**, 495–502 (2007).

39. Voura, E.B. *et al.* Proteolysis during tumour cell extravasation in vitro: metalloproteinase involvement across tumour cell types. *PLoS One* **8**, e78413 (2013).

40. Tokui, N. *et al.* Extravasation during bladder cancer metastasis requires cortactin-mediated invadopodia formation. *Mol. Med. Rep.* **9**, 1142–1146 (2014).

41. Sutoh Yoneyama, M. *et al.* Vimentin intermediate filament and plectin provide a scaffold for invadopodia, facilitating cancer cell invasion and extravasation for metastasis. *Eur. J. Cell Biol.* **93**, 157–169 (2014).

42. Freeman, S.A. *et al.* Preventing the activation or cycling of the Rap1 GTPase alters adhesion and cytoskeletal dynamics and blocks metastatic melanoma cell extravasation into the lungs. *Cancer Res.* **70**, 4590–4601 (2010).

43. Leong, H.S. et al. Intravital imaging of embryonic and tumour neovasculature using viral nanoparticles. Nat. Protoc. 5, 1406–1417 (2010).

44. Nowak-Sliwinska, P. et al. Angiostatic kinase inhibitors to sustain photodynamic angio-occlusion. J. Cell. Mol. Med. 16, 1553–1562 (2012).

45. Jeon, J.S., Zervantonakis, I.K., Chung, S., Kamm, R.D. & Charest, J.L. In vitro model of tumor extravasation. PLoS. One. 8, e56910 (2013).

46. Chen, M.B., Whisler, J.A., Jeon, J.S. & Kamm, R.D. Mechanisms of tumour cell extravasation in an in vitro microvascular network platform. Integr. Biol. (Camb). 5, 1262–1271 (2013).

47. Kramer, R.H. & Nicolson, G.L. Interactions of tumour cells with vascular endothelial cell monolayers: a model for metastatic invasion. Proc. Natl. Acad. Sci. USA 76, 5704–5708 (1979).

48. Liu, L. et al. A microfluidic device for continuous cancer cell culture and passage with hydrodynamic forces. Lab Chip 10, 1807–1813 (2010).

49. Goulet, B. et al. Nuclear localization of maspin is essential for its inhibition of tumour growth and metastasis. Lab. Invest. 91, 1181–1187 (2011).

50. Leong, H.S. et al. Imaging the impact of chemically inducible proteins on cellular dynamics *in vivo*. PLoS One 7, e30177 (2012).

51. Leong, H.S., Chambers, A.F. & Lewis, J.D. Assessing cancer cell migration and metastatic growth *in vivo* in the chick embryo using fluorescence intravital imaging. Methods Mol. Biol. 872, 1–14 (2012).

52. Koop, S. et al. Independence of metastatic ability and extravasation: metastatic ras-transformed and control fibroblasts extravasate equally well. Proc. Natl. Acad. Sci. USA 93, 11080–11084 (1996).

53. Jilani, S.M. et al. Selective binding of lectins to embryonic chicken vasculature. J. Histochem. Cytochem. 51, 597–604 (2003).

Chapter 3

3 Necroptosis Mediates Cancer Cell Extravasation and Metastasis throughout Cancer Cell Extracellular Vesicle Release

Contents of this chapter are currently under consideration of publication in *Cell Death and Differentiation*.

3.1 Introduction

Metastasis is the most lethal stage of cancer, contributing to over 90% mortality in cancer patients[1]. The most invasive cancers such as prostate cancer metastasize to several distant organs or tissues including the bone, brain, and lungs. Invasive cancer proceeds in metastasis through multiple cellular events and signaling pathways. For example, metastasis is comprised of different steps and each step is controlled by several cellular molecular pathways[2,3]. As such, a multipronged approach is required to effectively halt tumour metastasis[4]. Therefore, elucidating the underlying cellular and molecular processes involved in different cellular events and signaling pathways in metastasis is urgently needed.

To succeed in metastasis, single tumour cells must leave the primary tumour bed and proceed through the metastatic cascade[2,3]. Leaving tumour cells enter the circulation (intravasation), survive in the blood and lymphatic streams, arrest at a distant site, then escape into the stromal space of a secondary organ (extravasation) to form a colony[2]. Recently, inhibition of extravasation has been suggested to be detrimental to cancer cell surviving in the extracellular milieu, indicating that extravasation is a limiting step in the metastatic cascade[3]. Although this study points to extravasation as a realistic target in stopping cancer metastasis, other pre-existing underlying cellular mechanisms have also been loosely explored. Hoshino *et al.* and Sung *et al.* showed that extravasating cancer cells release extracellular vesicles (EVs) into the extracellular space[5,6]. EVs originate heterogeneously from multivesicular bodies, and may include microparticles, exosomes, oncosomes, and apoptotic bodies along a wide-size spectrum. While it is believed that cancer cell EVs may have a functional role in cancer progression, the significance and

potential role of EV release during extravasation have yet to be elucidated. Headley *et al*. recently showed that extravasated melanoma B16F10 cells decreased in size 24 hours after injection compared to cells at 2 hours after injection[9]. These studies suggest that EV release may potentially be involved in cancer cell extravasation. Here, we investigated the potential role of EV release in prostate cancer cell volume regulation during extravasation and whether potential cell volume changes modulate metastatic potential.

One cellular event that may regulate EV release is cell death. Programmed cell death processes induce cell membrane blebbing to maneuver EV biogenesis. It has also been demonstrated that necroptosis, a form of programmed necrosis, induces intravascular cancer cell death in a receptor-interacting serine/threonine-protein kinase 3 (RIPK3)- and mixed lineage kinase domain-like (MLKL)-dependent manner. Gong *et al*. showed that MLKL is directly involved in the scrambling of the plasma membrane to expose phosphatidylserine (PS) and membrane bleb formation and release, which are distinct from apoptotic blebs[7]. Regardless of the morphology of cells during necrosis and the secretion of intracellular contents, the process of necroptosis allows the formation of membrane blebs and induces EV release.

In this study, we investigated the biophysical function of EV release during cancer cell extravasation as a measure of the metastatic efficiency of cancer cells. We discovered that EV release led to significant cell volume reduction after extravasation, suppressing extravasation and secondary colony formation rates. Thus, our results suggest that a reduction in cell volume by EV release facilitates cancer cell extravasation at the cost of reduced efficiency in forming secondary colonies. Our results also show that necroptosis may potentially serve as a target to module EV generation, cell volume reduction, extravasation, and secondary colony formation.

3.2 Materials and methods

Cells culture and reagents

Human prostate cancer cell lines PC3 and PC-3M-LN4 (ATCC) were cultured and maintained in complete DMEM and RPMI media supplemented with 10% fetal bovine serum, respectively. All cells were routinely tested for mycoplasma contamination. To generate cells expressing green fluorescent proteins, vector pzsGreen-C1 (Clontech) was stably transfected into PC-3M-LN4 and PC-3 lines with XtremeGENE HP (Roche). Doxycycline-inducible MLKL-C-HA-3xFlag construct was kindly provided by Dr. Zhiago Wang at the University of Texas Southwestern Medical Center. Antibodies specific for phosphorylated MLKL (S358, ab187091) and MLKL (ab183770) were purchased from Abcam. RIPK3, MLKL, and caspases shRNA constructs were purchased from Dr. Jason Moffat and the Ontario Institute for Cancer Research (OICR) Genomics Facility. DyLight 649-Lectin conjugates (Lens Culinaris Agglutinin, Vector Laboratories), dextran-FITC (Sigma Aldrich), dextran-rhodamine B (ThermoFisher Scientific), wheat germ agglutinin-tetramethylrhodamine (ThermoFisher Scientific), and Hoechst (ThermoFisher Scientific) were diluted with 1x PBS (pH 7.4). Tumour necrosis factor- α (TNF-α; ThermoFisher Scientific) was diluted into 100 μg/mL with distilled water. Staurosporine (1285, STS, Tocris) and dimethyl fumarate (4512, DMF, Tocris) were diluted into 10 mM and 100 mM stocks, respectively, with DMSO. Necrostatin-1 (2324, Nec-1, Torcris) and Z-VAD-fmk (Abcam) were diluted into 50 mM and 10 mM stocks, respectively, with DMSO. pmAmetrine-DEVD-tdTomato was purchased from Addgene.

Quantification of CAM blood vessel permeability

To quantify blood vessel permeability of chorioallantoic membranes (CAMs) at different ages, dextran-FITC (150kDa) was injected using a microinjection needle into the CAMs of day 9, 13, and 18 chicken embryos. Real-time imaging of the CAM was performed using confocal microscopy at 0.5, 4, 6, 12, and 24 hours post-injection. Real-time imaging was performed as previously described[35]. To calculate the mean fluorescence intensity, the fluorescence of dextran-FITC channel in each picture was measured by ImageJ.

Quantification of cancer cell EV release *in vitro* and *in vivo*

To quantify cancer cell EV release *in vitro*, PC-3 zsGreen and PC-3M-LN4 zsGreen cancer cells were cultured in DMEM and RPMI complete media with 10% FBS and grown to 80%

confluency. Cells were cultured in serum-free medium (RPMI) with 5% exosome-depleted serum and treated for 24 h. Treatments included: DMSO (control), STS, TNF-α, ZVAD-fmk, TNF-α/ZVAD-fmk/Smac mimetic, DMF, and Nec-1. Conditioned media were pre-centrifuged for 5 minutes at 1000 x *g* to remove cells and only supernatant was collected. Samples from each well were analyzed immediately with nFC (Apogee Inc.) after collection or stored at -80 ºC. To quantify cancer cell EVs *in vivo*, PC-3 zsGreen and PC-3M-LN4-zsGreen cancer cells treated as indicated above were injected into the CAM of chicken embryos at day 9, 13, or 18. After 24 hours, blood samples were collected from the CAM of each chicken embryo and centrifuged for 30 minutes at 2,500 x *g* to isolate plasma from the blood samples. The plasma samples were tested immediately by nFC after collection or stored in -80ºC. Twenty µL of each condition media and plasma sample was added to 180 µL of PBS and analyzed by nFC.

In vitro and *in vivo* FRET imaging of cancer cell EV release and caspase-3 activity

To visualize the activation of caspase-3 in PC-3M-LN4 cancer cells *in vitro*, cells were stably transfected with pmAmetrine-DEVD-tdTomato (Addgene) by X-tremeGENE HP DNA transfection reagent (Roche) for 24 h, and then selected by neomycin (Thermo Fisher). pmAmetrine-DEVD-tdTomato-positive PC-3M-LN4 cells were resuspended in PBS, and injected into the CAM of day 13 chicken embryos. Real-time intravital FRET imaging of DEVD expressing cancer cells in the bloodstream was performed with an upright resonant laser scanning confocal microscope (Nikon Fast A1R+, 60x objective) as described previously[11]. Mean fluorescent intensity analysis of pmAmetrine and tdTomato expression was performed with Image J software.

In vivo extravasation efficiency and metastatic colony formation assay

The chicken CAM assay for *ex ovo* metastasis and extravasation efficiency was performed as previously described[35]. In brief, PC-3 and PC-3M-LN4 cells were grown to 80-90% confluency. PC-3 and PC-3M-LN4 cancer cells were then injected intravenously into the CAM of day 9, 13, or 18 embryos using a microinjector, and incubated in the 37 °C for 24 h. Intravascular and extravasated cells were counted in a marked area by an aluminum foil window (1 inch x 1 inch) at $T = 0$ h and $T = 24$ h using wide-field fluorescence microscopy

and 10x objective. At least 100 cells per region of interest were examined at $T = 0$ h. Extravasation efficiency of each group per embryo was calculated by dividing the number of extravasated cells at $T = 24$ h by the number of intravascular cells at $T = 0$ h. Then, mean extravasation efficiencies in the embryos were calculated. Metastatic colonies in each embryo were also counted by epifluorescence microscopy after an additional 7-day incubation post-extravasation efficiency analysis. The Z-stack images of cells in the bloodstream, in the course of extravasation and in the stroma were obtained by an upright resonant laser scanning confocal microscope (Nikon Fast A1R+, 60x objective), as described previously[11].

Induction and inhibition of cancer cell death processes

PC-3 and PC-3M-LN4 cancer cell line were treated with STS, TNF-α, TNF-α/ZVAD-fmk/Smac mimetic (TZS), or DMF. DMSO was used as a control. To inhibit apoptosis and necroptosis, cancer cells were treated with ZVAD-fmk and necrostatin-1, respectively. shRNA-mediated mRNA knockdown was also used to inhibit apoptotic and necroptotic processes. Knockdown efficiency was tested by immunostaining and immunoblotting of RIPK3 and MLKL.

Cancer cell EV isolation

PC-3 zsGreen cells were grown to 80% confluency in complete medium. Cells were then cultured in RPMI medium containing exosome-depleted FBS with DMSO (vehicle) and 100 μM of DMF for 48 h. The conditioned medium was collected and centrifuged at 1000 x g for 10 min to remove cellular debris and apoptotic bodies. The number of EVs (size >100 nm) was counted by nFC.

Immunoblotting

Each group of PC-3 zsGreen cells with different treatments were lysed in NP-40 (Invitrogen) with protease inhibitor cocktail (Thermo Fisher Scientific), then rotated for 30 mins at 4 °C. Supernatant was collected after a spin at 13000 x g for 30 minutes, and the protein concentration was determined by the BCA assay (Thermo Fisher Scientific). PC-3 zsGreen Cell and EV lysates were heated at 70 °C for 10 minutes under non-reducing

conditions. Samples were subjected to SDS-PAGE, transferred to nitrocellulose (NC) membranes (Thermo Fisher Scientific). and blocked with 5% bovine serum albumin in Tris-buffered saline with 0.1% Tween-20 (TBST). Blots were incubated with indicated primary antibodies and HRP-conjugated secondary antibodies (Invitrogen). Protein bands were visualized using an enhanced chemiluminescent (ECL) horseradish peroxidase (HRP) substrate (Supersignal West Pico PLUS, Thermo Scientific).

shRNA-mediated gene knockdown

The expression of both human RIPK3 and MLKL was knocked down using lentiviral-expressed shRNA.

qRT-PCR

The primers for RIPK3 were as follows: forward: 5'-GACTCCAGAGACCTCAACTTTC-3'; reverse:5'-CCAGTTCATGCCTTGTCTCT-3'. The primers for MLKL were as follows: forward:5'AACTCAAGGCTACCAAGTGAAG3'; reverse:5'CCAGTTCCTGAGGTGAGAGATA-3'. mRNA levels were determined by qRT-PCR.

Statistics and Reproducibility

Comparison between groups were analyzed by Kolmogorov-Smirnov or Kruskal-Wallis tests and multigroup comparisons were analyzed by Kruskal-Wallis test using GraphPad Prism V6 software. Comparison between a control group and treatment groups were analyzed by unpaired t-test using GraphPad Prism V6 software. All data were presented as Mean ± Standard Deviation in each figure. Data with P values < 0.05, 0.01, 0.001, 0.0001 were considered significant.

3.3   Results

3.3.1   Extravasating cancer cells experience a significant cell volume reduction

Cancer cells confront physical stresses during extravasation[8] and may be affected significantly by the extracellular mllieu[9]. To reveal how efficiently invasive prostate cancer cells extravasate into the stroma, we first measured the differential permeability of the chicken CAM vasculature by injecting a FITC-conjugated Dextran into the CAMs[10] (**Figure 10**). The CAM of day 9 chicken embryos showed the most permeable blood vasculature leaking FITC-conjugated dextran more rapidly compared to day 13 and 18 CAMs (**Figure 10A**). Mean fluorescence intensity (MFI) analysis of dextran in the CAM also showed that the vasculature of day 18 CAM had higher intensity of dextran over 24 hours (**Figure 10B**). Next, we injected PC-3M-LN4 zsGreen cells into the CAM of day 9 and 13 chicken embryos and observed similar extravasation rates (approximately 36.1% and 34.3%), whereas PC-3M-LN4 zsGreen cells injected into the day 18 chicken embryos exhibited extravasation rates of approximately 6.8% (**Figure 11A**). These differences in extravasation capacity of PC-3M-LN4 cells injected at different times were associated with differential metastatic colony formation (**Figure 11B**). This was expected as cancer cell extravasation is a key step in metastasis. Previous studies have shown that impaired cancer cell extravasation is detrimental to colony formation in the CAM of chicken embryos[3]. Cancer cells injected into the CAM of day 9 formed the most secondary colonies ($\approx$36 colonies on average) (**Figure 11B, ii**). Although extravasation rates of PC-3M-LN4 cells in day 9 and 13 CAMs were similar, cancer cells in the CAMs of day 9 chicken embryos formed significantly more colonies than day 13 CAMs (**Figure 11B, ii**). To gain an insight into potential underlying cellular events in the differential PC-3M-LN4 zsGreen extravasation rates, we performed confocal microscopy-based intravital imaging of PC-3M-LN4 zsGreen cells before and after extravasation. Confocal imaging captured both intravascular and extravasated PC-3M-LN4 zsGreen cells in Z-stack (**Figure 11C, i-iii**) and the cell volume of each cell was measured (**Figure 11C, iv**). PC-3M-LN4 zsGreen cells injected into the CAM of day 18 chicken embryos exhibited the smallest cell volume after extravasation by losing $\approx$51.6% of their original cell volume, whereas cells injected into the CAM of day 9 chicken embryos exhibited the biggest cell volume showing only

<10 % cell volume loss after extravasation. Meanwhile, PC-3M-LN4 zsGreen cells in the CAM of day 13 chicken embryos exhibited ≈31.2% cell volume loss, exhibiting a moderate level of cell volume reduction after extravasation. These results show that cancer cells extravasation is associated with cell volume reduction but the latter can represent a limiting factor for successful metastatic dissemination and colony formation as we observed there is a strong correlation between an increase in cell volume reduction and decreases in cancer cell extravasation and secondary colony formation rates.
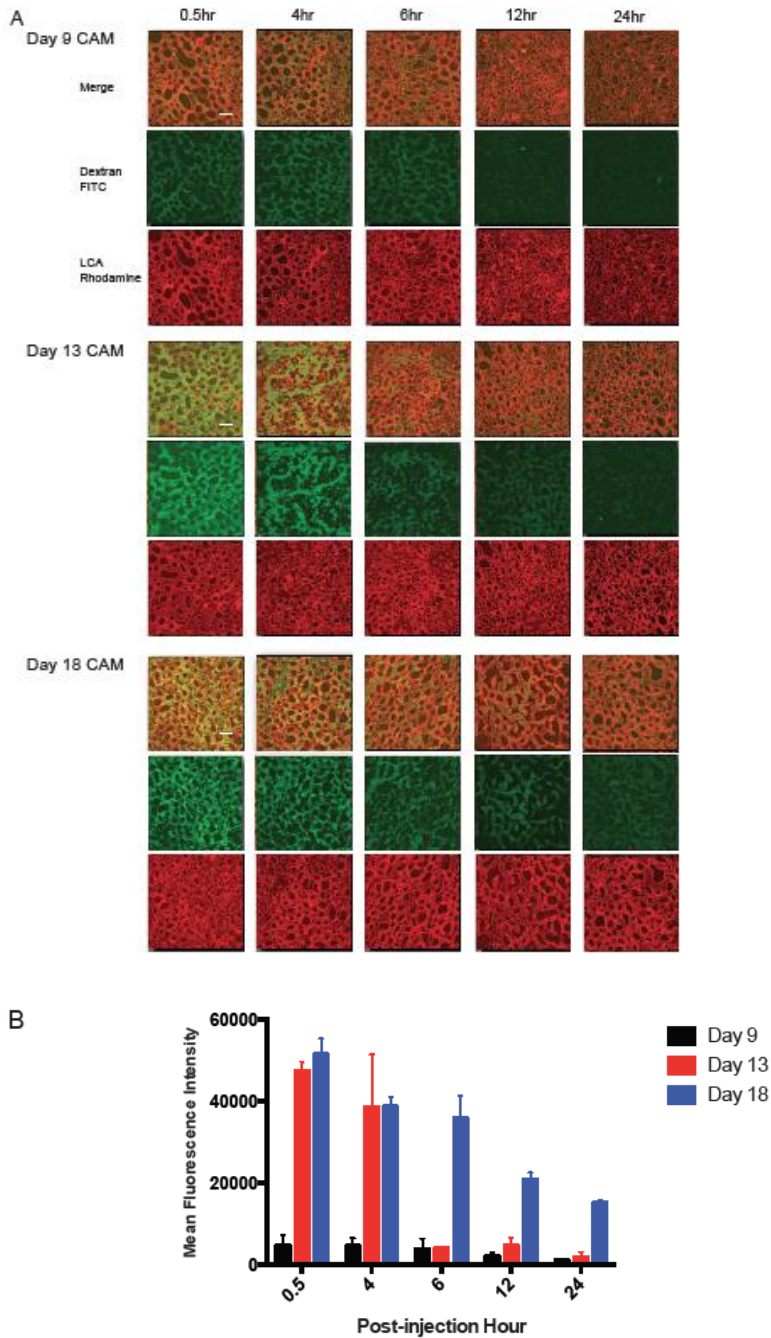
Figure 10: Evaluation of vasculature permeability of the CAMs at different embryonic development. (A) Confocal microscopy-based intravital imaging displays different permeability of the CAM vasculature of day 9, 13, 18 chicken embryos by showing the degree of FITC-tagged 150 kDa dextran retention. Representative images depict that the endothelium labeled with Rhodamine-Lens culinaris agglutinin and the lumen labeled with FITC-dextran. The CAM vasculature was imaged at 30 min, and at 4, 6, 12, 24 h points post-dextran injection. (B) Mean fluorescence intensity analysis of FITC-dextran images in the CAM vasculature of day 9, 13, 18 chicken embryos at different time points to show different vasculature permeability (n=3).
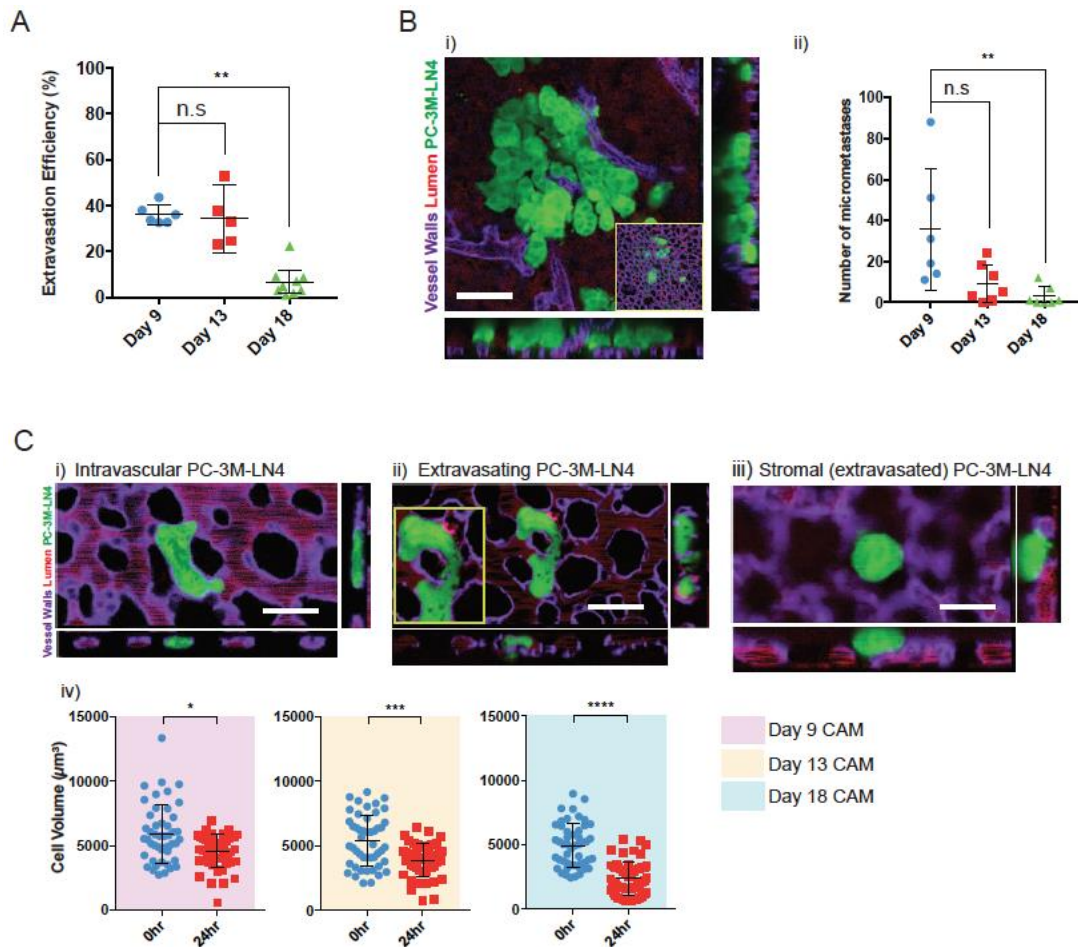
Figure 11: The correlation between cell volume reduction and extravasation efficiency of PC-3M-LN4 human prostate cancer cells. (A) Quantification of PC-3M-LN4 zsGreen cell extravasation in the CAM. PC-3M-zsGreen cells were injected into the CAM of day 9, 13, and 18 chicken embryos and their extravasation efficiencies were analyzed by epifluorescence microscopy-based imaging. Injected PC-3M-LN4 zsGreen cells were counted at $T=0$ and $T=24$ h post-injection to analyze extravasation efficiency (n≥5 animals/group). (B) Metastatic colony formation of PC-3M-LN4 zsGreen cells in the CAM after 4-7 days post-injection was imaged by confocal microscopy. Scale bar, 50 µm, original magnification is 60x (i). The number of micrometastases formed by PC-3M-LN4 zsGreen cells were counted and analyzed by epifluorescence microscopy-based imaging (n ≥ 6 animals/group) (ii). (C) Confocal microscopy-based analysis of cell volume reduction after PC-3M-LN4 zsGreen cell extravasation. Representative images depict that zsGreen fluorescent protein expressing PC-3M-LN4 cell gets arrested in a local capillary (i), undergoes extravasation by forming an invadopodium (ii), and dwells in the stroma after extravasation (iii). The endothelium and lumen of the vasculature are labeled with Lens culinaris agglutinin-Dylight 647 (purple) and rhodamine-dextran (red) respectively. Scale, 20 µm, original magnification is 60x. PC-3M-LN4 cell volumes in the CAM of day 9, 13, 18 chicken embryos at $T=0$ and $T=24$ h post-injection was analyzed by confocal

microscopy (n≥47 cells/group) (iv). All error bars represent S.D. *P<0.05, **P<0.01, ***P<0.001, ****P<0.0001, unpaired t-test.

3.3.2 Invasive cancer cells spontaneously release EVs greater than 100 nm into the bloodstream during cancer cell extravasation

Emerging evidence has shown that invasive cancer cells spontaneously release EVs less than 1000 nm both *in vitro* and *in vivo*[9]. Our *in vivo* imaging studies also revealed that extravasating PC-3M-LN4 zsGreen cells released plasma membrane-derived EVs along a variable size spectrum (>200 nm) into the bloodstream (**Figure 12A-C**). Most of the EVs directly released from the main cell body into the bloodstream varied in size between 300 nm and 1600 nm (**Figure 12C**). This release was observed most frequently from extravasating cancer cells, which were arrested within the intravascular space (**Figure 12A**). Intravascular cancer cells consistently generated membrane blebs that were either retracted or released into the bloodstream as EVs (**Figure 12A**). Although most EVs from the main cell body were observed in the bloodstream, we also observed that both extravasating and extravasated cancer cells released EVs into the stromal space, providing evidence that EV release is not only limited to an intravascular event but also to an extravascular event (**Figures 12D**-**G**). Lastly, we observed that PC-3M-LN4 zsGreen cells injected into the CAM of day 18 chicken embryos released the highest number of circulating EVs ($\approx 1.3 \times 10^4$ events/µL and $\approx 8.3 \times 10^3$ events/µL in average) whereas cancer cells in day 9 showed the lowest amount of circulating EV release ($\approx 0.61 \times 10^3$ events/µL and $\approx 1.1 \times 10^3$ events/µL in average) (**Figure 12H**). Collectively, these data demonstrate that extravasating cancer cells release EVs greater than 100 nm and ramp up EV release, potentially to confront exterior environments, including blood vessels with reduced permeability.
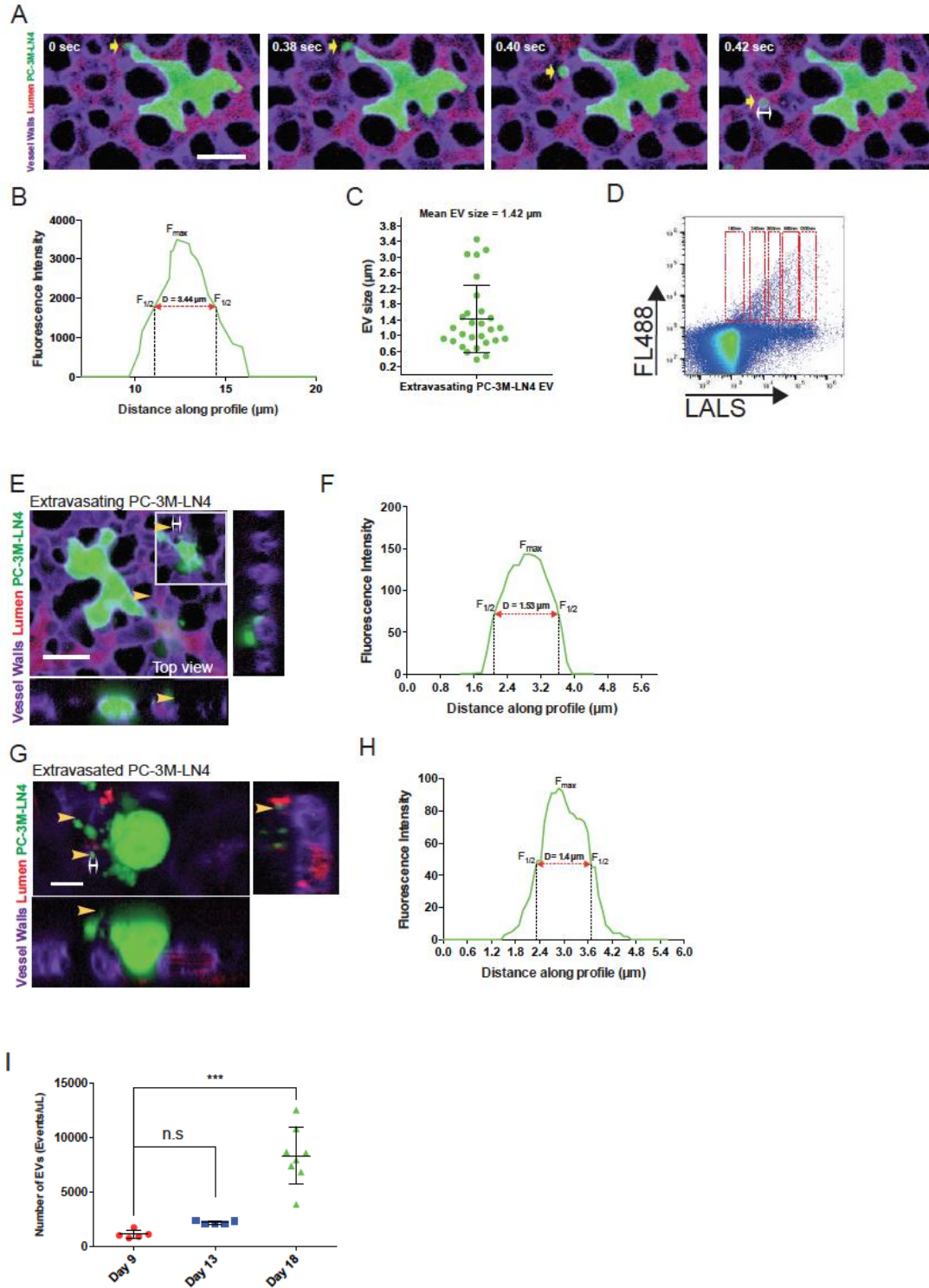
Figure 12: Extravasating human prostate cancer cells spontaneously release large EVs in the CAM model. (A) Representative time-lapse images of extravasating PC-3M-LN4 zsGreen cells showing dynamic EV release into the bloodstream. Yellow arrows point to EV release into the bloodstream. The blood vessel and lumen of the CAM are marked

by Lens culinaris agglutinin-Dylight 647 (purple) and rhodamine-dextran (red), respectively. The stroma is dark space between blood vessels. Scale, 20 µm, original magnification is 60x. (B) Size measurement of EV released from PC-3M-LN4 zsGreen cell from (A) by measuring EV fluorescence intensity distribution. (C) Size distribution of EV released by extravasating PC-3M-LN4 cells. Sizes of PC-3M-LN4 EVs were measured by fluorescence intensity distribution. (D) nFC-based size identification of PC-3M-LN4 zsGreen cell EV in plasma samples of chicken embryos. Representative cytogram shows most PC-3M-LN4 zsGreen EVs are distributed between 180 nm and 1300 nm. LALS and FL488 represent large-angle light scattering that measures size of EVs and fluorescent intensities of GFP-positive EVs, respectively. (E) Representative image of EV release from an invadopodium of extravasating PC-3M-LN4 zsGreen cell (pointed by a yellow arrow) into the stroma. The plane underneath the blood vessel is displayed in the white box showing that the invadopodium released the EV into the stroma. The released EV is also pointed by a yellow arrow in XZ plane view. The blood vessel and lumen of the CAM are marked by lectin-Dylight 647 (purple) and rhodamine-dextran, respectively. The stroma represents dark space between blood vessels. Scale bar, 20 µm, original magnification is 60x. (F) Size measurement of EV released from PC-3M-LN4 zsGreen cell from (E) by measuring EV fluorescence intensity distribution. (G) EV release into the stroma by extravasated PC-3M-LN4 zsGreen cell. PC-3M-LN4 zsGreen cell EVs (Green) released into the stroma are pointed with yellow arrows. Blood vessel and lumen are marked by lectin-Dylight 647 (purple) and rhodamine-dextran (red), respectively. The stroma is dark space between blood vessels. Scale bar, 20 µm, original magnification is 60x. (H) Size measurement of PC-3M-LN4 zsGreen cell EV release into the stroma by measuring EV fluorescence intensity distribution. (I) nFC based quantification of circulating PC-3M-LN4 zsGreen cell EVs in plasma samples of chicken embryos. PC-3M-LN4 cells were injected into the CAM of day 9, 13, 18 chicken embryos and the blood of all chicken embryos were collected at T=24 post-injection. All error bars represent S.D. ***P<0.05, unpaired t-test.

3.3.3 Cancer cell EV generation during cancer cell extravasation is not predominantly regulated by apoptosis

We investigated whether apoptosis is responsible for EV biogenesis from extravasating cancer cells, because apoptosis mainly leads to cell membrane blebbing, which is a source of EV biogenesis. To induce apoptosis in cancer cells, PC-3M-LN4 cells were treated with 1 μM of staurosporine (STS). STS is a cell-permeable alkaloid that readily induces apoptotic cell death. STS-treated PC-3M-LN4 cells displayed high mAmetrine and low tdTomato fluorescence signals whereas vehicle-treated PC-3M-LN4 cells showed both high mAmetrine and tdTomato fluorescence signals (**Figure 13A**). In agreement with a previous study by Ai *et al.*, the mean fluorescent intensity ratios (MFI between tdTomato:mAmetrine) of control and apoptotic PC-3M-LN4 cells were 1:1.99 and 1:5.32 respectively[11] (**Figure 13B**). Compared to *in vitro* images of mAmetrine and tdTomato expression in healthy and apoptotic cells, intravital FRET imaging of cancer cell EV release revealed that not only the main cell body had both high mAmetrine and tdTomato fluorescence signals but also the released EV did (**Figure 13C**; marked by yellow arrows). The fluorescent intensity of each channel showed that the MFI of EV release in PC-3M-LN4 cells (1:2.13) was closer to that of intact PC-3M-LN4 cells than apoptotic PC-3M-LN4 cells (1:5.32) (**Figure 13D**). These data show that other cellular mechanisms may dominantly maneuver the EV generation and release, however this cell death pathway is still involved in the stimulation of EV release.

To build on our results, we exposed PC-3 zsGreen cells to tumour necrosis factor-α (TNF-α) or pan-caspase inhibitor ZVAD-fmk (carbobenzoxy-valyl-alanyl-aspartyl-[O-methyl]-fluoromethylketone) and measured EV release. TNF-α (2-10 ng/mL) increased EV release *in vitro* (>2 folds), whereas caspase inhibitor ZVAD-fmk (3&5μM) showed an approximately 2-fold decrease in EV release (**Figure 14A**). These results were recapitulated by the quantification of EV release *in vivo*: TNF-α (5 ng/mL) treated PC-3 zsGreen cells exhibited an increase in EV release, compared to vehicle treated cells (**Figure 14B**). TNF-α (1 ng/mL) treated PC-3 zsGreen cells also showed a significant decrease in their extravasation rates (≈30%), compared to vehicle (≈50%) (**Figure 14C**). This readout was mirrored by STS (65 and 130 nM) showing significant decreases in PC-3 zsGreen cell

extravasation rates (<30%) (**Figure 14D**). Inhibiting apoptosis by ZVAD-fmk (3, 5µM) significantly increased extravasation rates (>60%) (**Figure 14E**), although that apoptosis inhibition by shRNA-mediated caspase-3 knockdown did not show a significant alteration in extravasation rates (**Figure 14F**). These results suggest that apoptotic signaling negatively affects cancer cell extravasation, possibly through increasing EV release.
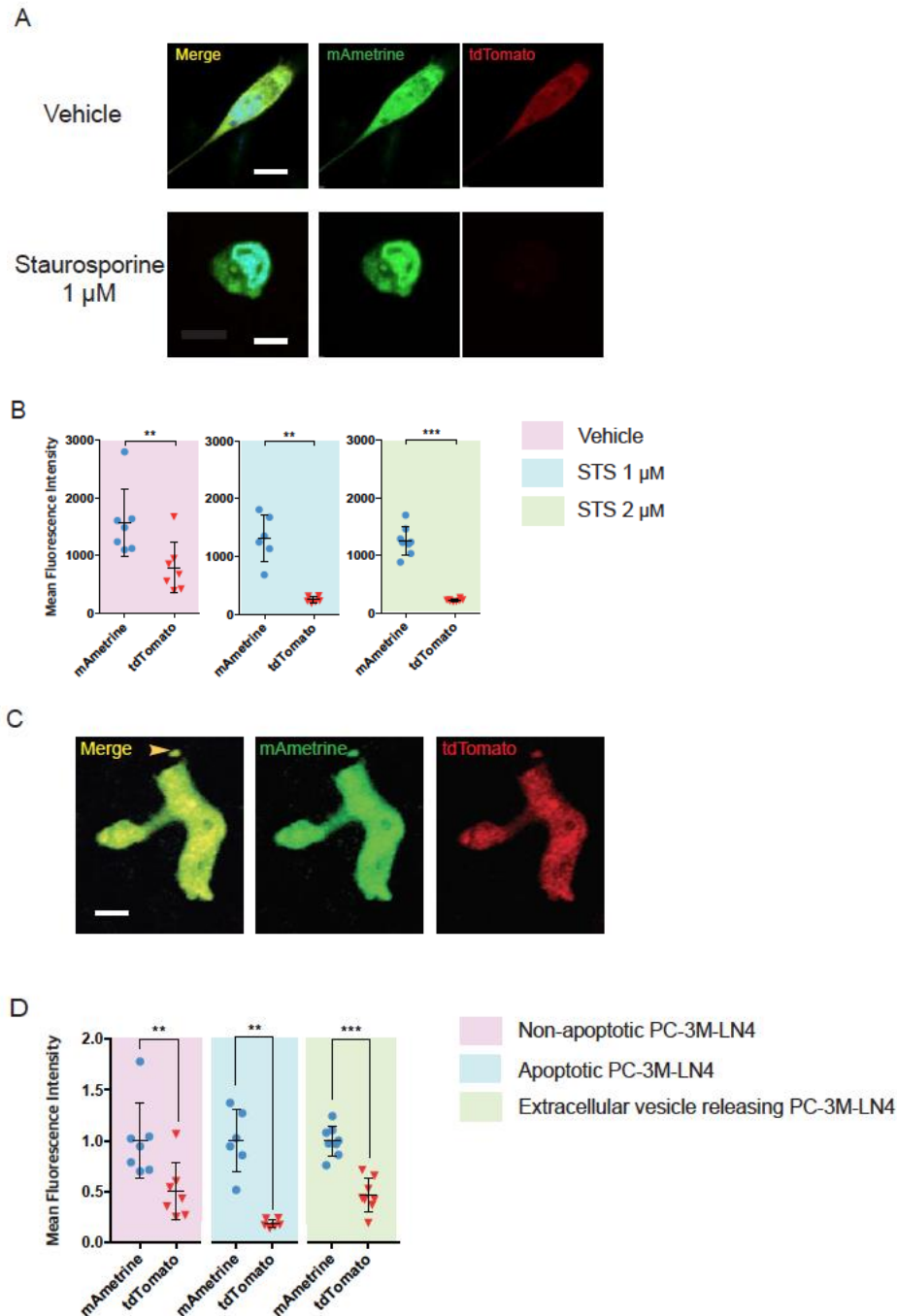
Figure 13: FRET imaging of extracellular vesicle release by mAmetrin-DEVD-tdTomato expressing cancer cells. (A) Representative confocal imaging of caspase-3 activation in apoptotic and non-apoptotic PC-3M-LN4 cells. PC-3M-LN4 cells were treated with vehicle (DMSO) or staurosporine (1 μM) for 24 hours. Scale bar, 20 μm, original magnification is 60x. (B) Mean fluorescence intensity analysis of mAmetrine and tdTomato in PC-3M-LN4 cells treated with vehicle (DMSO), 1 μM or 2 μM of staurosporine (STS) for 24 h. Images of PC-3M-LN4 cells under each treatment (n≥6 cells/group) were taken by confocal microscopy and fluorescent intensities of mAmetrine

68

and tdTomato in each cell were analyzed by ImageJ. (C) Intravital FRET imaging of caspase-3 levels during *in vivo* PC-3M-LN4 cell EV release, as assessed by mAmetrine-DEVD-tdTomato fluorescence. PC-3M-LN4 cells were injected into day 13 chicken embryos for the intravital FRET imaging. A yellow arrow indicates the EV release from the main cell body. Scale bar, 20 µm, original magnification is 60x. (D) The comparison of mean fluorescent intensity ratio (MFI) of mAmetrin and tdTomato expressions in EV releasing PC-3M-LN4 cells with non-apoptotic (with DMSO) and apoptotic (with 1 µM STS) PC-3M-LN4 cells. All error bars represent S.D. **P<0.01, ***P<0.001, unpaired student t-test.
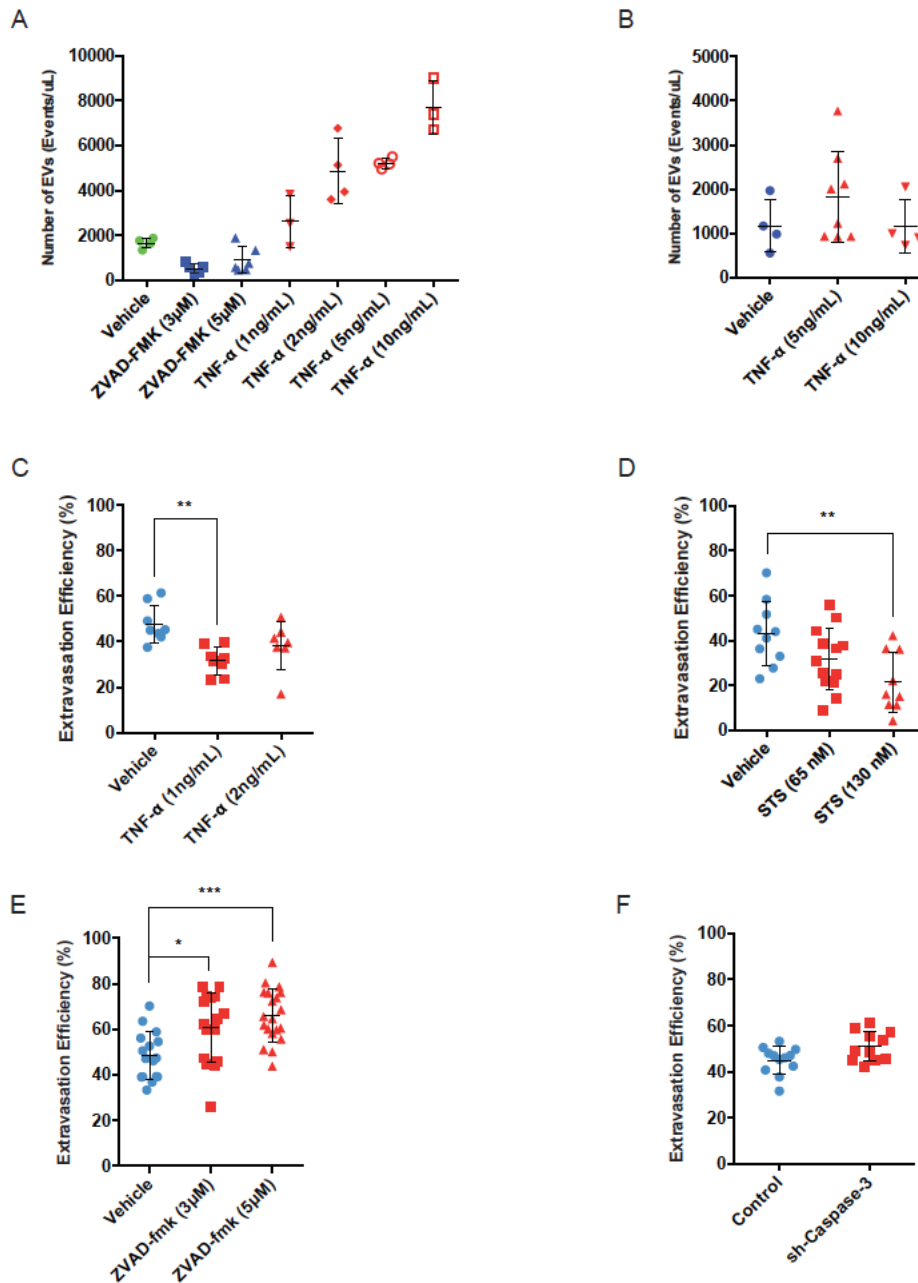
Figure 14: The effect of apoptosis on PC-3 cell EV release and extravasation. (A) Pro-apoptotic and anti-apoptotic effects to PC-3 cell EV release *in vitro*. PC-3 zsGreen cells were treated with TNF-α (1, 2, 5, 10 ng/mL) or ZVAD-fmk (3, 5μM) for 24 h. The conditioned medium was analyzed by nFC to quantify the EV release (n=3 independent experiments). (B) Effect of apoptotic PC-3 zsGreen cells *in vivo*. PC-3 zsGreen cells were treated with DMF or TNF-α (5, 10 ng/mL) and injected in (n≥4 animals/group). The conditioned medium of PC-3 zsGreen cells for each treatment was analyzed by nFC. (C) Pro-apoptotic effects of TNF-α (1 ng/mL and 2 ng/mL) on PC-3 zsGreen cancer cell extravasation efficiency. PC-3 zsGreen cells with each treatment were injected and extravasation efficiency was measured by counting the number of cells at T=0 and T=24 (n≥7 animal/group). (D) Pro-apoptotic effects of STS (65 nM and 130 nM) on PC-3

zsGreen cancer cell extravasation efficiency. Injected PC-3 zsGreen upon each treatment were counted at T=0 and T=24 (n≥9 animal/group). (E) Anti-apoptotic effects of ZVAD-fmk on PC-3 zsGreen cell extravasation efficiency. PC-3 zsGreens cells treated with ZVAD-fmk (3μM and 5μM) for 24 h were injected and the numbers of PC-3 cells were counted at T=0 and T=24 (n≥14 animal/group) to analyze PC-3 cell extravasation efficiency. (F) The effect of shRNA derived caspase-3 knockdown on PC-3 cancer cell extravasation efficiency. shRNA targeting caspase-3 introduced PC-3 cells were injected into the CAM of day 13 and PC-3 cells were counted at T=0 and T=24 to evaluate PC-3 cell extravasation efficiency (n≥14 animal/group). All error bars represent S.D. *P<0.05, **P<0.01, ***P<0.001, unpaired student t-test.

3.3.4 Necroptosis-induced EV release in human prostate cancer cells

Emerging studies have shown that a combination of tumour necrosis factor-α (TNF-α) with ZVAD-fmk (carbobenzoxy-valyl-alanyl-aspartyl-[O-methyl]-fluoromethylketone) and Smac mimetic (small-molecule inhibitor of apoptosis antagonists) robustly induces necroptosis[12]. In addition, dimethyl fumarate (DMF, Tecifera) has been highlighted as a promising necroptosis inducer and is already approved by the FDA[13]. Using this platform, we tested whether necroptosis induces EV release in prostate cancer cells. As a proxy for necroptosis induction, we measured the levels of mixed lineage kinase domain-like (MLKL), a critical regulator of necroptotic cell death. PC-3 cells treated with TNF-α (100ng/mL), ZVAD-fmk (20μM), Smac mimetic (100 nM) or TZS (combination), and DMF (100μM) showed significant increases in MLKL mRNA levels compared to vehicle treated PC-3 cells (**Figure 15A**). The levels of MLKL mRNA in TZS- and DMF-treated PC-3 cells were as high as doxycycline-inducible MLKL overexpressing PC-3 cells (>4 folds) (**Figure 15A, 17F**). PC-3 cells overexpressing MLKL treated with TZS exhibited the highest MLKL and phosphorylated MLKL levels (**Figure 15B**). Although TZS or DMF treated PC-3 cells showed increased MLKL and phosphorylated MLKL, DMF treatment induced significantly higher phosphorylated MLKL compared to both TZS and vehicle (**Figure 15B**). MLKL-knockdown in PC-3 cells showed a significant decrease in both mRNA and protein levels of MLKL (**Figure 15A, B**). We then investigated the effect of DMF-induced necroptosis on cancer cell EV release during extravasation. nFC analysis of conditioned medium of PC-3 cells treated with TZS and DMF showed that both TZS and

DMF-mediated necroptosis induced PC-3 EV release. However, DMF treated PC-3 zsGreen cells exhibited greater than a 3-fold-increase in the number of EV release *in vitro* (**Figure 15C, D**). Next, TZS treated PC-3 cells were injected into the CAM of day 13 chicken embryos. After 24 hours post-injection, both TZS and DMF treatments induced significant PC-3 zsGreen cell EV release compared to vehicle treated PC-3 zsGreen cells, with DMF treatment causing a higher increase (> 3 fold) *in vivo* (**Figure 16A, B**). These results show that DMF induces necroptosis by increasing MLKL and phosphorylated MLKL levels in PC-3 cells and causes necroptosis-mediated PC-3 cell EV release. These results also suggest that DMF-induced cancer cell necroptosis can potentially increase cancer cell EV release during extravasation, more so than TZS treatment.
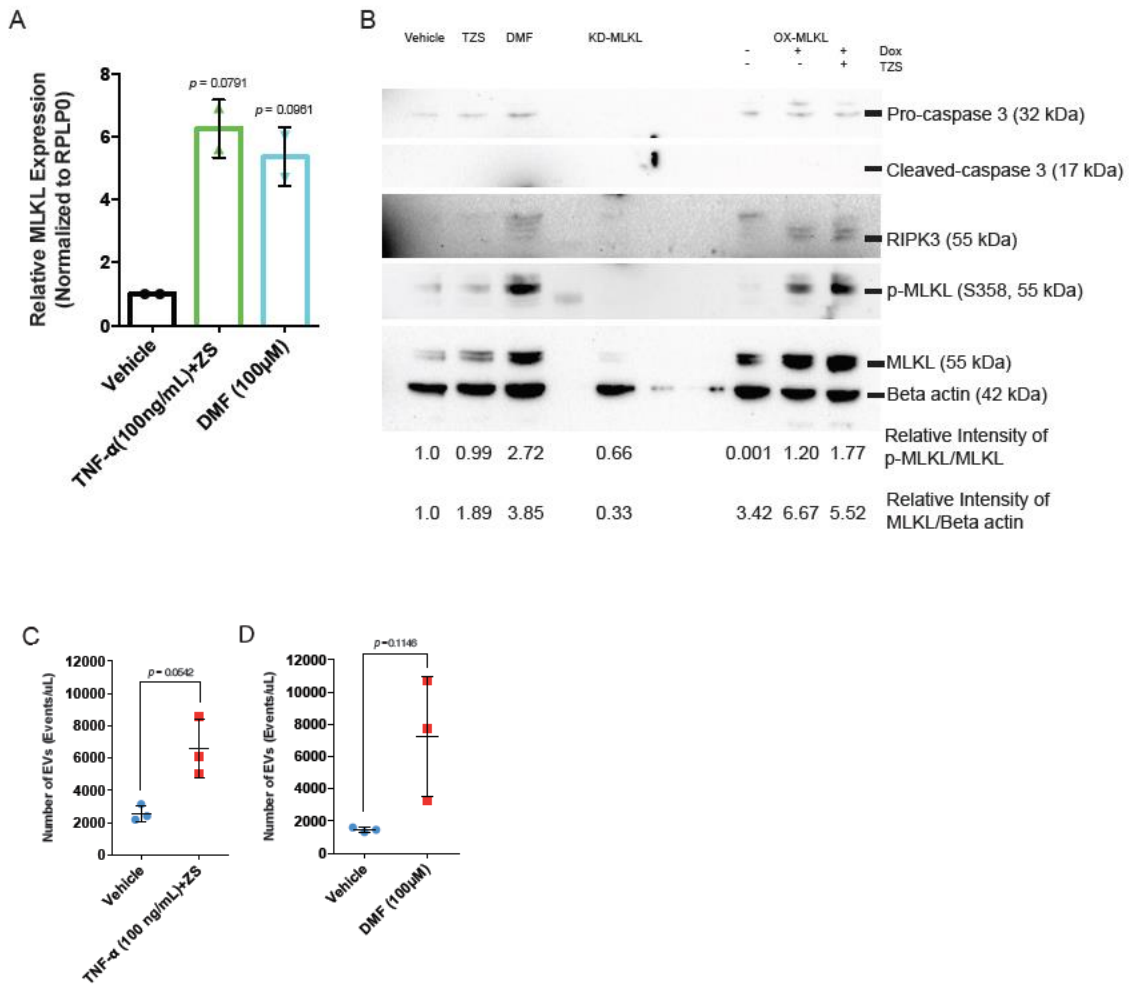
Figure 15: DMF induced necroptosis pathway is involved in cancer cell EV release. (A) Real-time PCR-based mRNA quantification of MLKL gene in TZS and DMF treated PC-3 cells (n=2 independent experiments). RPLP0 gene was used as a housekeeping gene for normalization. (B) Protein quantification of MLKL, phosphorylated MLKL, RIPK3, and active caspase-3 in PC-3 cells with TZS, DMF, and MLKL knockdown and overexpression (n=2 independent experiments). Lysates from PC-3 cells in each treatment were subjected to western blotting. (C) nFC based quantification of *in vitro* PC-3 zsGreen cell EV release with TZS treatment. (n=3 independent experiments) (D) Quantification of DMF (100 μM) treated PC-3 zsGreen cell EV release *in vitro* by nFC-based analysis (n=3 independent experiments). All error bars represent S.D. Unpaired t-test.
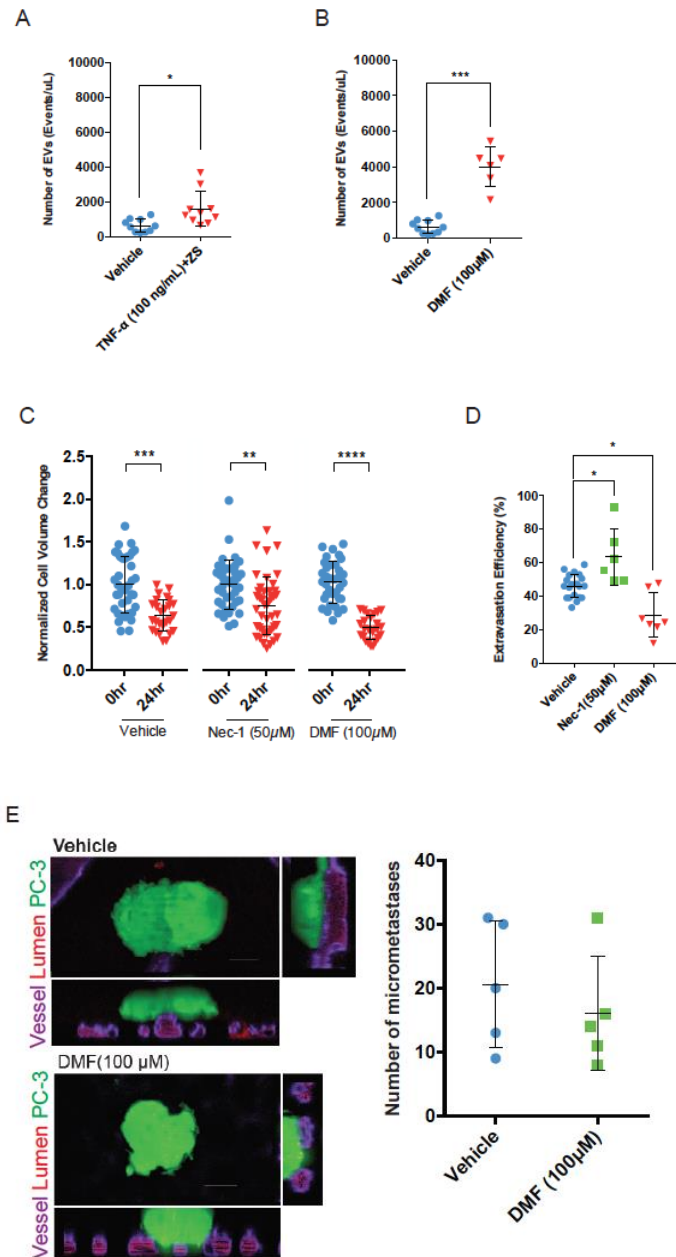
Figure 16: DMF induced PC-3 cell necroptosis, increased EV release, and reduced PC-3 metastasis. (A) nFC analysis of *in vivo* EV release from PC-3 zsGreen cells treated with DMSO and TZS in the CAM. PC-3 zsGreen cells were injected into the CAM of day 13 chicken embryos. Plasma samples from each chicken embryo was collected at T=24 h post-injection (n=10 animals/experiments). (B) nFC analysis of *in vivo* EV release from PC-3 zsGreen cells treated with DMSO and 100μM of DMF. Plasma samples from each chicken embryo was collected at T=24 h post-injection (n≥6 animals/group). PC-3 zsGreen cells with each treatment were injected into the CAM of day 13 chicken embryos (n≥6 animals/group). (C) Confocal imaging-based cell volume change analysis of PC-3 zsGreen cell under DMSO, Nec-1 (50 μM) and DMF (100 μM) treatments (n≥24 cells/group) after injections into the day 13 chicken embryos. PC-3 cells with each treatment were imaged at

T=0 and T=24 h post-injection. (D) *In vivo* PC-3 cell extravasation assay under Nec-1 (50μM) and DMF (100μM) treatments. PC-3 zsGreen cells with each treatment injected into the CAM (n≥6 animals/group) of day 13 chicken embryo. The numbers of PC-3 cells were counted at T=0 and T=24 h post-injection. (E) Epifluorescence imaging-based *in vivo* metastatic colony assay of PC-3 zsGreen cell under necroptosis in the CAM. Representative images metastatic colony formations by DMSO and DMF (100μM) treated PC-3 zsGreen cells. Scale bar 20 µm, original magnification is 60x. PC-3 zsGreen cells with each treatment injected into the CAM of day 9 chicken embryo and secondary colonies were quantified after 4 days (n=5 animals/group). All error bars represent S.D. *P<0.05, **P<0.01, ***P<0.001, ****P<0.0001. Unpaired t-tests.

3.3.5 Increased necroptosis-derived EV release is detrimental to the metastatic efficiency of invasive cancer cells

Our studies showing necroptosis-mediated EV release prompted us to investigate whether this process is associated with cell volume changes, extravasation rates and metastatic potential. To test this, we treated cells with vehicle, DMF, and necrostatin-1, an inhibitor of necroptosis. Our results show that differential amounts of EV release induce different levels of cell volume reduction after extravasation. The DMF (100 μM) group showed the most cell volume loss (≈51.0%) compared to the vehicle group (≈36.1%), whereas necrostatin-1 treated PC-3 zsGreen cells showed the least cell volume loss (≈25.2%) (**Figure 16C**). As PC-3 zsGreen cancer cells lost more cell volume due to excessive EV release under DMF treatment, DMF treated PC-3 zsGreen cells exhibited a significant decrease in their extravasation rates (≈28.8%) after 24 hours in the CAM compared to vehicle treated PC-3 zsGreen cells. However, PC-3 zsGreen cells with necrostatin-1 treatment exhibited a significant increase in extravasation efficiency (≈63.7%) (**Figure 16D**). DMF-induced necroptosis decreased not only the number (≈ 0.75-fold), but also the magnitude (≈ 0.5-fold) of metastatic colony formation by PC-3 zsGreen cells in the CAM (**Figure 16E**). To recapitulate the effects of necrostatin-1 on cancer cell necroptosis during extravasation, we determined whether knocking down RIPK3 and MLKL by shRNAs significantly affects cancer cell extravasation. Firstly, knockdown of RIPK3 and MLKL were very efficient in reducing the levels of RIPK3 and MLKL mRNA and protein in PC-3 cells (**Figure 17A**). shRNA-mediated RIPK3 and MLKL knockdown resulted in a decrease in the expression of RIPK3 and MLKL (**Figure 17B**). Although knockdown of

RIPK3 did not affect PC-3 zsGreen cell EV release, knockdown of MLKL significantly reduced the number of EVs released as compared to the control group (**Figure 17C**). However, the knockdown of both RIPK3 and MLKL led to a significant increase ($\approx$61.9% and $\approx$56.5%, respectively) in extravasation rates of PC-3 zsGreen cells compared to the control group ($\approx$43.5%) (**Figure 17D**). This further confirmed that intravascular necroptosis significantly regulated cancer cell extravasation. The knockdown of MLKL led to an increase in metastatic colony formation ($\approx$31 micrometastases) whereas the RIPK3 knockdown did not improve the metastatic colony formation of PC-3 zsGreen cells ($\approx$18 micrometastases) (**Figure 17E**).

Doxycycline-inducible MLKL overexpression in PC-3 cells was confirmed by measuring mRNA and protein levels, showing increases in both MLKL and phosphorylated MLKL (**Figure 17F, G**). In addition, MLKL overexpression with TZS treatment showed a significant decrease in PC-3 cell extravasation efficiency (**Figure 17H**). Altogether, our results show that cancer cell necroptosis promotes cell volume reduction by inducing excessive EV release during extravasation, resulting in a significant decrease in cancer cell metastatic capacity.
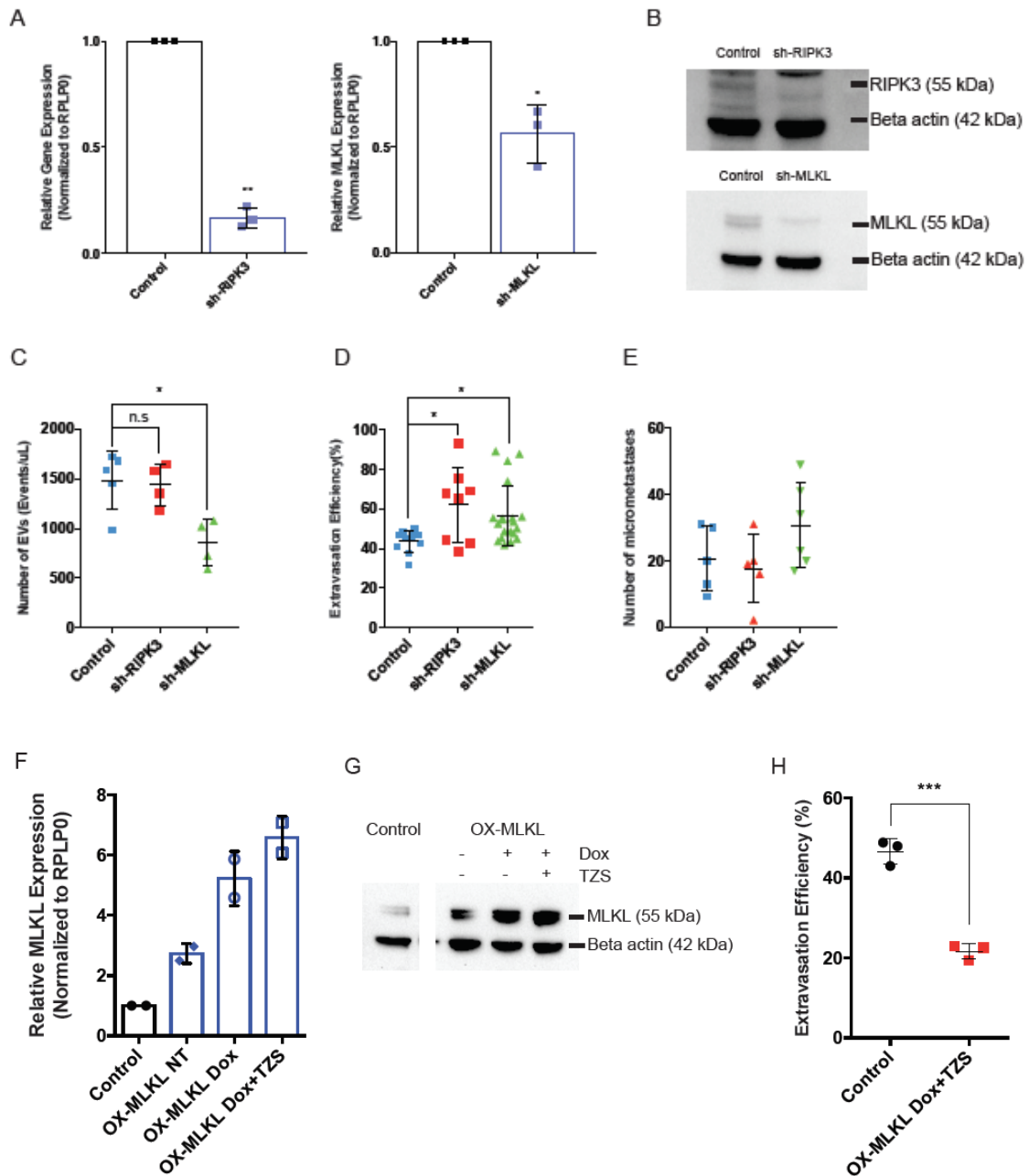
Figure 17: Genetic modulation of necroptosis and the corresponding changes in PC-3 EV release and metastatic potential. (A) qRT-PCR analysis of RIPK3 and MLKL mRNA in PC-3 cells. PC-3 cells were transduced with lentivirus expressing shRNA targeting RIPK3 and MLKL (n=3 independent experiments). (B) MLKL proteins in PC-3 cells expressing RIPK3 and MLKL shRNA. (C) nFC based quantification of shRNA expressing PC-3 zsGreen cell EV release. PC-3 zsGreen cells were injected into the CAM of day 13 chicken embryos. Plasma samples of chicken embryos were collected at T=24 h post injection (n≥4 animals/group) (D) *In vivo* extravasation assay of PC-3 zsGreen with

RIPK3 and MLKL shRNA. PC-3 cells were injected into the CAM of day 13 chicken embryos (n≥8 animals/group). The number of extravasated cells at T=0 and T=24 h post-injection counted by epifluorescence microscopy. (E) *In vivo* metastatic colony assay of PC-3 zsGreen shRNA clones in the CAM of chicken embryo (n≥6 animals/group). All PC-3 shRNA clones were injected into the CAM of day 13 chicken embryos and the number of extravasated cells on 7th day post-injection was analyzed by epifluorescence microscopy. (F) qRT-PCR analysis of MLKL mRNA in MLKL overexpressing PC-3 cells (n=2 independent experiments). PC-3 cells were stably transfected with a doxycycline-inducible MLKL expressing construct. RPLP0 was used as a housekeeping gene. (G) MLKL protein quantification. Doxycycline-inducible MLKL overexpressing PC-3 cells treated with PBS, doxycycline only, and doxycycline with TZS were subjected to western blot for MLKL. (H) *In vivo* extravasation assay of MLKL-overexpressing PC-3 zsGreen cells. Control vector (control) and MLKL overexpressing PC-3 cells were injected into the CAM of day 13 chicken embryos (n≥3 animals/group). The number of extravasated cells at T=0 and T=24 h post-injection counted by epifluorescence microscopy. All error bars represent S.D. *$P<0.05$. Unpaired t-tests.

3.4 Discussion

Cancer cell volume reduction may be a prerequisite to a metastatic phenotype of extravasating cancer cells since endothelial integrity (i.e. gap junctions) of the blood vessel is a barrier to successful extravasation[8, 16, 17]. Due to the size restriction of cancer cells in the transendothelial space, cell volume reduction by EV release[8, 17, 18] may be a strategy by the cancer cells to succeed in extravasation, as evidenced by our studies (**Figures 11C**). Even if cells succeed in crossing the endothelial wall, the stromal environment, comprised of connective tissues, is another barrier to extravasation. The stroma creates an ideal niche for cancer cell growth and progression of secondary colonies[19-27], but extravasating cancer cells also confront spatial restrictions when entering the stroma. Our *in vivo* extravasation assays with the CAM of chicken embryos showed that fluorescently labeled PC-3M-LN4 cells spent over 24 hours to extravasate into the stroma and continuously released large EVs into the bloodstream (**Figures 11C** and **12A, 12C, 12H**). While it was previously unclear whether large EV release reduces cell volume during extravasation, our results (**Figures 11C** and **12H**) provide evidence showing that an increase in large EV release is correlated with a decrease in cancer cell volume after extravasation. As previous studies showed that cancer cells have a higher chance of extravasation if they rapidly extravasate into the stroma, cells would reduce cell volume by releasing excessive EVs into the bloodstream[8, 17, 18]. A recent study by Lyons *et al.* showed that most invasive cancers acquire a smaller cell volume over time[28]. In addition, using intravital imaging (**Figure 11C**), we observed that most cancer cells in the stroma exhibit reduced cell volume and size, potentially allowing the cancer cells to extravasate. When cancer cells reduced their cell volume (**Figure 11C**), extravasation efficiency significantly decreased (**Figure 11D**). Thus, we suggest that a reduction in cancer cell volume by cancer cell EV release facilitates cancer cell extravasation, but excessive EV release is counterproductive to metastatic capacity. As such, future studies regarding the cellular processes of cancer cell volume reduction during extravasation are warranted.

Various cellular processes are involved in driving heterogeneity in EV biogenesis. In this study, we focused on determining key cellular pathway targets in which membrane-derived EVs are initiated. A reliable source of cell membrane blebbing is during programmed cell

death that includes apoptosis and necroptosis. Although cancer cells spread to distant sites throughout the circulatory system, the extracellular milieu of cancer cells in the bloodstream is detrimental to cell viability and successful extravasation. Most intravascular cancer cells must be trapped in the capillaries near secondary organs in order to be successful in extravasation, though they cannot escape from cell death upon detaching from endothelial cells or from geometrical pressure[29]. Apoptosis releases apoptotic bodies which can be a principal mechanism for intravascular programmed cancer cell death. We recapitulated the study of Dr. Weiss in 1985 by performing intravital imaging of extravasating cancer cells in the CAM. We initially hypothesized that apoptosis may be the main cue of cancer cell membrane blebbing and EV release since intravascular cancer cells are exposed to many apoptosis inducing factors (for example, reactive oxygen species, nutrient accessibility, immune attack). While apoptotic intravascular cancer cells exhibited increased circulating EVs (**Figure 14A, B**), real time FRET imaging of EV-releasing cancer cells in the bloodstream did not show elevated caspase-3 activity, while increased activity was noted *in vitro* (**Figures 13A**, **B**). As EV-releasing cancer cells maintained the fluorescence of both mAmetrine and tdTomato without FRET quenching, the results are indicative of a lack of caspase-3 activity (**Figures 13C**, **D**)[11].

Regardless of whether EV release is regulated by apoptosis, intravascular cancer cells still exhibit cell death in the bloodstream. The lack of a real-time necroptosis reporter still leaves the origin of cancer cell EV release obscure. A recent study provides evidence that membrane blebbing and release are initiated by phosphorylated MLKL[7]. Numerous cancer cell types express basal RIPK3 and MLKL that can initiate membrane blebbing[30]. Circulating necroptosis inducing factors, such as TNF-α, might induce intravascular cancer cell necroptosis[31,32]. Here, we also introduced DMF as a potential necroptosis inducer[13] showing increased levels of MLKL and phosphorylated MLKL (**Figure 15B**). Confronting intravascular necroptosis, inevitably some cancer cells could survive and succeed in extravasation to form metastatic colonies as evidence from our studies (**Figures 15D,E**). One possible cellular process involved in EV release may be the removal of detrimental proteins such as MLKL. It is widely known that endosome-derived EVs require ESCRT-III machinery[33]. However, release of large EVs containing MLKL is also facilitated by the recruitment of ESCRT-III complex, comprised of CHMP2A and CHMP4B[7]. Such

discharge of EVs containing MLKL may not only remove a detrimental protein, but may also defer MLKL induced-plasma membrane damage[7,34]. Regardless of the potential plasma membrane recovery mechanism described previously, our studies show that an increase in PC-3 EV release by DMF correlates with cell volume reduction, and a failure of extravasation and metastatic colony formation. Knockdown of MLKL led to a significant decrease in PC-3 cell EV generation and implicated that PC-3 cells may avoid excessive cell volume reduction which significantly reduces extravasation and metastatic colony formation (**Figure 16**). We do note that the expression of RIPK3 and MLKL has yet to be tracked in real time during EV release.

Overall, since many invasive cancers are apoptosis-resistant, it is likely advantageous to exploit the nature of necroptosis, in which more cancer cell EV release can be stimulated, to sensitize cancer cells to intravascular death before they cross the endothelial border.

3.5 References

1. Mehlen, P. & Puisieux, A. Metastasis: a question of life or death. *Nat. Rev. Cancer* **6,** 449–58 (2006).

2. Chambers, A. F., Groom, A. C. & MacDonald, I. C. Dissemination and growth of cancer cells in metastatic sites. *Nat. Rev. Cancer* **2,** 563–72 (2002).

3. Leong, H. S. *et al.* Invadopodia Are Required for Cancer Cell Extravasation and Are a Therapeutic Target for Metastasis. *Cell Rep.* **8,** 1558–1570 (2014).

4. Dhillon, A. S., Hagan, S., Rath, O. & Kolch, W. MAP kinase signalling pathways in cancer. *Oncogene* **26,** 3279–3290

5. Hoshino, D. *et al.* Exosome Secretion Is Enhanced by Invadopodia and Drives Invasive Behavior. *Cell Rep.* **5,** 1159–1168 (2013).

6. Sung, B. H., Ketova, T., Hoshino, D., Zijlstra, A. & Weaver, A. M. Directional cell movement through tissues is controlled by exosome secretion. *Nat. Commun.* **6,** 7164 (2015).

7. Gong, Y.-N. *et al.* ESCRT-III Acts Downstream of MLKL to Regulate Necroptotic Cell Death and Its Consequences. *Cell* **169,** 286–300.e16 (2017).

8. Strilic, B. & Offermanns, S. Cancer Cell Review Intravascular Survival and Extravasation of Tumour Cells. (2017).

9. Headley, M. B. *et al.* Visualization of immediate immune responses to pioneer metastatic cells in the lung. *Nature* **531,** 513–517 (2016).

10. Pink, D. B. S., Schulte, W., Parseghian, M. H., Zijlstra, A. & Lewis, J. D. Real-Time Visualization and Quantitation of Vascular Permeability In Vivo: Implications for Drug Delivery. *PLoS One* **7,** e33760 (2012).

11. Ai, H., Hazelwood, K. L., Davidson, M. W. & Campbell, R. E. Fluorescent protein FRET pairs for ratiometric imaging of dual biosensors. *Nat. Methods* **5,** 401–403 (2008).

12. Liu, S. *et al.* MLKL forms disulfide bond-dependent amyloid-like polymers to induce necroptosis. *Proc Natl Acad Sci USA* **114**, E7450-E7459 (2017).

13. Xie, X. *et al.* Dimethyl fumarate induces necroptosis in colon cancer cells through GSH depletion/ROS increase/MAPKs activation pathway. *Br. J. Pharmacol.* **172,** 3929–3943 (2015).

14. Biggs, C. N. *et al.* Prostate extracellular vesicles in patient plasma as a liquid biopsy platform for prostate cancer using nanoscale flow cytometry. *Oncotarget* **7,** 8839–8849 (2016).

15. Brett, S. I., Kim, Y., Biggs, C. N., Chin, J. L. & Leong, H. S. Extracellular vesicles such as prostate cancer cell fragments as a fluid biopsy for prostate cancer. *Prostate Cancer Prostatic Dis* **18,** 213–220 (2015).

16. Kienast, Y. *et al.* Real-time imaging reveals the single steps of brain metastasis formation. *Nat. Med.* **16,** 116–122 (2010).

17. Weiss, L. Biomechanical interactions of cancer cells with the microvasculature during hematogenous metastasis. *Cancer Metastasis Rev.* **11,** 227–35 (1992).

18. Becker, A. *et al.* Extracellular Vesicles in Cancer: Cell-to-Cell Mediators of Metastasis. *Cancer Cell* **30,** 836–848 (2016).

19. Sleeman, J. P. The metastatic niche and stromal progression. *Cancer Metastasis Rev* **31**, 239-40 (2012).

20. Kaplan, R. N. *et al.* VEGFR1-positive haematopoietic bone marrow progenitors initiate the pre-metastatic niche. *Nature* **438,** 820–827 (2005).

21. Oskarsson, T. *et al.* Breast cancer cells produce tenascin C as a metastatic niche component to colonize the lungs. *Nat. Med.* **17,** 867–874 (2011).

22. Malanchi, I. *et al.* Interactions between cancer stem cells and their niche govern metastatic colonization. *Nature* **481,** 85–89 (2012).

23. Gao, D. *et al.* Myeloid Progenitor Cells in the Premetastatic Lung Promote Metastases by Inducing Mesenchymal to Epithelial Transition. *Cancer Res.* **72,** 1384–1394 (2012).

24. Erler, J. T. *et al.* Hypoxia-Induced Lysyl Oxidase Is a Critical Mediator of Bone Marrow Cell Recruitment to Form the Premetastatic Niche. *Cancer Cell* **15,** 35–44 (2009).

25. Kii, I. *et al.* Incorporation of Tenascin-C into the Extracellular Matrix by Periostin Underlies an Extracellular Meshwork Architecture. *J. Biol. Chem.* **285,** 2028–2039 (2010).

26. Kim, D.-K. *et al.* EVpedia: a community web portal for extracellular vesicles research. *Bioinformatics* **31,** 933–939 (2015).

27. Hiratsuka, S. *et al.* MMP9 induction by vascular endothelial growth factor receptor-1 is involved in lung-specific metastasis. *Cancer Cell* **2,** 289–300 (2002).

28. Lyons, S. M. *et al.* Changes in cell shape are correlated with metastatic potential in murine and human osteosarcomas. (2016).

29. Weiss, L., Dimitrov, D. S. & Angelova, M. The hemodynamic destruction of intravascular cancer cells in relation to myocardial metastasis. *Proc. Natl. Acad. Sci.*

U. S. A. **82,** 5737–5741 (1985).

30. Qu, Y. *et al.* RIPK3 interactions with MLKL and CaMKII mediate oligodendrocytes death in the developing brain. *Cell Death Dis.* **8,** e2629–e2629 (2017).

31. Degterev, A. *et al.* Chemical inhibitor of nonapoptotic cell death with therapeutic potential for ischemic brain injury. *Nat. Chem. Biol.* **1,** 112–119 (2005).

32. Pobezinskaya, Y. L. *et al.* The function of TRADD in signaling through tumour necrosis factor receptor 1 and TRIF-dependent Toll-like receptors. *Nat. Immunol.* **9,** 1047–1054 (2008).

33. Yoon, S., Kovalenko, A., Bogdanov, K. & Wallach, D. MLKL, the Protein that Mediates Necroptosis, Also Regulates Endosomal Trafficking and Extracellular Vesicle Generation. *Immunity* **47,** 51–65.e7 (2017).

34. Babiychuk, E. B., Monastyrskaya, K., Potez, S. & Draeger, A. Blebbing confers resistance against cell lysis. *Cell Death Differ.* **18,** 80–9 (2011).

35. Kim, Y. *et al.* Quantification of cancer cell extravasation in vivo. *Nat. Protoc.* **11,** 937–948 (2016).

Chapter 4

4   Conclusions and future directions

4.1   Quantification of Cancer Cell Extravasation *In Vivo*

4.1.1   Summary of findings and conclusions

The key findings from the first part (chapter 3) of my thesis show morphological changes of cancer cells in the course of extravasation in the chorioallantoic membrane (CAM) of chicken embryo. The observation of morphological changes also permits to assess precisely whether cancer cells succeed in extravasation and perform powerful quantification of cancer cell extravasation as well. Chapter 3 ultimately shows the CAM model is suitable for evaluation of potential pharmacological or genetic treatments on anti-cancer extravasation *in vivo* in a high-throughput manner. Many substantial studies already proved its reliability and reproducibility as a better animal model system by collaborating with us.

Research into methods that could allow the investigation of the key cellular steps in metastasis initiated the body of this work. This work established not only a robust animal model for the quantification of cancer cell extravasation, but also a suitable system to observe underlying cellular and molecular events during cancer metastasis. The analysis of cell extravasation efficiency directly links to the evaluation of cancer cell invasiveness. Previous quantification methods of cancer cell extravasation have relied heavily on the mouse or zebrafish model as *in vivo* systems or the matrigel degradation assay as an *in vitro* system. In chapter 3, I introduced the CAM of chicken embryo as providing all the advantages of the CAM model and resolving limitations associated with the previous models. In addition, the optimization of the CAM-based quantification of cancer cell extravasation has provided researchers with a highly effective model in the field.

The CAM model is accessible to confocal-based intravital imaging techniques to visualize cancer cell extravasation from the blood vessels and into the stroma. The only prerequisite technique is an intravenous injection of cancer cells, and fluorophore-conjugated dextrans (to highlight vessel lumens) and lectins (binding to glycocalyx on the endothelial cell wall).

I investigated which embryonic day is suitable to inject cancer cells and monitored rapid cancer cell extravasation in the CAM. The CAM of day 13 chicken embryos provided a well-developed vasculature and allowed cancer cells to extravasate within 2-6 h post-injection, compared to older chicken embryos ($\geq$ day 14 chicken embryos, $>$ 9 hours post-injection). In chapter 4, the vascular permeability of the vasculature of day 9, 13, 18 chicken embryos was evaluated by measuring the level of FITC-dextran retention. This observation was also evaluated by another group (Willetts *et al.*) and published following my Nature protocols article[1,2], highlighting the importance as well as the reproducibility of my work.

The CAM assay has been used by several of our collaborators to quantify different cancer cell lines following different genetic and pharmacological treatments. A study by Mesci *et al.* showed that MDA-MB-231 cells (MDA.330-3p) transfected with microRNA miR-330-3p exhibit a significant decrease in extravasation efficiency and metastatic colony formation, using the CAM assay. Intravital imaging of MDA.330-3p cells in the CAM also showed impaired invadopodia formation, suggestive of reduced invasiveness[3]. Another study by Stender *et al.* using the CAM assay showed that MCF-7 breast cancer cells with estrogen receptor-α knocked out exhibit significantly decreased extravasation efficiency in response to interleukin-1β and TNF-α[4]. Lastly, Tornin *et al.* reported that FUS-CHOP, an oncogene that increases a metastatic potential, significantly increases extravasation efficiency of bone marrow mesenchymal stem cells (BM-MSCs)[5]. These studies highlight the utility of the CAM extravasation model for quantification purposes. Although my work optimized the protocol of the CAM-based cancer extravasation method, such a tool may also be used to examine intravasation, *in vivo* EV release from circulating tumor cells and cells at the primary tumor sites. Lastly, the CAM model can be utilized to study the interaction between tumor cells and immune cells. Therefore, the model provides a highly valuable experimental platform.

4.1.2   Future directions for CAM modeling

4.1.2.1   Tracking tumor EV release and EV transfer in xenografted tumors

An emerging concept that would be important to investigate in future studies is EV transfer between cells. Very recently, EVs derived from glioma cells were shown to deliver oncogenes such as c-myc and EGF-RvIII to donor cells, inducing mitogen-activated protein kinase (MAPK) and Akt pathway and promoting anchorage-independent cell growth and survival[6]. A study by Yu *et al*. also showed that EVs from colorectal carcinoma could transfer tissue factor (TF) that activated K-RAS in donor cells and contributed to tumorigenic and angiogenic phenotype[7]. Conversely, Luhtala and Hunter showed that K-Ras embedding U-87MG human glioblastoma cell EV transfer did not evoke K-Ras function in donor cells[8]. EVs attaching to donor cells were found to be less than 2% and only 0.08-0.10% of total K-Ras fusion proteins were shown to be released into EVs. Instead of that donor cells taking up EVs containing oncogenes, this study suggested that U-87MG EVs might affect cancer cell migration by providing more anchors or increasing chemoattractant release. To validate whether cancer cells deliver EV cargoes to donor cells and induce oncogene functions, a model system providing physiological environment is required. To this end, I propose implanting invasive cancer cell lines such as PC-3, MDA-MB-231 cells with or without GFP expression in distant or close proximity. After a week to allow tumor growth, we may collect tumors for histological analyses and assessment of protein levels by immunoblotting. Once we confirm the presence of protein transfer by donor EVs, we can perform a proteomic analysis to investigate whether the types of transferred proteins are their functional significances from pathway analysis. We may also perform an intravital imaging of tumor EV transfer. This may be achieved through implanting GFP- and RFP-expressing cells and observing GFP or RFP EV transfers. Studies by Verweij *et al*. and Hyenne *et al*. showed that cancer cell-derived EVs injected into the blood vessels of zebrafish embryos were captured by the endothelium and circulating macrophages[9,10]. These studies did not report direct EV-derived oncogene transfer to recipient cells but suggested that cancer cell-derived EVs may reprogram the fate of macrophages to adopt a pro-inflammatory phenotype. Since the CAM provides a

systemic environment for tumors and circulating EVs, the platform may yield valuable information on cancer cell EV transfer.

4.1.2.2   Studying tumor intravasation

Studying cancer cell intravasation mostly relies on the mouse xenograft model in which human cells or tissues are implanted in mice. Studies by Deryugina and Kiosses show human fibrosarcoma cell variants with low and high invasiveness (HT-lo/diss and HT-high/diss, respectively) exhibit different levels of cancer metastasis when implanted in mice[11]. Although the researchers noted intravasating cells with low and high levels of invasiveness, advanced imaging analyses were lacking. Specifically, techniques to process acquired pictures and determine the score of cancer cell intravasation would have provided greater knowledge. Peng *et al*. coupled an *in vitro* transwell system and a mouse subcutaneous xenograft model to study the degree of cancer cell intravasation[12]. They plated human microvascular endothelial cells at the bottom of a transwell and then overlaid human breast cancer which induced endothelial permeability. They also implanted MDA-MB-231 subcutaneously in mice and then intravenously administered TiO_2 nanoparticles to induce vessel permeability. The combination of the *in vivo* and *in vitro* assays was used to quantify the degree of cancer cell intravasation. One could argue that real-time imaging of cancer cell intravasation would circumvent the challenges of coupling multiple systems and drawing limited conclusions. Another limitation of these studies mentioned above, is that the currently used models do not allow for simultaneous assessment of morphological changes in cells such as invadopodia formation, which is required for intravasation. The CAM model is a robust model to observe any underlying cellular events such as cell shape/size changes, invadopodia formation, and EV release during intravasation by using confocal microscopy-based intravital imaging. To establish the CAM model for quantification of cancer intravasation, GFP-expressing cancer cells with different degree of invasiveness may be selected. For example, human prostate cancer cell lines PC-3, DU-145, and LnCap show the highest, medium, lowest invasiveness, respectively, and may provide useful information. The cells may then be implanted on the CAM of day 9 chicken embryos which will provide the highest permeability to the CAM vasculature. Then, we

can incubate the CAM until tumors are visible ($\approx$ 4-7 days). Imaging the CAM vasculature near the tumors will allow us to evaluate the presence of intravasated cancer cells. Once we confirm the presence of cancer cells in the blood stream, we can also perform a real-time imaging of the edges of the tumors to capture the events of cancer cell intravasation. Quantification of cancer cell intravasation can be performed by capturing pictures of the CAM vasculature surrounding the primary tumors followed by counting GFP positive individual cancer cells.

4.1.2.3   Developing a humanized CAM model to study tumor and immune cell interaction

Another exciting future study will be to use the CAM model to investigate tumor-immune cell interaction. Currently, immune system interaction with tumors is commonly studied in mice. Yamaguchi *et al*. have cultured peripheral blood mononuclear cell-derived dendritic cells, melanoma antigen recognizing T cells (MART-Ts), and human melanoma tumor infiltrating lymphocytes and introduced the cells into non-obese diabetic mice[13]. In this model, immune cells proliferated and exhibited anti-tumor activity when implanted in mice. Likewise, humanized mice are also being widely used to develop cancer immunotherapy by using patient-derived xenografts (PDXs)[14]. However, generating these humanized mice is expensive and time-consuming. Perhaps the CAM model may be used to study these cell-cell interactions in a cost-effective and high-throughput manner. To achieve this, we can possibly introduce human peripheral blood mononuclear cells via intravenous injection in the CAM model. We can then collect blood samples at different time points post-injection to examine the survival of injected cells. Once we establish such a cell transfer to be feasible, tumor cells or portions of tumor tissues may be implanted. This study may allow us to perform immunohistochemistry to evaluate the presence of tumor infiltrating lymphocytes. This study may also lead to a next generation animal model to study potential immunotherapy.

4.2 Necroptosis: A Key Mediator of Cancer Cell Extracellular Vesicle Biogenesis and Regulator of Cancer extravasation

4.2.1 Summary of findings and conclusions

The key findings from the second part of my thesis show the two main events during cancer cell extravasation: 1) the reduction of cancer cell volume during cancer cell extravasation as an invasive phenotype of extravasating cancer cells, and 2) cancer cell EV release as a potential cellular process leading to the cell volume loss. Although the cell volume reduction at certain threshold may help cancer cells execute to extravasate, excessive cell volume loss is detrimental to cancer cell metastasis. In addition, the body of this work evidences that necroptosis is a potential trigger to induce excessive cancer cell EV release leading to subsequent excessive cell volume reduction, resulting in a failure in cancer metastasis.

Studying underlying events during cancer cell extravasation may lead to the discovery of new targets to stop cancer metastasis. In chapter 4, I showed that cancer cells reduce cell volume after extravasation. Confocal microscopy revealed that cancer cells spontaneously release large EVs into the blood stream. My results also suggest that there is a threshold for EV release generating subsequent desired outcomes for the cancer cells. Specifically, cancer cell EV release may reduce cell volumes, facilitating endothelial transmigration and extravasation. Increasing further EV release may reduce extravasation by inducing cell death. Although other researchers have focused on what signal these EVs may be providing to bystander cells, my research focused on the direct phenotypic modulation of cancer cell through EV release.

Research into cancer cell EVs has led to seminal findings, including the observation that vascular endothelial cells may be activated by taking up cancer cell-derived EVs and regulate angiogenesis and vascular permeability. Both vascular permeability and angiogenesis are essential for tumor growth, at least in solid tumors. A study by Zeng *et al*. showed that cancer cell-derived large EVs contained miR-25-3p that increased the expression of vascular endothelial growth factor receptor-2 (VEGFR2) in endothelial cells.

Such an increase contributed to vascular permeability and angiogenesis[15]. Similarly, Paggeti *et al.* reported that leukemia cell-derived EVs induce proliferation in normal endothelial cells, and increase invasiveness by remodeling of the actin cytoskeleton[16]. Schillaci *et al.* also showed that metastatic colorectal cancer cell (SW620)-derived EVs confer an invasive phenotype in non-metastatic colorectal cancer cells (SW480) and human endothelial cells (HUVEC) by activating the RhoA/ROCK pathway[17]. Cancer cell EVs are also believed to induce endothelial-to-mesenchymal transition (EndMT) to facilitate tumor growth[18]. These studies underscore the importance of cancer-derived EVs in promoting tumor growth and metastasis.

Cell phenotype changes are also important for cancer progression. McGrail *et al.* demonstrated that more invasive cancer cells are more contractile[19]. Bakal *et al.* showed that highly invasive cancer cells had active changes in cytoskeletal gene expression, resulting in morphologic changes[20]. Based on these observations, Lyons *et al.* demonstrated the morphologic differences between invasive and non-invasive human and murine osteosarcoma cell lines. Although there was variation in large and small cell volume in metastatic osteosarcoma cells, highly metastatic cancer cells exhibited significantly smaller mean cell area and volumes compared to less metastatic cancer cells[21]. These results were the first observation of the relationship between cancer cell volume and metastatic efficiency. Therefore, it is conceivable that metastatic cancer cells require a certain level of cell volume reduction to maneuver extravasation more efficiently. The strong correlation between EV release and cancer cell volume reduction in my studies showed that excessive reduction of cancer cell volume is significantly detrimental to metastatic efficiency. My studies also identified that MLKL-mediated necroptosis significantly increases cancer cell EV release, which can further decrease cancer cell metastatic efficiency. Therefore, my findings implicate MLKL-mediated necroptosis as a novel target to stop invasive cell metastasis.

4.2.2 Future directions in the role of cancer cell morphology change and necroptotic cancer cell death

4.2.2.1 Elucidating ESCRT-III complex participation in necroptosis-induced EV release

In chapter 4, I have shown that DMF significantly increased both MLKL and phosphorylated MLKL levels in PC-3 cells. DMF also increased EV release *in vitro* and *in vivo*. These results suggest that MLKL may be involved in necroptosis activation as well as EV release. Gong *et al*. showed that phosphorylated MLKL translocated to the plasma membrane and ESCRT-III complex was recruited to the site of MLKL oligomer recruitment, resulting in shedding EVs[22]. Therefore, one future direction may be to elucidate whether the ESCRT-III complex is also recruited by necroptosis induced by DMF. To test this, PC-3 cells may be treated with DMF, and the levels of CHMP2B and CHMP4B expression may be assessed. High resolution imaging may also be utilized to show ESCRT-III complex at the site of EV release. This proposed study will elucidate whether DMF-induced necroptosis also shares a common MLKL and ESCRT-III-derived EV biogenesis mechanism.

4.2.2.2 RNAseq and proteomic analysis of DMF treated PC-3 cells

I have used DMF as a potential inducer of necroptosis. Although DMF showed a significant increase in both MLKL and phosphorylated MLKL, it is important to elucidate the downstream gene expression profile for two reasons. First, this profile may uncover new downstream pathways to target in cancer cells. Second, the results may generate fundamental insight into necroptosis. To achieve these goals, we could expose PC-3 cells to DMF and perform RNA sequencing. We can also compare RNA sequencing data of control and MLKL-silenced PC-3 cells exposed to DMF to confirm changes in the expression of downstream genes.

4.2.2.3 Investigating molecular pathways involved in cancer cell volume reduction

Although Lyons *et al*. introduced the relationship between small cancer cell volume and a higher degree of invasiveness, the underlying mechanisms of cancer cell volume reduction during extravasation are still elusive[21]. McGrail *et al*. showed that solid tumors derived from MCF7 breast cancer cells resist compressive stress from the tissue environment by increasing sodium efflux and actin polymerization, and preventing cell death[23,24]. One potential study to offer greater insight may focus on determining whether cancer cell volume change is dependent on modulating tonicity and osmotic pressure. Stably transfected PC-3 cells with a vector expressing GFP-tagged NHE1 (sodium-hydrogen antiporter 1) and exposure to DMF may be utilized to achieve this goal. One could study whether DMF increases the expression of NHE1 and induces cell volume changes *in vitro*. Osmotic stressors may also be investigated in this platform. This study may add to the underlying cellular process during necroptosis that regulates EV release.

4.3   Bibliography

1.   Willetts, L., Bond, D., Stoletov, K. & Lewis, J. D. Quantitative Analysis of Human Cancer Cell Extravasation Using Intravital Imaging. *Methods Mol Biol* **1458**, 27-37 (2016).

2.   Kim, Y. *et al.* Quantification of cancer cell extravasation in vivo. *Nat. Protoc.* **11,** 937–948 (2016).

3.   Mesci, A. *et al.* Targeting of CCBE1 by miR-330-3p in human breast cancer promotes metastasis. *Br. J. Cancer* **116,** 1350–1357 (2017).

4.   Stender, J. D. *et al.* Structural and Molecular Mechanisms of Cytokine-Mediated Endocrine Resistance in Human Breast Cancer Cells. *Mol. Cell* **65,** 1122–1135.e5 (2017).

5.   Tornin, J. *et al.* FUS-CHOP Promotes Invasion in Myxoid Liposarcoma through a SRC/FAK/RHO/ROCK-Dependent Pathway. *Neoplasia* **20,** 44–56 (2018).

6.   Al-Nedawi, K. *et al.* Intercellular transfer of the oncogenic receptor EGFRvIII by microvesicles derived from tumour cells. *Nat. Cell Biol.* **10,** 619–24 (2008).

7.   Yu, J. L. *et al.* Oncogenic events regulate tissue factor expression in colorectal cancer cells: implications for tumor progression and angiogenesis. *Blood* **105,** 1734–1741 (2005).

8.   Luhtala, N. & Hunter, T. Failure to detect functional transfer of active K-Ras protein from extracellular vesicles into recipient cells in culture. *PLoS One* **13,** e0203290 (2018).

9.   Verweij, F. J. *et al.* Live Tracking of Inter-organ Communication by Endogenous Exosomes In Vivo. *Dev. Cell* **48,** 573–589.e4 (2019).

10.   Hyenne, V. *et al.* Studying the fate of tumor extracellular vesicles at high spatio-temporal resolution using the zebrafish embryo. *bioRxiv* 380238 (2018).

11. Deryugina, E. I. & Kiosses, W. B. Intratumoral Cancer Cell Intravasation Can Occur Independent of Invasion into the Adjacent Stroma. *Cell Rep.* **19,** 601–616 (2017).

12. Peng, F. *et al.* Nanoparticles promote in vivo breast cancer cell intravasation and extravasation by inducing endothelial leakiness. *Nat. Nanotechnol.* **14**, 279-286 (2019).

13. Yaguchi, T. *et al.* Cellular & Molecular Immunology advance online publication. (2017). doi:10.1038/cmi.2017.106

14. Choi, Y. *et al.* Studying cancer immunotherapy using patient-derived xenografts (PDXs) in humanized mice. *Exp. Mol. Med.* **50,** 99 (2018).

15. Zeng, Z. *et al.* Cancer-derived exosomal miR-25-3p promotes pre-metastatic niche formation by inducing vascular permeability and angiogenesis. *Nat. Commun.* **9,** 5395 (2018).

16. Paggetti, J. *et al.* Exosomes released by chronic lymphocytic leukemia cells induce the transition of stromal cells into cancer-associated fibroblasts. *Blood* **126,** 1106–1117 (2015).

17. Schillaci, O. *et al.* Exosomes from metastatic cancer cells transfer amoeboid phenotype to non-metastatic cells and increase endothelial permeability: their emerging role in tumor heterogeneity. *Sci Rep* **7**,4711.

18. Yeon, J. H. *et al.* Cancer-derived exosomes trigger endothelial to mesenchymal transition followed by the induction of cancer-associated fibroblasts. *Acta Biomater.* **76,** 146–153 (2018).

19. McGrail, D. J., Kieu, Q. M. N., Iandoli, J. A. & Dawson, M. R. Actomyosin tension as a determinant of metastatic cancer mechanical tropism. *Phys. Biol.* **12,** 026001 (2015).

20. Bakal, C., Aach, J., Church, G. & Perrimon, N. Quantitative Morphological

Signatures Define Local Signaling Networks Regulating Cell Morphology. *Science.* **316,** 1753–1756 (2007).

21. Lyons, S. M. *et al.* Changes in cell shape are correlated with metastatic potential in murine and human osteosarcomas. *Biol Open* **5**, 289-99 (2016).

22. Gong, Y.-N. *et al.* ESCRT-III Acts Downstream of MLKL to Regulate Necroptotic Cell Death and Its Consequences. *Cell* **169,** 286–300.e16 (2017).

23. McGrail, D. J. *et al.* Osmotic Regulation Is Required for Cancer Cell Survival under Solid Stress. *Biophys J* **109**, 1334-7 (2015).

24. Jiang, H. & Sun, S. X. Cellular Pressure and Volume Regulation and Implications for Cell Mechanics. *Biophysj* **105,** 609–619 (2013).

Curriculum Vitae

Name:	Yohan Kim
Post-secondary Education and Degrees:	The University of Western Ontario London, Ontario, Canada 2005-2010 Hon. BSc. Biology The University of Western Ontario London, Ontario, Canada 2012-2014 MSc. Microbiology and Immunology The University of Western Ontario London, Ontario, Canada 2015-2019 PhD. Pathology and Laboratory Medicine
Honours and Awards:	Edwin R. Jarmain Entrance Scholarship 2005 Laurene Paterson Estate Scholarship 2009 Dean's Honor List 2009, 2010 Ontario Graduate Scholarship 2016
Related Work Experience	Undergraduate Summer Research Assistant The University of Western Ontario 2007-2008 Research Assistant The University of Western Ontario 2012-2014 Research Technician Lawson Health Research Institute 2014-2015 Research Assistant The University of Western Ontario 2015-Present

Research Assistant
Mayo Clinic
2017-Present

Publications:

1. **Kim Y***, Williams KC*, Gavin CT, Jardin E, Chambers AF, and Leong HS. Quantification of Cancer Cell Extravasation *In vivo*. *Nature Protocols*. 2016. May;11(5):937-48. Impact factor – 11.30

2. Yin C*, **Kim Y**, Argintaru D, Heit Bryan. Rab17 Mediates Differential Antigen Sorting Following Efferocytosis and Phagocytosis. *Cell Death and Disease*. 2016. December; 7, e2529. Impact Factor – 5.97

3. Stander JD*, Nwachukwu JC, Kastrati I, **Kim Y,** Strid T, Yakir M, Youffe P, Lin C, Frasor J, Leong HS, and Glass CK. Structural and Molecular Mechanisms of Cytokine-Mediated Endocrine Resistance in Human Breast Cancer Cells. *Molecular Cell*. 2017. March; 65(6):1122-1135. Impact factor – 14.71

4. Mesci A*, Huang X, Taeb S, Jahangiri S, **Kim Y**, Fokas E, Bruce J, Leong HS, Liu SK. Targeting of CCBE1 by miR-330-3p in Human Breast Cancer Promotes Metastasis. *British Journal of Cancer*. 2017. April; 116:1350-1357. Impact Factor – 6.18

5. Gomes J*, Lucien F*, Cooper TT, **Kim Y**, Williams KC, Liao X, Kaufman L, Lagugné-Labarthet F, Kenyon O, Boysen J, Kay NE, McIntyre CW, Leong HS. Analytical Considerations in Nanoscale Flow Cytometry of Extracellular Vesicles to Achieve Data Linearity. *Thromb Haemost*. 2018. August. Doi: 10.1055/s-0038-1668544. Impact Factor – 4.952

6. Brett SI*, Lucien F, Guo C, Williams KC, **Kim Y**, Durfee PN, Brinker CJ, Chin JL, Yang J, and Leong HS. Immunoaffinity Based Methods are Superior to Kits for Purification of Prostate Derived Extracellular Vesicles from Plasma Samples. *The Prostate*. 2017. August; ep:pros.23393 Impact factor – 3.82

7. Brett SI*, **Kim Y**, Biggs CN, Chin JL, and Leong HS. Extracellular Vesicles Such as Prostate Cancer Fragments as a Fluid Biopsy for Prostate Cancer. *Prostate Cancer and Prostatic Diseases*. 2015. Sept;18(3):213-20. Impact factor – 3.72

8. Williams KC*, Cepeda MA, Javed S, Searle K, Parkins KM, Makela A, Hamilton AM, Soukhtehzari S, **Kim Y**, Tuck AB, Ronald JA, Foster PJ, Chamber AF, Leong H. Invadopodia are Chemosensing Protrusions that Guide Cancer Cell Extravasation to Promote Brain Tropism in Metastasis. *Oncogene*. 2019. May;38(19):3598-3615. Impact Factor- 6.85

9. Tornin J*, Hermida-Prado F, Padda RS, Gonzalez MV, Alvarez-Fernandez C, Rey V, Martinez-Cruzado L, Estupiñan O, Menendez ST, Fernandez-Nevado L, Astudillo A, Rodrigo JP, Lucien F, **Kim Y**, Leong HS, Garcia-Pedrero JM, Rodriguez R. FUS-CHOP Promotes Invasion in Myxoid Liposarcoma through a SRC/FAK/RHO/ROCK-Dependent Pathway. *Neoplasia*. 2018. January; 20(1):44-56.

10. Joshi B*, Pawling J, Shankar J, Pacholczyk K, **Kim Y**, Tran W, Meng F, Foster L, Leong H, Dennis J, Nabi I. Caveolin-1 Y14 Phosphorylation Supresses Tumour Growth while Promoting Invasion. *Oncotarget*. 2019. In Press.